DOCTORAL DISSERTATION

博 士 論 文

FUNDAMENTAL STUDY OF LIQUEFACTION AND HYDRAULIC COLLAPSE OF UNSATURATED SOILS

（不飽和土の液状化現象と浸水崩壊現象に関する基礎的研究）

Yokohama National University

Graduate School of Urban Innovation

国立大学法人　横浜国立大学大学院都市イノベーション学府

VEERAYUT KOMOLVILAS

ヴィラユット コモルヴィラス

September 2017

2017 年 9 月

FUNDAMENTAL STUDY OF LIQUEFACTION AND HYDRAULIC COLLAPSE OF UNSATURATED SOILS

(不飽和土の液状化現象と浸水崩壊現象に関する基礎的研究)

by

VEERAYUT KOMOLVILAS
ヴィラユット コモルヴィラス

A Dissertation Submitted to the Graduate School of Urban Innovation, Yokohama National University in Partial Fulfillment of the Requirement for the Degree of

Doctor of Engineering

Yokohama National University, Graduate School of Urban Innovation
国立大学法人　横浜国立大学大学院都市イノベーション学府

Examination Committee

Associate Professor, Dr. Mamoru KIKUMOTO (Chair)
Professor, Dr. Kazuo KONAGAI
Professor, Dr. Kimitoshi HAYANO
Associate Professor, Dr. Ying CUI
Associate Professor, Dr. Toshiyasu UNNO

September 2017
2017 年 9 月

ABSTRACT

Soil can be classified into two main states depended on the saturated conditions which are saturated state and unsaturated state. Saturated state is the state that the voids in soil are fully filled with water, while the unsaturated state is the state that soil is composed of three phrases, namely, soil particle phrase, water phrase, and air phrase. The difference in air pressure and water pressure of unsaturated soil is defined as suction pressure which the variation in suction has a dominant effect on the unsaturated soil behaviors. It is generally known that the behaviors of unsaturated soil are different from that of saturated soil. The unsaturated soil shows stiffer behavior and retain a looser void ratio comparing with saturated soil under the same confining stress condition. However, the stiffness of unsaturated soil decreases as an increase in degree of saturation.

The hydraulic collapse behavior is one of the phenomena related to variation in suction; i.e. unsaturated soil experiences the volumetric contraction or failure due to the reduction in suction or soaking. This soaking induced collapse phenomenon can cause unintentional problems in civil engineering, for example, the settlement of embankments during or after construction due to the heavy rain or flooding. Another behavior is the cyclic behavior of unsaturated soil. The cyclic behavior of unsaturated soil has recently been concerned in liquefaction phenomena. Several researchers have reported that the mean effective stress of unsaturated soil with a relatively high degree of saturation gradually decreases under fully undrained cyclic loading condition, and such soils can be finally liquefied like saturated soil.

In this dissertation, the hydraulic collapse behavior and the cyclic behavior of unsaturated soil were studied through a series of simulations by using a three-dimensional extension of the simple elastoplastic constitutive model proposed by Kikumoto et al. (2010). The proposed model is a critical state soil model formulated using Bishop's effective stress tensor, which incorporates the following concepts: (a) the volumetric movement of state boundary surface containing the critical state line and normal consolidation line owing to the variation of degree of saturation which controls the volumetric behavior and the peak strength of unsaturated soil; (b) the soil water characteristic curve considering the effects of specific volume and hydraulic hysteresis; and (c) the subloading surface concept for considering the effect of density. Void air is assumed to be an ideal gas obeying Boyle's law in this dissertation. In addition, this model is formulated on the basis of the isotropic hardening concept which the modified Cam clay model is selected as the critical state soil model. The proposed model was validated through comparisons with past experiment results.

The simulation results showed that the proposed model properly described the hydraulic collapse behavior of unsaturated soil under both isotropic and anisotropic conditions such as the

soaking induced volumetric strain and the soaking induced deviatoric strain. The effects of density, mean net stress, and deviatoric stress on the hydraulic collapse behavior were investigated through a parametric study. Moreover, the effects of soaking history on the hydraulic collapse behavior and the soaking induced instability of unsaturated soil were explained. Regarding to the cyclic behavior of unsaturated soil, the fully undrained cyclic behaviors of unsaturated soils such as liquefaction, compression behavior, and an increase in the degree of saturation due to cyclic loading were also suitably described by the proposed model. The effects of the degree of saturation, void ratio, and confining pressure on the cyclic strength of unsaturated soils were described by the simulation results.

Finally, an extension of the elastoplastic constitutive model for unsaturated soil to anisotropy is proposed. This model is modified from the model proposed by Kikumoto et al. (2010) by incorporating the rotational hardening concept (Hashiguchi and Chen, 1998) and the critical state soil model for rotational hardening (Dafalias, 1986). The simulation results of the proposed model including rotational hardening revealed that the proposed model is able to simulate the effect of anisotropy on the unsaturated soil behaviors.

ACKNOWLEDGEMENT

I am very grateful to Assoc. Prof. Mamoru Kikumoto, my academic advisor, for his valuable advice and kind supports throughout my PhD study. I am greatly indebted to my academic advisor for his enthusiasm and encouragement, and especially for pushing me farther than I thought I could go. It is a great honor to work under his supervision.

To Prof. Kazuo Konagai and Prof. Kimitoshi Hayano, I would like to express my deepest appreciation for your assistance and guidance to my study and research. I would also like to extend my sincere appreciation to all committee members: Assoc. Prof. Ying Cui and Assoc. Prof. Toshiyasu Unno for their comments and suggestions to improve this dissertation.

A debt of gratitude is also owed to my colleagues and all good friends in Yokohama National University for their support and friendship. Their friendship means much to me. Moreover, I would like thank all staff in Yokohama National University for their kind co-operation in documentation and formalities.

I would like to give my sincere thanks to my best friend, Mr. Keita Nakamura, who always helped and encouraged me in my studies and shared all good and bad experiences with me throughout my student life in Japan.

I would like to take this opportunity to express my sincere gratitude to Yokohama National University and Ministry of Education, Culture and Sports, Science and Technology, Japan for providing me the great opportunity and a full financial support to fulfill my PhD degree.

Finally, I would like to thank my family for all their loves, understanding and support; none of this would have been possible without you.

TABLE OF CONTENTS

LIST OF TABLES

LIST OF FIGURES

CHAPTER 1

INTRODUCTION

1.1 RESEARCH BACKGROUND

Soil can be classified into two main states depending on the saturated conditions which are saturated state and unsaturated state. Saturated state is the state that the voids in soil are fully filled with water (e.g., the subsoil layer below the groundwater table), while the unsaturated state is the state that soil is composed of three phrases, namely, soil particle phrase, water phrase, and air phrase (e.g., the subsoil layer over the capillary zone of ground water table).

It is generally known that the behaviors of unsaturated soil are different from that of saturated soil. The difference in air pressure and water pressure of unsaturated soil is defined as suction pressure which the variation in suction has a dominant effect on the unsaturated soil behaviors. The unsaturated soil shows stiffer behavior and retains a looser void ratio comparing with saturated soil under the same confining stress condition. However, the stiffness of unsaturated soil decreases as an increase in the degree of saturation. This increase in the degree of saturation can cause the deformation or failure of the unsaturated soil which is called the hydraulic collapse behavior. Another behavior is the cyclic behavior of unsaturated soil which has recently been concerned in liquefaction phenomena. Several researchers (e.g., Unno et al., 2008; Okamura and Noguchi, 2009; Tsukamoto et al., 2014) have reported that the mean effective stress of unsaturated soil with a relatively high degree of saturation gradually decreases under fully undrained cyclic loading condition, and such soils can be finally liquefied like saturated soil.

One example of the geo-structures which is typically under unsaturated condition is embankment. Embankment can be suffered from the hydraulic collapse or liquefaction phenomena, for example, the embankment which is subjected to the heavy rain or earthquake. Figures 1.1 shows the collapse of highway embankments due to heavy rain in Yamaguchi prefecture (Japan, 2005). In addition, the Sanriku-Minami earthquake triggered a landslide in the town of Tsukidate in Japan on May 26, 2003 as shown in Figure 1.2. An artificial fill in this area classified as a volcanic sandy soil lost its effective stress under cyclic loading although the degree of saturation is about 70%. However, not only rainfall and seismic intensities determine the stability of geo-structures but also the quality of construction.

Regarding to the construction of embankment, the compaction curves are usually used for the quality control by defining the optimum water content and maximum dry density at each

level of applied maximum stress in compaction process. The simulations of compaction curves have already been well simulated by using one dimensional constitutive model for unsaturated soils proposed by Kikumoto et al. (2010). However, the behaviors of compacted soil after construction due to the heavy rain and earthquake have not yet been studied, and as the behaviors of compacted soil depend on the variations in density, degree of saturation, and stress condition as usually defined in the compaction curves. Therefore, the effects of these variations on the unsaturated soil behaviors under the earthquake and heavy rainfall conditions should be studied theoretically. Moreover, the studies of saturated soil behaviors have been widely conducted and proposed by many researchers through both experiment tests and numerical analyses, but the number of studies of unsaturated soil behaviors is still limited because of the difficulty in experiment tests and the complexity of constitutive modelling for unsaturated soils. Therefore, the unsaturated soils should be more researched about their behaviors as soils are often under unsaturated conditions in practical situations.

Figure 1.1 Collapse of highway embankment due to heavy rain in Yamaguchi, 2005

Figure 1.2 Landslide due to liquefaction in Tsukidate, 2003 (Photo by Prof. Kazuo Konagai)

1.2 RESEARCH OBJECTIVES

The main objectives of this research are to study the unsaturated soil behaviors through the numerical simulations and propose the elastoplastic constitutive model for unsaturated soils, which can be explained as follows:

1. To develop the elastoplastic constitutive model for unsaturated soils based on the model proposed by Kikumoto et al. (2010). *(Chapter 2*)
2. To study the hydraulic collapse behavior of unsaturated soils. *(Chapter 3)*
    - Applying the model to investigate the effects of density, stress conditions and soaking history on the hydraulic collapse behavior of unsaturated soils under isotropic and anisotropic conditions.
    - To explain the soaking induced instability of unsaturated soils.
3. To study the cyclic behavior of unsaturated soils. *(Chapter 4)*
    - To present a series of simulations of fully undrained cyclic loading on unsaturated soils.
    - To propose a standard for the liquefaction resistance of unsaturated soils in relation to the degree of saturation, density, and confining pressure.
4. To propose an extension of the elastoplastic constitutive model for unsaturated soils to anisotropy by incorporating rotational hardening. *(Chapter 5)*

1.3 OUTLINE OF DISSERTATION

Chapter1 Introduction

Research background and research objectives of this study are described in this chapter including the outline of this dissertation and mathematical notation.

Chapter 2 An elastoplastic constitutive model for unsaturated soils

Chapter 2 explains the important concepts used to develop the elastoplastic constitutive model for unsaturated soils based on the model proposed by Kikumoto et al. (2010). In the introduction, the existing constitutive models for unsaturated soil are firstly reviewed. Then the formulation of an elastoplastic constitutive model for unsaturated soils is described. The proposed model is a critical state soil model formulated using Bishop's effective stress tensor, which incorporates the following concepts: (a) the volumetric movement of state boundary surface containing the critical state line and normal consolidation line owing to the variation of degree of saturation which controls the volumetric behavior and the peak strength of unsaturated soil; (b) the soil water characteristic curve considering the effects of specific volume and hydraulic hysteresis;

and (c) the subloading surface concept for considering the effect of density. Void air is assumed to be an ideal gas obeying Boyle's law in this dissertation. In addition, this model is formulated on the basis of the isotropic hardening concept which the modified Cam-clay model is selected as the critical state soil model. In the following chapters, the simulation of the hydraulic collapse behavior and the cyclic behavior of unsaturated soils are calculated by using the model proposed in Chapter 2.

Chapter 3 Numerical study of the hydraulic collapse behavior of unsaturated soils

The literature reviews of the hydraulic collapse behavior of unsaturated soils are proposed in the introduction part of Chapter 3 including the related experimental and numerical works. The validation of the model proposed in Chapter 2 is then verified by comparing with the one-dimensional compression tests under constant suction and the soaking tests under isotropic and anisotropic conditions for assuring the performance of the proposed model on the hydraulic collapse behavior of unsaturated soils. Finally, the parametric study of the hydraulic collapse behavior of unsaturated soils under isotropic and anisotropic conditions is proposed to provide the typical hydraulic collapse behavior of unsaturated soils under a wide range of densities and stress conditions which it is difficult to conduct the experiment tests. Moreover, the effects of soaking history on the hydraulic collapse behavior and the soaking induced instability of unsaturated soils are also explained.

Chapter 4 Numerical study of the cyclic behavior of unsaturated soils

Chapter 4 presents the numerical study of the cyclic behavior of unsaturated soils. The liquefaction phenomenon of unsaturated soils is also discussed in Chapter 4. The literature reviews of both the experimental and numerical studies of the cyclic behavior of unsaturated soils are proposed in the introduction part. The validity of the proposed model in Chapter 2 is verified through a series of cyclic triaxial tests on saturated and unsaturated soils under fully undrained conditions and through the water retention tests for assuring the performance of the proposed model on the cyclic behavior of unsaturated soils. Finally, the effects of the degree of saturation, void ratio, and confining pressure on the cyclic strength of unsaturated soils are presented through a series of simulations of cyclic triaxial tests under fully undrained condition.

Chapter 5 Extension of the constitutive model for unsaturated soils to anisotropy

An extension of the constitutive model for unsaturated soils to anisotropy is proposed in

Chapter 5. This proposed model is modified from the model described in Chapter 2 by incorporating the rotational hardening concept (Hashiguchi and Chen, 1998) and the critical state soil model for rotational hardening (Dafalias, 1986). The background and the formulation of the model are firstly explained. Then, the simulation results calculated by using the proposed model are discussed to reveal the performance of the new model.

Chapter 6 Concluding remarks and future research

Chapter 6 concludes the substantive findings and the novelty of this research and provides the prospects for the future research.

1.4 MATHEMATICAL NOTATION

As for the notations and symbols, bold letters denote vectors and matrices; "·" denotes an inner product of two vectors (e.g., $\mathbf{a}\cdot\mathbf{b}=a_ib_i$) or a single contraction of adjacent indices of two tensors (e.g., $(\mathbf{c}\cdot\mathbf{d})_{ij}=c_{ik}d_{kj}$); ":" denotes an inner product of two second-order tensors (e.g., $\mathbf{c}\!:\!\mathbf{d}=c_{ij}d_{ij}$) or a double contraction of adjacent indices of tensors of rank two and higher (e.g., $(\mathbf{e}\!:\!\mathbf{c})_{ij}=e_{ijkl}c_{kl}$); $\otimes$ denotes a tensor product of two vectors (e.g., $(\mathbf{a}\otimes\mathbf{b})_{ij}=a_ib_j$) or a tensor product of two second-order tensors (e.g., $(\mathbf{c}\otimes\mathbf{d})_{ijkl}=a_{ij}b_{kl}$); "‖ ‖" denotes the norm of a first-order tensor (e.g., $\|\mathbf{a}\|=\sqrt{\mathbf{a}\cdot\mathbf{a}}=\sqrt{a_ia_i}$) or a second-order tensor (e.g., $\|\mathbf{c}\|=\sqrt{\mathbf{c}\!:\!\mathbf{c}}=\sqrt{c_{ij}c_{ij}}$); $\mathbf{1}$ is the second-order identity tensor; $\boldsymbol{I}$ is the fourth-order identity tensor $\left(I_{ijkl}=\frac{1}{2}\left(\delta_{ik}\delta_{jl}+\delta_{il}\delta_{jk}\right)\right)$; "$\dot{}$" denotes the time derivative; and the subscript zero denotes the initial state (e.g., v_0 = initial specific volume). These regulations of notations and symbols are entirely used for all chapters in this dissertation.

CHAPTER 2

AN ELASTOPLASTIC CONSTITUTIVE MODEL FOR UNSATURATED SOILS

Over the last few decades, many researchers have proposed the elastoplastic constitutive model to study the behavior of unsaturated soils. The elastoplastic constitutive model for partially saturated soils was firstly formulated within the framework of hardening plasticity using suction and net stress as the stress variables, which is able to predict the stress-strain behavior of unsaturated soils by proposing the loading-collapse (LC) yield curve and the suction increase (SI) yield curve (e.g., Alonso et al., 1990; Wheeler and Sivakumar, 1995); however, this model is unable to predict the wetting and drying water retention curves of unsaturated soils. Gallipoli et al. (2003) proposed the elastoplastic constitutive model with single yield curve, which the stress variables and the bonding variable are calculated by the degree of saturation, suction and net stress to simulate the hydraulic hysteresis of unsaturated soils. Wheeler et al. (2003) developed the elastoplastic constitutive model incorporating the coupling mechanical and hydraulic behavior of unsaturated soils by considering the effect of variation in degree of saturation on the stress-strain behavior as the stress variables including the degree of saturation and the effect of variation in volumetric strain on the hydraulic behavior through the modified suction which depended on the ordinary suction and porosity, nevertheless, Wheeler et al. (2003) stated that the water retention curve in the model should be improved. Gallipoli et al. (2003a) proposed the water retention curve model considering the effect of density on the variation in degree of saturation, however, the effect of hydraulic hysteresis did not include in the model.

Recently, many researchers have proposed the coupling of an elastoplastic constitutive model and a water retention curve model to capture the cyclic behavior of unsaturated soils. Khalili et al. (2008) proposed coupled flow and deformation models based on the effective stress concept for cyclic analysis using the bounding surface plasticity, the hydraulic hysteresis considering the change in density, and the coupled effect of suction hardening. Yang et al. (2008) developed a constitutive model for unsaturated cemented soils under cyclic loading using the bond damage theory for considering cemented soils, the Barcelona Basic Model for describing the effect of suction on cohesion, and the bounding surface plasticity concept for modeling the strain due to cyclic loading. Liu and Muraleetharan (2012) proposed a coupled hydro-mechanical constitutive model in the general stress space for unsaturated sands and silts. They considered the hysteretic properties of the soil-water characteristic curve (SWCC) using the bounding surface plasticity

concept. In addition, they investigated the effect of suction on hardening through the irrecoverable water content calculated using the SWCC model. However, thus far, the liquefaction of unsaturated soils has not been simulated using the above-mentioned models. Meanwhile, Unno et al. (2013) proposed a simplified elastoplastic constitutive model combined with the three-phase porous media theory and the modified SWCC model to study the effect of pore air pressure on the cyclic behavior of unsaturated sandy soils, however, the suction does not affect the yield surface of unsaturated soils in this model.

Kikumoto et al. (2010) proposed a simple critical state model for unsaturated soils considering the degree of saturation-induced hardening and the effects of hydraulic hysteresis and density on the water retention curve, which is capable of describing hydraulic collapse and compaction behaviors. The main objective of this chapter is to develop the elastoplastic constitutive model for unsaturated soils proposed by Kikumoto et al. (2010) to three-dimensional problems in order to predict the hydraulic collapse behavior and the liquefaction behavior of unsaturated soils. The basic concepts applied to formulate the model are described in this chapter.

2.1 THE EFFECTIVE STRESS FOR UNSATURATED SOILS

Sivakumar (1993) indicated that the critical state stress ratio is uniquely defined by Bishop's mean effective stress versus the deviator stress plane regardless of the degree of saturation. Hence, a unique critical state friction angle can be assumed in a model for unsaturated soils if it is formulated on the basis of Bishop's effective stress tensor (Bishop, 1959).

Thus, we formulate the model for unsaturated soils on the basis of Bishop's effective stress tensor $\boldsymbol{\sigma''}$, defined by:

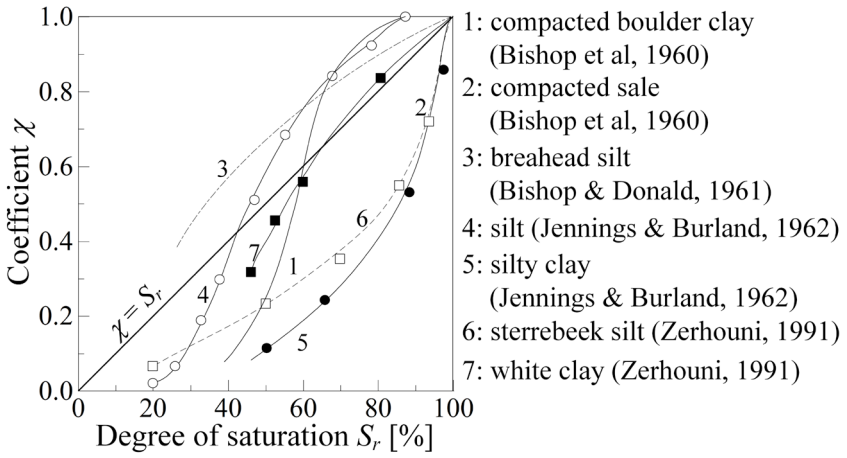

Figure 2.1 Observed relations between degree of saturation S_r and effective stress parameter χ (Gens, 1996)

$$\boldsymbol{\sigma}'' = \boldsymbol{\sigma} - (1-\chi)u_{\mathrm{a}}\mathbf{1} - \chi u_{\mathrm{w}}\mathbf{1} = (\boldsymbol{\sigma} - u_{\mathrm{a}}\mathbf{1}) + \chi(u_{\mathrm{a}} - u_{\mathrm{w}})\mathbf{1} = \boldsymbol{\sigma}_{\mathrm{net}} + \chi s\mathbf{1} \tag{2.1}$$

where $\boldsymbol{\sigma}$, $\boldsymbol{\sigma}_{\mathrm{net}}$, u_{a}, u_{w}, and s represent Cauchy's total stress tensor, Cauchy's net stress tensor, air pressure, water pressure, and suction, respectively. Further, χ is an effective stress parameter given by a monotonic increasing function of the degree of saturation S_{r} ranging from 0 for dry conditions to 1 for fully saturated conditions; for simplicity, it is assumed to be equal to S_{r} in this study.

$$\boldsymbol{\sigma}'' = \boldsymbol{\sigma} - (1-S_{\mathrm{r}})u_{\mathrm{a}}\mathbf{1} - S_{\mathrm{r}}u_{\mathrm{w}}\mathbf{1} = \boldsymbol{\sigma}_{\mathrm{net}} + S_{\mathrm{r}}s\mathbf{1} \tag{2.2}$$

Equation (2.2) has been first proposed by Schrefler (1984) in a similar expression as Bishop's effective stress, but using the degree of saturation S_{r} instead of χ. Figure 2.1 shows the observed relations between the effective stress parameter χ and degree of saturation S_{r} of several types of soils (Gens, 1996). Borja (2006) has also derived Equation (2.2) by using the principles of thermodynamics.

2.2 SOIL WATER CHARACTERISTIC CURVES (SWCCs)

The behavior of unsaturated soils is influenced by the coupling effects between mechanical and hydraulic behaviors. Therefore, the proper soil water characteristic curves need to be implemented into the constitutive model for unsaturated soils. Considering the possible range of the degree of saturation S_{r}, the effective degree of saturation S_{e} is given by

$$\frac{S_{\mathrm{r}} - S_{\mathrm{min}}}{S_{\mathrm{max}} - S_{\mathrm{min}}} = S_{\mathrm{e}} \tag{2.3}$$

where S_{max} and S_{min} are the maximum and minimum degrees of saturation, respectively. Classical SWCC models give the effective degree of saturation S_{e} as a monotonic decreasing, single-valued function of suction s ranging from 0 to 1 (e.g., Gardner, 1958; Brooks and Corey, 1964; Fredlund and Xing, 1994; van Genuchten, 1980). Any of such classical models can be applied to the proposed SWCC model presented here. For this study, we selected the following function proposed by van Genuchten (1980).

$$S_{\mathrm{e}} = S_{\mathrm{e}}(s) = \{1 + (\alpha s)^n\}^{-m} \tag{2.4}$$

where α, n, and m are material parameters.

However, past experimental studies (e.g. Tarantino and Tombolato, 2005; Sun et al., 2007) indicate that volumetric behavior influences the SWCC and that denser soils tend to retain a higher S_{r} as shown in Figure 2.2. Therefore, we extended classical SWCC models that assume a unique relationship between suction and degree of saturation using a modified suction s^*, where the effect of density is incorporated as

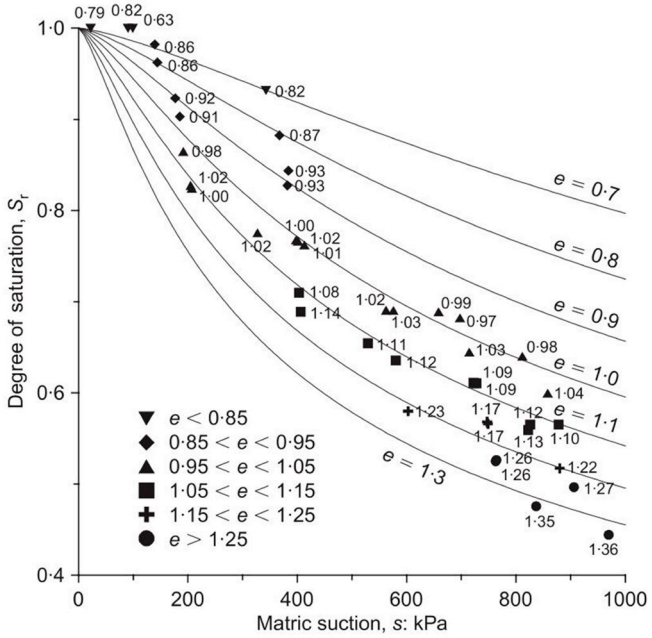

Figure 2.2 The effect of density on SWCCs (Tarantino and Tombolato, 2005)

$$s^* = s\left(\frac{e}{e_{\mathrm{ref}}}\right)^{\xi_{\mathrm{e}}} \tag{2.5}$$

where e is the void ratio, e_{ref} is a reference void ratio for which we use the void ratio of saturated, normally consolidated soils under atmospheric pressure p_{a} (= 98 kPa), and ξ_{e} is a parameter controlling the effect of density. Thus, using s^*, we can rewrite Equation (2.4) as

$$S_{\mathrm{e}} = S_{\mathrm{e}}(s^*) = \{1 + (\alpha s^*)^n\}^{-m}. \tag{2.6}$$

Further, it is well known that SWCCs trace hysteretic paths according to drying and wetting histories (Haines, 1930; Topp and Miller, 1966; Huang et al., 2005). Therefore, we define the main drying and wetting curves by Equation (2.6) as the highest and lowest boundaries of the degree of saturation, $S_{\mathrm{r}}^{\mathrm{d}}$ and $S_{\mathrm{r}}^{\mathrm{w}}$, as follows:

$$\frac{S_{\mathrm{r}}^{\mathrm{A}} - S_{\min}}{S_{\max} - S_{\min}} = S_{\mathrm{e}}^{\mathrm{A}}(s^*) = \left\{1 + \left(\alpha^{\mathrm{A}} s^*\right)^n\right\}^{-m}, \qquad \mathrm{A} = \mathrm{d}, \mathrm{w} \tag{2.7}$$

where d and w denote the main drying and wetting curves, respectively. The main drying and wetting paths are schematically illustrated in Figure 2.3. We need to set different values for the parameters α^{d} and α^{w} for the main drying and wetting curves, respectively, whereas we use the same values for the other parameters, namely n and m. As $S_{\mathrm{r}}^{\mathrm{d}}$ is always larger than $S_{\mathrm{r}}^{\mathrm{w}}$ at the same suction value, α^{d} should be set to a smaller value than α^{w}.

To define the current state (s^*, S_{r}), we use a ratio I_{h} of interior division of the current state between two reference states on the main curves under the same modified suction as follows:

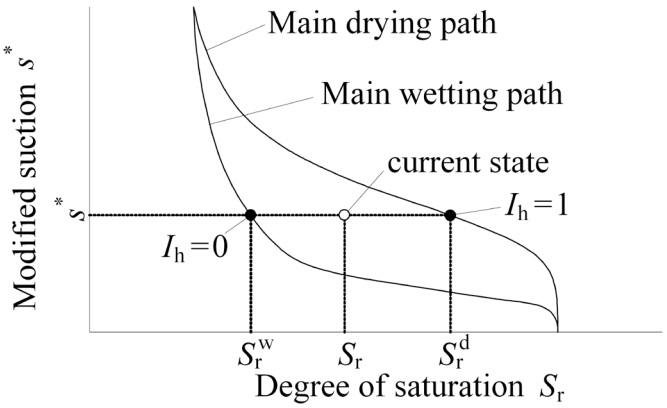

Figure 2.3 Modeling of hysteresis in water retention curve

$$I_h = \frac{S_r - S_r^w}{S_r^d - S_r^w}. \tag{2.8}$$

As the current state (s^*, S_r) is always located between the two main curves, I_h always takes a value between 0 and 1. Further, I_h can be used as a key state variable that reflects the wetting and drying histories. It increases monotonically to 1 with decreasing S_r (drying) as the current state approaches the main drying curve, and it decreases monotonically to 0 with increasing S_r (wetting) as the current state approaches the main wetting curve. Thus, an evolution law for I_h must satisfy the following requirements.

$$\dot{I_h} \begin{cases} \geq 0 & \text{when} \quad \dot{S_r} \leq 0 \\ \leq 0 & \text{when} \quad \dot{S_r} \geq 0 \\ = 0 & \text{when} \quad I_h = 0 \text{ or } I_h = 1 \end{cases}. \tag{2.9}$$

An evolution law given by the following equation satisfies this requirement and is employed in the present study:

$$\dot{I_h} = \frac{dI_h}{dS_r}\dot{S_r} \text{ where } \frac{dI_h}{dS_r} = \begin{cases} -\xi_h(1-I_h)^3 & \text{when } \dot{S_r} \leq 0 \\ -\xi_h {I_h}^3 & \text{when } \dot{S_r} > 0 \end{cases} \tag{2.10}$$

where ξ_h is a material constant controlling the effect of suction histories.

From Equations (2.5), (2.7), and (2.8), the time derivative of the degree of saturation is given by increments of suction *s*, void ratio *e*, and variable I_h as

$$\dot{S_r} = \frac{\partial S_r}{\partial s}\dot{s} + \frac{\partial S_r}{\partial e}\dot{e} + \frac{\partial S_r}{\partial I_h}\dot{I_h}. \tag{2.11}$$

Substituting Equation (2.10), we finally get

$$\dot{S_r} = \frac{\frac{\partial S_r}{\partial s}\dot{s} + \frac{\partial S_r}{\partial e}\dot{e}}{1 - \frac{\partial S_r}{\partial I_h}\frac{dI_h}{dS_r}}. \tag{2.12}$$

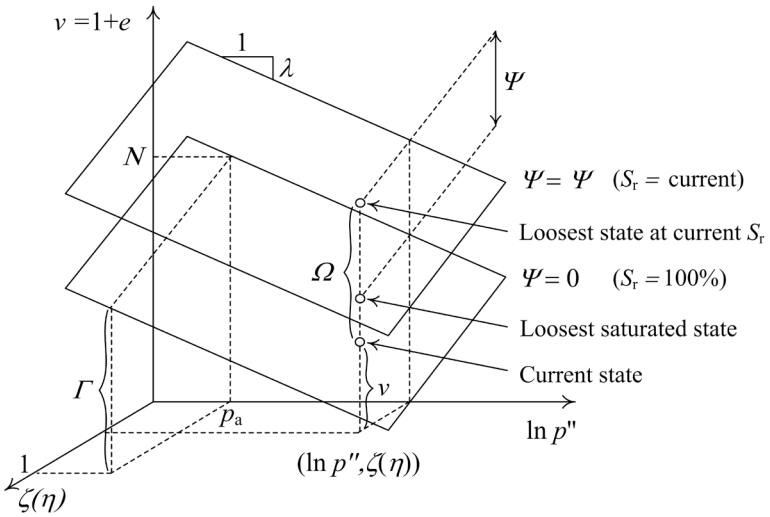

Figure 2.4 State boundary surface moving with S_r and state variable Ω under the effect of packing density

2.3 STRESS–STRAIN RELATIONSHIP FOR UNSATURATED SOILS

A critical state soil model for unsaturated soils was formulated by Kikumoto et al. (2010) on the basis of the modified Cam clay model (Roscoe and Burland, 1968), which incorporates the subloading surface concept (Hashiguchi and Ueno, 1977) and the volumetric movement of the state boundary surface owing to the variation in S_r as shown in Figure 2.4. We extend this model to three-dimensional problems herein. For the model, we first assume additive decomposition of the total strain rate tensor as

$$\dot{\boldsymbol{\varepsilon}} = \dot{\boldsymbol{\varepsilon}}^{\mathrm{e}} + \dot{\boldsymbol{\varepsilon}}^{\mathrm{p}} \tag{2.13}$$

where $\dot{\boldsymbol{\varepsilon}}^{\mathrm{e}}$ and $\dot{\boldsymbol{\varepsilon}}^{\mathrm{p}}$ are elastic and plastic strain rate tensors, respectively.

2.3.1 Elastic stress–strain relationship

For the elastic stress–strain relationship, we use a conventional, nonlinear elastic bulk modulus for soils, given by

$$K = \frac{v_0}{\kappa} p'' \tag{2.14}$$

where v_0 is the initial specific volume, κ is the swelling index that represents the slope of the elastic volumetric relationship in the semi-logarithmic ln p''–v plane, and Poisson's ratio ν_{e} is assumed to be constant. Thus, the rate form of the elastic relationship is given by

$$\dot{\boldsymbol{\sigma}}'' = \boldsymbol{D}^{\mathrm{e}} : \dot{\boldsymbol{\varepsilon}}^{\mathrm{e}} \tag{2.15}$$

where $\dot{\boldsymbol{\sigma}}''$ is the rate of Bishop's effective stress tensor and $\boldsymbol{D}^{\mathrm{e}}$ is the elastic stiffness tensor given by

$$\boldsymbol{D}^{\mathrm{e}} = K\mathbf{1} \otimes \mathbf{1} + 2G\left(\boldsymbol{I} - \frac{1}{3}\mathbf{1} \otimes \mathbf{1}\right) \tag{2.16}$$

where G is the shear modulus given by

$$G = \frac{3K(1-2\nu_{\mathrm{e}})}{2(1+\nu_{\mathrm{e}})}. \tag{2.17}$$

As an inverse tensor of the elastic stiffness tensor $\boldsymbol{D}^{\mathrm{e}}$ always exists, we get

$$\dot{\boldsymbol{\varepsilon}}^{\mathrm{e}} = \boldsymbol{D}^{\mathrm{e}-1} : \dot{\boldsymbol{\sigma}}''. \tag{2.18}$$

2.3.2 Yield function for unsaturated soil based on subloading surface concept

The specific volume $v_{\mathrm{sbs}}^{\mathrm{sat}}$ of a saturated soil on the state boundary surface that defines the loosest state (maximum specific volume) of the saturated soil for the given mean effective stress p' and deviator stress q can be expressed as

$$v_{\mathrm{sbs}}^{\mathrm{sat}} = N - \lambda \ln\frac{p'}{p_{\mathrm{a}}} + (\Gamma - N)\zeta(\eta) \tag{2.19}$$

where p' is the mean effective stress $\frac{\boldsymbol{\sigma}':\mathbf{1}}{3}$, η is the stress ratio q/p', $q\left(=\sqrt{\frac{3}{2}\boldsymbol{s}:\boldsymbol{s}}\right)$ is the deviator stress, and $\boldsymbol{s}(=\boldsymbol{\sigma} - p\mathbf{1})$ is the deviator stress tensor. Further, N and Γ are the reference specific volumes of saturated, normally consolidated soil under atmospheric pressure p_{a} in the isotropic stress state (η = 0) and critical state (η = M), respectively, λ is the compression index, and $\zeta(\eta)$ is a monotonic increasing function of η that satisfies 0 on the NCL with η = 0 and 1 on the CSL with η = M. We employ the following function based on the modified Cam clay model (Roscoe and Burland, 1968):

$$\zeta(\eta) = \frac{\ln\left\{1 + \left(\frac{\eta}{M}\right)^2\right\}}{\ln 2} \tag{2.20}$$

where M is the stress ratio in the critical state.

As an unsaturated soil exhibits a relatively high stiffness and tends to retain a larger specific volume than a saturated soil, the state boundary surface is assumed to shift upward (downward) as the degree of saturation S_{r} decreases (increases) in the direction of the specific volume axis. Thus, using a new variable $\Psi(S_{\mathrm{r}})$ to represent the upward shift of the state boundary surface in the v direction, we define the specific volume $v_{\mathrm{sbs}}^{\mathrm{unsat}}$ on the state boundary surface of the unsaturated soil using Bishop's mean effective stress p'' in a manner similar to Equation (2.19) as

$$v_{\mathrm{sbs}}^{\mathrm{unsat}} = N - \lambda \ln\frac{p''}{p_{\mathrm{a}}} + (\Gamma - N)\zeta(\eta) + \Psi \tag{2.21}$$

where Ψ is assumed to be a monotonic decreasing function of the degree of saturation S_{r}, which always takes a non-negative value and is equal to 0 under the fully saturated condition (S_{r} = 1). Thus, we introduce a simple linear relationship for Ψ as

$$\Psi = \psi(1 - S_{\mathrm{r}}) \tag{2.22}$$

where ψ is a material parameter representing the volumetric distance of the state boundary surface for dried and saturated states in the specific volume direction.

In order to consider the effect of specific volume, the subloading surface concept (Hashiguchi and Ueno, 1977) is applied to our model. According to this concept, soil exhibits elastoplastic, irreversible deformation even below the state boundary surface and then gradually approaches the state boundary surface with loading. Therefore, the cyclic behavior of unsaturated soils can therefore be predicted relatively well using this concept. On the other hand, classical models without the subloading surface concept will predict purely elastic behavior within the yield surface and cannot simulate the cyclic behavior of soil. Taking a state variable Ω as the difference between the specific volume of the current state and that on the state boundary surface under the same stress (p', η), we can represent an arbitrary specific volume v of an unsaturated soil using Ω as

$$v = v_{\mathrm{sbs}}^{\mathrm{unsat}} - \Omega = N - \lambda \ln \frac{p''}{p_{\mathrm{a}}} + (\Gamma - N)\zeta(\eta) + \Psi(S_{\mathrm{r}}) - \Omega. \tag{2.23}$$

The definition of the state variable $\Omega(\geq 0)$ is shown in Figure 2.4. Although Been and Jefferies (1985) proposed a similar state parameter as the volumetric distance of the soil from the reference state on the steady state line under the current mean effective stress, our parameter Ω always refers to the volumetric distance from the current state to the loosest state of the soil (specific volume on the state boundary surface) under the current stress condition (p', q) and the current degree of saturation S_{r}. As Ω necessarily decreases with the development of plastic deformation and finally converges to 0, an evolution law of Ω can be represented by

$$\frac{\dot{\Omega}}{v_0} = -\omega\Omega|\Omega|\left\|\dot{\boldsymbol{\varepsilon}}^{\mathrm{p}}\right\| \tag{2.24}$$

where ω is a parameter controlling the effect of density.

We can get the current specific volume v from Equation (2.23), and we can get the initial specific volume v_0 by substituting the initial states $v = v_0$, $\Psi = \Psi_0$, $\Omega = \Omega_0$, $p'' = p_0''$, and q = 0 into Equation (2.23).

$$v_0 = N - \lambda \ln \frac{p_0''}{p_{\mathrm{a}}} + \Psi_0 - \Omega_0 \tag{2.25}$$

The total volumetric strain (compression is taken to be positive) generated from the initial state to

the current state is given by

$$\varepsilon_{\mathrm{v}} = -\frac{\mathrm{d}v}{v_0} = \frac{v_0 - v}{v_0} \tag{2.26}$$

By substituting Equations (2.23) and (2.25) into Equation (2.26), we get

$$\varepsilon_{\mathrm{v}} = \frac{1}{v_0}\left\{\lambda \ln\frac{p''}{p_0''} + (N-\Gamma)\zeta(\eta) - (\Psi - \Psi_0) + (\Omega - \Omega_0)\right\}. \tag{2.27}$$

Taking the trace on both sides of Equation (2.15), we get the elastic volumetric strain as

$$\varepsilon_{\mathrm{v}}^{\mathrm{e}} = \frac{\kappa}{v_0}\ln\frac{p''}{p_0''}. \tag{2.28}$$

The plastic volumetric strain can be determined by taking the difference between the total volumetric strain and the elastic volumetric strain. From Equations (2.27) and (2.28), we get

$$\varepsilon_{\mathrm{v}}^{\mathrm{p}} = \frac{1}{v_0}\left\{(\lambda-\kappa)\ln\frac{p''}{p_0''} + (N-\Gamma)\zeta(\eta) - (\Psi - \Psi_0) + (\Omega - \Omega_0)\right\}. \tag{2.29}$$

From Equation (2.29), the yield function *f* for an unsaturated soil can be written as

$$f = \frac{1}{v_0}\left\{(\lambda-\kappa)\ln\frac{p''}{p_0''} + (N-\Gamma)\zeta(\eta) - (\Psi - \Psi_0) + (\Omega - \Omega_0)\right\} - \varepsilon_{\mathrm{v}}^{\mathrm{p}}. \tag{2.30}$$

An associated flow is assumed in the model and the function *f* is used as the plastic potential function as

$$\dot{\boldsymbol{\varepsilon}}^{\mathrm{p}} = \langle\dot{\Lambda}\rangle\frac{\partial f}{\partial \boldsymbol{\sigma}''} \tag{2.31}$$

where $\dot{\Lambda}$ is the rate of the plastic multiplier and $< >$ are Macaulay brackets, which denote the ramp function as $< \mathrm{x} >= \begin{cases} \mathrm{x} & \text{if } \mathrm{x} > 0 \\ 0 & \text{if } \mathrm{x} \le 0 \end{cases}$.

As the soil exhibits an unlimited distortional strain in the critical state without any change in stress or volume, the derivatives of the yield function $f\left(\boldsymbol{\sigma}'', \Psi, \Omega, \varepsilon_{\mathrm{v}}^{\mathrm{p}}\right)$ with respect to p'' becomes 0 when $\eta = M$. Thus, $(\lambda - \kappa)$ is equal to $(N-\Gamma)\ln 2$ when Equation (2.20) is applied. Equation (2.30) can be finally rearranged as

$$f = \frac{\lambda-\kappa}{v_0}\left[\ln\frac{p''}{p_0''} + \ln\left\{1 + \left(\frac{\eta}{M}\right)^2\right\}\right] - \frac{\Psi - \Psi_0}{v_0} + \frac{\Omega - \Omega_0}{v_0} - \varepsilon_{\mathrm{v}}^{\mathrm{p}} \tag{2.32}$$

2.3.3 Elastoplastic stress–strain relationship

Regarding the loading condition, soil exhibits elastic deformation if the stress condition is under the yield surface ($f < 0$) which there is no plastic deformation ($\langle\dot{\Lambda}\rangle = 0$), while soil exhibits plastic deformation if the stress condition remains on the yield surface ($f = 0$) which the plastic multiplier exists ($\langle\dot{\Lambda}\rangle > 0$). Therefore, we could write the possible relationship between f

and $\langle\dot{\Lambda}\rangle$ as

$$\langle\dot{\Lambda}\rangle f = 0 \tag{2.33}$$

which is called the Khun-Tucker conditions (Kuhn and Tucker, 1951). Taking the time derivative of Equation (2.33), we get

$$\langle\dot{\Lambda}\rangle \dot{f} = 0 \tag{2.34}$$

which the time derivative of the yield function will equal to 0 ($\dot{f} = 0$) if the plastic multiplier exists ($\langle\dot{\Lambda}\rangle > 0$), called consistency conditions. From the consistency conditions, taking the time derivative of the yield function $f(\boldsymbol{\sigma}'', \Psi, \Omega, \varepsilon_{\mathrm{v}}^{\mathrm{p}})$ given by Equation (2.32), we get the consistency condition as

$$\dot{f} = \frac{\partial f}{\partial \boldsymbol{\sigma}''} : \dot{\boldsymbol{\sigma}''} + \frac{\partial f}{\partial \Psi}\dot{\Psi} + \frac{\partial f}{\partial \Omega}\dot{\Omega} + \frac{\partial f}{\partial \varepsilon_{\mathrm{v}}^{\mathrm{p}}}\dot{\varepsilon_{\mathrm{v}}^{\mathrm{p}}} = 0. \tag{2.35}$$

Substituting Equation (2.31) and the evolution laws of Ψ and Ω, given by Equations (2.22) and (2.24), respectively, into Equation (2.35), we get

$$\frac{\partial f}{\partial \boldsymbol{\sigma}''} : \dot{\boldsymbol{\sigma}''} + \frac{\psi}{v_0}\dot{S}_{\mathrm{r}} - \omega\Omega|\Omega|\langle\dot{\Lambda}\rangle \left\|\frac{\partial f}{\partial \boldsymbol{\sigma}''}\right\| - \langle\dot{\Lambda}\rangle \frac{\partial f}{\partial \boldsymbol{\sigma}''} : \mathbf{1} = 0. \tag{2.36}$$

From Equations (2.13) and (2.18), the stress rate tensor is given by

$$\dot{\boldsymbol{\sigma}''} = \boldsymbol{D}^{\mathrm{e}} : (\dot{\boldsymbol{\varepsilon}} - \dot{\boldsymbol{\varepsilon}^{\mathrm{p}}}) = \boldsymbol{D}^{\mathrm{e}} : \left(\dot{\boldsymbol{\varepsilon}} - \langle\dot{\Lambda}\rangle \frac{\partial f}{\partial \boldsymbol{\sigma}''}\right) \tag{2.37}$$

We get the rate of the plastic multiplier from Equations (2.36) and (2.37) as follows.

$$\langle\dot{\Lambda}\rangle = \left\langle \frac{\frac{\partial f}{\partial \boldsymbol{\sigma}''} : \boldsymbol{D}^{\mathrm{e}} : \dot{\boldsymbol{\varepsilon}} + \frac{\psi}{v_0}\dot{S}_{\mathrm{r}}}{\frac{\partial f}{\partial \boldsymbol{\sigma}''} : \mathbf{1} + \omega\Omega|\Omega| \left\|\frac{\partial f}{\partial \boldsymbol{\sigma}''}\right\| + \frac{\partial f}{\partial \boldsymbol{\sigma}''} : \boldsymbol{D}^{\mathrm{e}} : \frac{\partial f}{\partial \boldsymbol{\sigma}''}} \right\rangle \tag{2.38}$$

where $\frac{\partial f}{\partial \boldsymbol{\sigma}''} : \mathbf{1} + \omega\Omega|\Omega| \left\|\frac{\partial f}{\partial \boldsymbol{\sigma}''}\right\|$ is the hardening parameter H of the proposed model. Soils show a hardening behavior when $H > 0$, a perfectly plastic behavior when $H = 0$, and a softening behavior when $H < 0$ as shown in Figure 2.5.

Finally, we get the rate form of the elastoplastic stress–strain relationship from Equations (2.13), (2.18), (2.31), and (2.38).

$$\dot{\boldsymbol{\sigma}''} = \boldsymbol{D}^{\mathrm{e}} : \dot{\boldsymbol{\varepsilon}} - \left\langle \frac{\frac{\partial f}{\partial \boldsymbol{\sigma}''} : \boldsymbol{D}^{\mathrm{e}} : \dot{\boldsymbol{\varepsilon}} + \frac{\psi}{v_0}\dot{S}_{\mathrm{r}}}{\frac{\partial f}{\partial \boldsymbol{\sigma}''} : \mathbf{1} + \omega\Omega|\Omega| \left\|\frac{\partial f}{\partial \boldsymbol{\sigma}''}\right\| + \frac{\partial f}{\partial \boldsymbol{\sigma}''} : \boldsymbol{D}^{\mathrm{e}} : \frac{\partial f}{\partial \boldsymbol{\sigma}''}} \right\rangle \boldsymbol{D}^{\mathrm{e}} : \frac{\partial f}{\partial \boldsymbol{\sigma}''} \tag{2.39}$$

When the rate of the plastic multiplier $\dot{\Lambda}$ is positive, the rate form of the elastoplastic stress–strain relationship can be expressed as

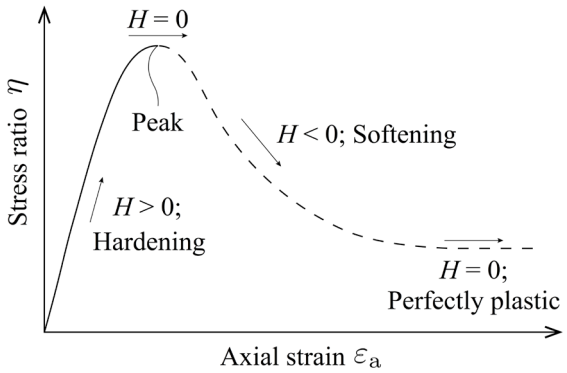

Figure 2.5 Typical stress-strain relationship of over consolidated soils

$$\dot{\boldsymbol{\sigma}}'' = \boldsymbol{D}^{\mathrm{ep}}:\dot{\boldsymbol{\varepsilon}} - \boldsymbol{D}^{\mathrm{Sr}}\dot{S}_{\mathrm{r}} \tag{2.40}$$

where $\boldsymbol{D}^{\mathrm{ep}}$ and $\boldsymbol{D}^{\mathrm{Sr}}$ are defined as follows.

$$\boldsymbol{D}^{\mathrm{ep}} = \boldsymbol{D}^{\mathrm{e}} - \frac{\boldsymbol{D}^{\mathrm{e}}:\frac{\partial f}{\partial \boldsymbol{\sigma}''} \otimes \frac{\partial f}{\partial \boldsymbol{\sigma}''}:\boldsymbol{D}^{\mathrm{e}}}{\frac{\partial f}{\partial \boldsymbol{\sigma}''}:\mathbf{1} + \omega\Omega|\Omega|\left\|\frac{\partial f}{\partial \boldsymbol{\sigma}''}\right\| + \frac{\partial f}{\partial \boldsymbol{\sigma}''}:\boldsymbol{D}^{\mathrm{e}}:\frac{\partial f}{\partial \boldsymbol{\sigma}''}} \tag{2.41}$$

$$\boldsymbol{D}^{\mathrm{Sr}} = \frac{\boldsymbol{D}^{\mathrm{e}}:\frac{\partial f}{\partial \boldsymbol{\sigma}''}\frac{\psi}{v_0}}{\frac{\partial f}{\partial \boldsymbol{\sigma}''}:\mathbf{1} + \omega\Omega|\Omega|\left\|\frac{\partial f}{\partial \boldsymbol{\sigma}''}\right\| + \frac{\partial f}{\partial \boldsymbol{\sigma}''}:\boldsymbol{D}^{\mathrm{e}}:\frac{\partial f}{\partial \boldsymbol{\sigma}''}} \tag{2.42}$$

2.4 CALIBRATION OF MODEL PARAMETERS

The model parameters for the water retention curve can be calibrated by fitting the water retention curve. Note that $S_{\min}$, $S_{\max}$, α^{w}, α^{d}, n, and m are parameters for the main wetting and drying curves described by the van Genuchten model, and ξ_{h} and ξ_{e} are the parameters controlling the effect of suction histories and density, respectively.

There are two sets of model parameters for the stress–strain characteristics. The first set (λ, κ, N, M, and ν_{e}) can be readily obtained from the results of elementary tests on saturated samples. The results of isotropic consolidation tests on saturated samples plotted in the e–ln p'' plane can be used to determine λ from the slope of the NCL, κ from the slope of the unloading part, and N from the specific volume on the NCL under atmospheric pressure. The slope of the CSL in the q–p'' plane, M, and Poisson's ratio, ν_{e}, are calibrated from the result of triaxial compression tests. The parameter ψ, which controls the effect of S_{r} on the position of the state boundary surface, can be determined by the result of soaking tests on dried or unsaturated soil samples or by the results of constant suction compression tests on unsaturated soil samples; however, it is deduced by fitting the simulations of cyclic loading tests under varying degrees of saturation to their corresponding experimental results in this study. The parameter ω, which controls the effect of density, is the only parameter that needs to be calibrated by a trial-and-error

procedure to fit the experimental results of the soils at different densities.

2.5 CONCLUSIONS

This chapter presented the formulation of a three-dimensional extension of the simple elastoplastic constitutive model proposed by Kikumoto et al. (2010). This proposed model is a critical state soil model formulated using Bishop's effective stress tensor, which incorporates the following concepts: (a) the volumetric movement of state boundary surface containing the critical state line and normal consolidation line owing to the variation of degree of saturation which controls the volumetric behavior and the peak strength of unsaturated soil; (b) the soil water characteristic curve considering the effects of specific volume and hydraulic hysteresis; and (c) the subloading surface concept for considering the effect of density. Void air is assumed to be an ideal gas obeying Boyle's law. In addition, this model is formulated on the basis of the isotropic hardening concept which the modified Cam-clay model is selected as the critical state soil model.

CHAPTER 3

NUMERICAL STUDY OF THE HYDRAULIC COLLAPSE BEHAVIOR OF UNSATURATED SOILS

In general, the stiffness of unsaturated soils decreases as an increase in the degree of saturation or a reduction in suction. The hydraulic collapse behavior is the deformation or failure of unsaturated soil due to soaking or a decrease in suction. This soaking induced collapse phenomena can cause unintentional problems in civil engineering, for example, the settlement of embankments during or after construction due to the heavy rain or flooding.

The experiment tests on unsaturated soils have been conducted by many researchers to study the hydraulic collapse behavior of unsaturated soils. Jennings and Burland (1962) conducted the one-dimensional compression and subsequent soaking tests on air dried silt. Air dried silt could stay in a looser region above the compression line of saturated sample during the compression process, then, its void ratio decreased approaching to the compression line of the saturated sample due to soaking under constant mean net stress condition. Tadepalli and Fredlund (1991) conducted soaking tests in the Oedometer ring on Indian Head silt. They found that an amount of volumetric collapse decreased with the increase in initial dry density and initial water content, and the variation in suction had a dominant effect on the volumetric collapse behavior of unsaturated soils. Honda (2000) conducted the one-dimensional compression tests under constant suction on Catapol clay. The unsaturated samples initially showed relatively higher stiffness and retained a larger void ratio compared with the saturated one under same stress level. However, the unsaturated samples exhibited significant compression resulted in the increase in the degree of saturation although the suction was kept constant. Kato and Kawai (2000) conducted a series of soaking tests under isotropic and anisotropic conditions, and repeated soaking tests under anisotropic condition by using triaxial apparatus on compacted clay. They concluded that the change in void ratio had a linear relationship with the change in water content during soaking under both isotropic and anisotropic conditions, and there was no hydraulic collapse due to the repeated soaking under anisotropic condition. Sun et al. (2007) conducted a series of soaking tests under isotropic and anisotropic conditions on unsaturated compacted clay with different densities and stress conditions by using triaxial apparatus. The experiment results show that the density and stress states affected the hydraulic collapse behavior of unsaturated soils under both isotropic and anisotropic conditions, while the soil water characteristic curve was only influenced by the density. Milatz et al. (2016)

conducted cyclic drying-wetting tests under oedometric stress conditions on medium coarse sand with different densities to study the hydraulic collapse behavior. The experiment results of all samples show that the significant hydraulic collapse was observed in the first soaking, then, it became smaller in the repeated soaking. However, conducting the experiment tests to study the hydraulic collapse behavior of unsaturated soils is quite complicated and time consuming especially at a wide range of density and stress conditions. Thus, the constitutive model needs to be developed for predicting the hydraulic collapse behavior.

The main objectives of this chapter are as follows: (1) to extend the simple elastoplastic constitutive model proposed by Kikumoto et al. (2010) to three-dimensional problems in order to predict the hydraulic collapse behavior of unsaturated soils; (2) to present a parametric study of the hydraulic collapse behavior of unsaturated soils under isotropic and anisotropic conditions using the above-mentioned model; (3) to propose the effects of soaking history on the hydraulic collapse behavior of unsaturated soils; and (4) to propose the soaking induced instability of unsaturated soils.

3.1 MODEL VALIDATION FOR THE HYDRAULIC COLLAPSE BEHAVIOR OF UNSATURATED SOILS

To verify the validity of the constitutive elastoplastic model proposed in Chapter 2, three series of the comparison between simulation and experimental results are presented. First is a series of simulation of one-dimensional compression test under constant suction on Catapol clay (Honda, 2000) which demonstrates the compression behavior of unsaturated soils. The other series are the simulation of soaking tests under isotropic and anisotropic conditions on Pearl clay (Sun et al., 2007) for describing the hydraulic collapse behavior of unsaturated soils. The model parameters of Catapol clay and Pearl clay are shown in Table 3.1 for stress-strain characteristics and Table 3.2 for soil-water characteristic curves.

3.1.1 One-dimensional compression test under constant suction

Honda (2000) conducted a series of one-dimensional compression tests under constant suction on Catapol clay at various suction pressures and densities to investigate the compression behavior of unsaturated soils. In the simulation, the saturated sample (s = 0 kPa) with the initial void ratio of 1.137 under the mean net stress of 5 kPa and the unsaturated samples with the initial suctions of 73.5, 147 and 294 kPa under the mean net stress of 10 kPa had been set as the initial conditions, and then one-dimensional compression tests were carried out under constant suction

(exhausted air and drained water conditions) until the vertical net stress reaching to 2450 kPa (as shown in Figure 3.1). The initial void ratios of the unsaturated samples are shown in Figure 3.2. Finally, the experimental results and the corresponding simulation results were compared (i.e., the relationship between vertical net stress and void ratio as shown in Figure 3.2a; the relationship between vertical net stress and degree of saturation as shown in Figure 3.2b).

Table 3.1 Parameters of Catapol clay and Pearl clay for stress–strain characteristics

Parameters	Catapol Clay	Pearl Clay	Descriptions
λ	0.140	0.100	Compression index
κ	0.010	0.001	Swelling index
M	1.1	1.1	Stress ratio in critical state
ν_{e}	0.2	0.2	Poisson's ratio
N	1.00	1.20	Reference specific volume on the state boundary surface under $p'' = p_{\mathrm{a}}$, $q = 0$, and $S_{\mathrm{r}} = 1$
ω	100.0	100.0	Effect of density
ψ	0.65	0.60	Effect of S_{r} on the position of the state boundary surface

Table 3.2 Parameters of Catapol clay and Pearl clay for water retention curves

Parameters	Catapol Clay	Pearl Clay	Descriptions
$S_{\max}$	1.00	1.00	Parameters for main wetting and drying curves described by van Genuchten's SWCC equation
$S_{\min}$	0.15	0.10	
α^{d} (1/kPa)	0.01	0.03	
α^{w} (1/kPa)	0.04	0.10	
n	1.80	1.50	
m	0.30	0.10	
ξ_{h}	100.0	100.0	Influence of suction histories
ξ_{e}	5.0	14.0	Influence of void ratio
e_{ref}	1.00	1.20	Reference void ratio

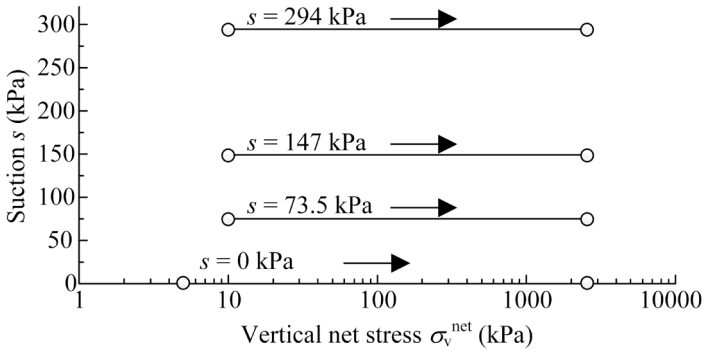

Figure 3.1 Stress paths of one-dimensional compression tests under constant suction

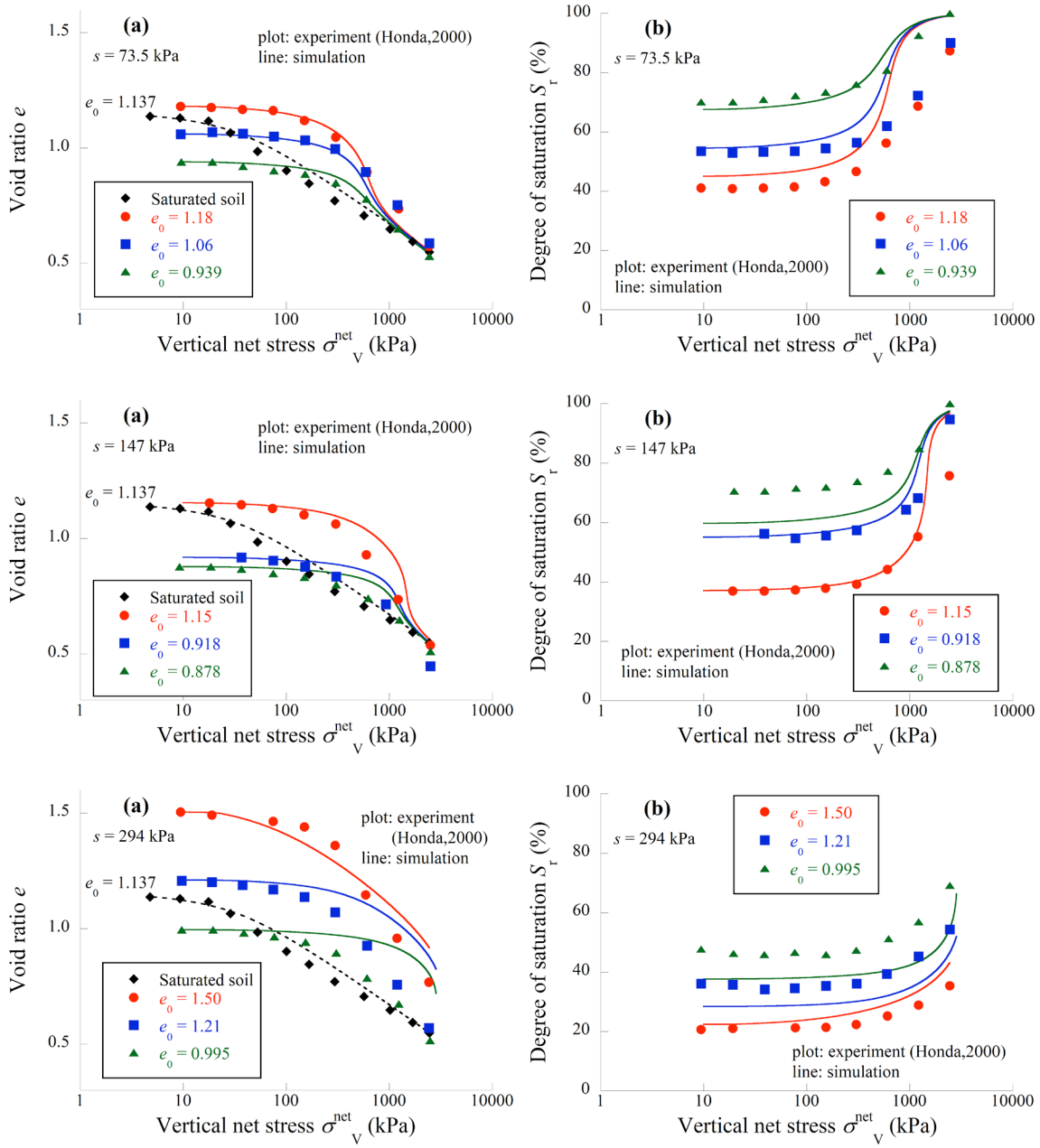

Figure 3.2 Comparison between the simulation results and the experimental results of one-dimensional compression tests under constant suction

The comparison between the simulation results and the experimental results shows that the proposed model precisely describes the compression behavior under constant suction of unsaturated soil at a wide range of suction pressures and densities. Figure 3.2a shows the compression lines during compression tests under constant suction. It is indicated that the unsaturated samples (see the red lines) initially exhibited relatively high stiffness which they could stay in a looser state comparing with the saturated samples (see the black broken line). This compression behavior could reproduce in the simulation by the proposed concept that the state

boundary surface shifts upward from the saturated state owing to the decrease in the degree of saturation. Then, the unsaturated samples showed a significant compression at a certain stress level which finally approached to the compression line of the saturated soil with the increase in degree of saturation. This increase in degree of saturation during compression process under constant suction (as shown in Figure 3.2b) was caused by the volumetric compression which were successfully predicted by using the modified suction in the proposed SWCC model as the modified suction decreases with a decrease in the void ratio though the suction remains constant. Then, this increase in the degree of saturation led to the downward movement of state boundary surface which finally approached to the saturated state.

It seems reasonable to conclude that the unsaturated soils having higher suction and lower degree of saturation show stiffer behavior. However, the stiffness of unsaturated soils is not only influenced by the suction and the degree of saturation but also by the density. Figure 3.2b shows that samples with higher initial density (i.e. lower void ratio) had higher initial degree of saturation under the same suction pressure. In the proposed SWCC model, the denser soils retain higher degree of saturation under the same suction conditions by implementing the modified suction. Therefore, the variation of the compression lines from the unsaturated state to the saturated state of the denser samples are also less than that of the looser samples under the same suction condition as the movement of the state boundary surface depends on the degree of saturation. Figures 3.2a shows that although denser samples had higher degree of saturation, the stiffness of denser samples (see the green lines) were higher than that of the looser samples (see the red lines) under the same suction condition.

3.1.2 Soaking tests under isotropic conditions

Sun et al. (2007) conducted a series of isotropic consolidation tests under constant suction and subsequent soaking tests under constant mean net stress on Pearl clay with different stress levels and densities to study the soaking induced collapse behavior of unsaturated soils under isotropic conditions. In the simulation, unsaturated samples with average void ratio of 1.36, 1.28, 1.17 and 1.05 had been consolidated from mean net stress of 20 kPa to the prescribed values (20, 49, 98, 196, 392, 588 kPa) under constant suction of 147 kPa, and samples were finally soaked by decreasing suction to 0 kPa under constant mean net stress. Stress paths of the simulation are shown in Figure 3.3.

Figure 3.4 shows the experimental results and the corresponding simulation results of isotropic consolidation test under constant suction and subsequent soaking test. It demonstrates

that the proposed model is able to capture the typical soaking induced collapse behavior under isotropic conditions of unsaturated soils. The compression behavior of unsaturated soils obtained from isotropic consolidation process under constant suction were same as above discussion in subject 3.1.1, which the compression lines of unsaturated samples could stay in a looser state comparing with the saturated samples and finally converged to the compression lines of saturated samples conforming to the increase in mean net stress. In the soaking process, the void ratio of unsaturated soils (s = 147 kPa) compressed during soaking process under constant mean net stress condition and finally approached to the compression lines of saturated samples (s = 0 kPa). This soaking induced collapse behavior can be reproduced from the proposed concept that the state boundary surface shifts downward owing to the increase in the degree of saturation which finally approaches to the saturated state. The density also influences the hydraulic collapse behavior. It is seen that an amount of volumetric compression during soaking process of denser sample was less than that of looser samples at the same mean net stress. This is because the denser samples had lower degree of saturation comparing with the looser samples under the same suction and mean net stress conditions. Therefore, the movement of the state boundary surface from the unsaturated state to the saturated state, which depends on the degree of saturation, was also smaller.

Figure 3.5 shows the magnitude of volumetric strains observed during soaking process at different stress levels and densities. The comparison between the simulation results and the experimental results shows that the proposed model properly predicts the magnitude of the hydraulic collapse considering the effects of confining stress and density, and can describe the soaking induced expansion of heavily over consolidated samples observed in the experimental results (see e_0 = 1.05).

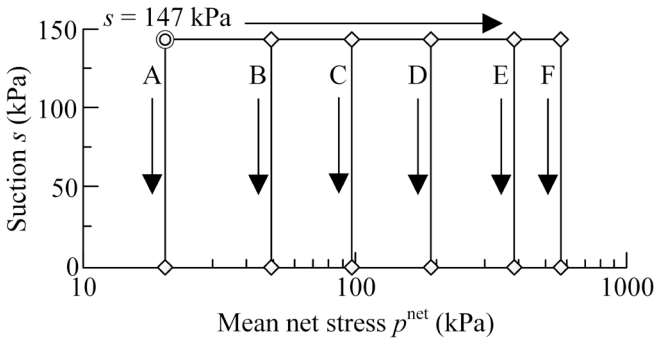

(A) p^{net} = 20 kPa, (B) p^{net} = 49 kPa, (C) p^{net} = 98 kPa,
(D) p^{net} = 196 kPa, (E) p^{net} = 392 kPa, (F) p^{net} = 588 kPa

Figure 3.3 Stress paths of isotropic consolidation tests under constant suction and subsequent soaking tests under isotropic conditions

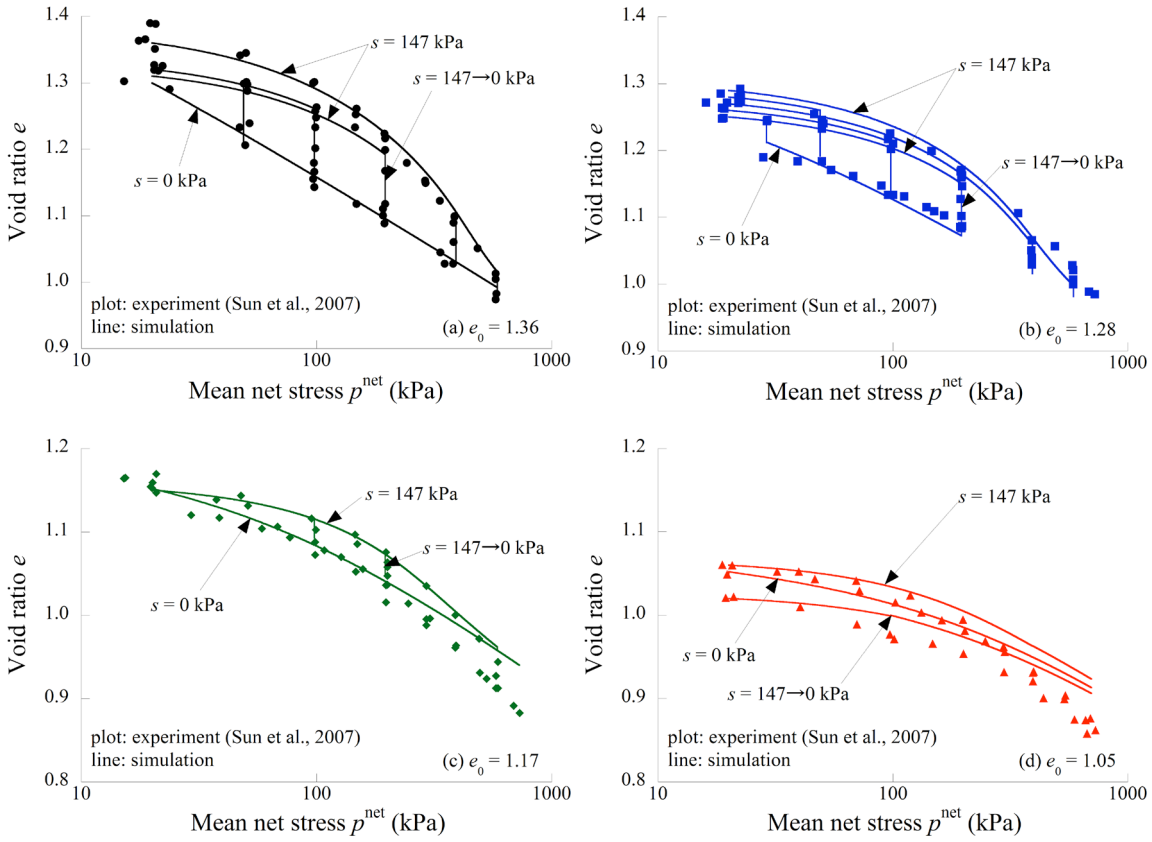

Figure 3.4 Comparison between the simulation results and the experimental results of isotropic consolidation tests under constant suction and subsequent soaking tests under isotropic conditions

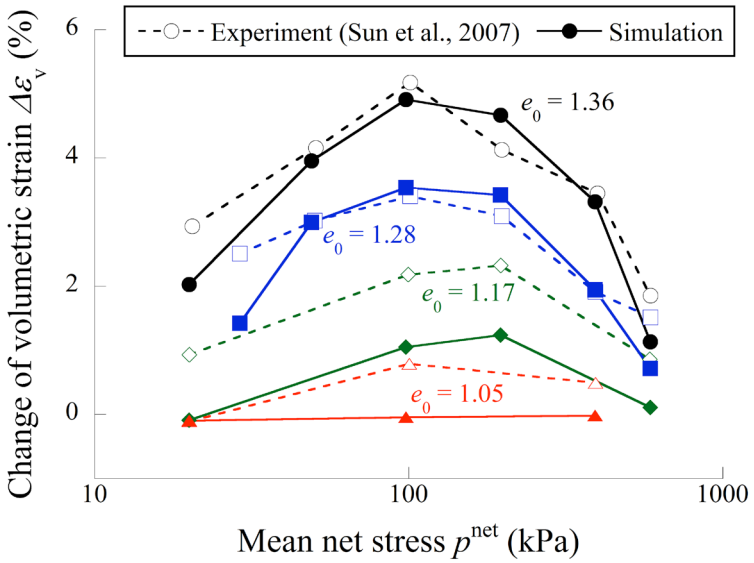

Figure 3.5 Change of volumetric strain due to soaking process at different mean net stress and density

3.1.3 Soaking tests under anisotropic conditions

Sun et al. (2007) performed a series of triaxial compression tests under constant suction and subsequent soaking tests on Pearl clay with different stress ratios and densities to study the soaking induced collapse behavior of unsaturated soils under anisotropic conditions. In the simulation, the samples with different initial void ratio (as shown in Figures 7 and 8) had been firstly consolidated from mean net stress of 20 kPa to 196 kPa under constant suction of 147 kPa. The triaxial compression tests under constant suction and constant mean net stress were, then, carried out to the prescribed principal stress ratio *R* of 1.5 and 2. Principal total stress ratio *R* is the ratio of the total axial stress σ_a to the total radial stress σ_r in triaxial compression test ($R = \sigma_a/\sigma_r$). After shearing, the samples were soaked by decreasing suction to 0 kPa while the principal stress ratio *R* and mean net stress are kept constant. Finally, triaxial compression tests under constant mean net stress at suction of 0 kPa were performed again until failure. Stress paths of the simulation are shown in Figure 3.6.

The experimental results and the corresponding simulation results are shown in Figures 3.7 to 3.9. Figure 3.7 shows the relationships between principal stress ratio *R* and axial strain, while Figure 3.8 shows the relationships between volumetric strain and axial strain. Figure 3.9a and 3.9b show the relationships between volumetric strain and initial void ratio, and between axial strain and initial void ratio, respectively. It can be seen from these figures that the effects of principal stress ratio *R* and density on the soaking induced collapse behavior of unsaturated soil under anisotropic conditions reported by sun et al. (2007) were well represented by the proposed model.

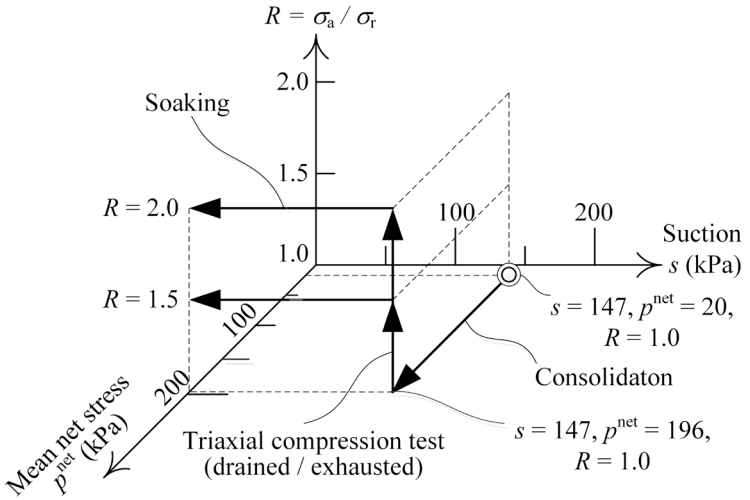

Figure 3.6 Stress paths of triaxial compression tests under constant suction and mean net stress and subsequent soaking tests under anisotropic conditions

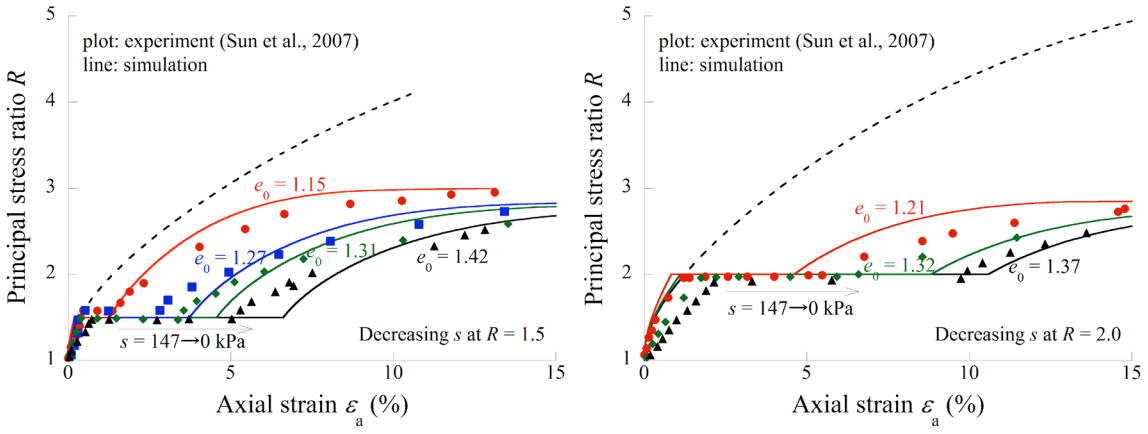

Figure 3.7 Comparison between the simulation results and the experimental results of triaxial compression tests under constant suction and subsequent soaking tests under anisotropic conditions

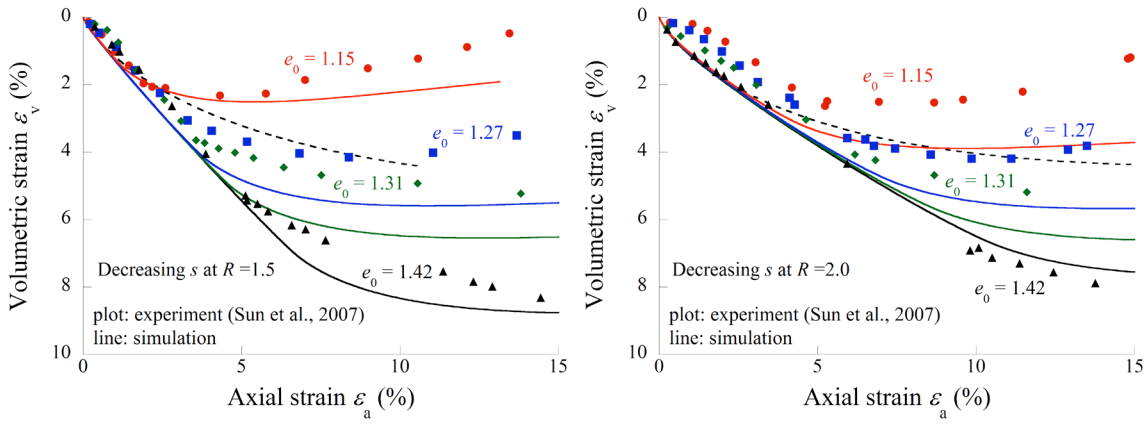

Figure 3.8 The relationships between volumetric and axial strains of triaxial compression tests under constant suction and subsequent soaking tests under anisotropic conditions

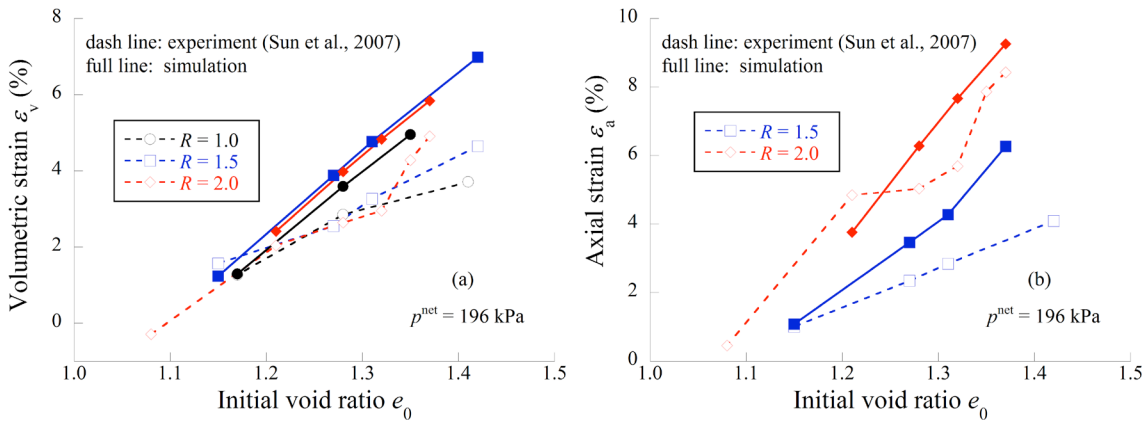

Figure 3.9 The effects of principal stress ratio *R* and initial void ratio e_0 on the volumetric and axial strains due to soaking under anisotropic conditions

Figure 3.7 shows that the principal stress ratio *R* had the significant effect on the collapse behavior of unsaturated samples. The unsaturated samples, subjected to the higher principal stress ratio *R*, had a larger induced axial strain due to soaking process. This is because the samples, subjected to the higher principal stress ratio *R* from shearing process, had higher initial stress ratio (q/p'') at the beginning of soaking path as the suction and mean net stress were kept constant during shearing process. In the soaking process, the mean effective stress ($p'' = p_{\text{net}} + sS_{\text{r}}$) of unsaturated samples decreased due to the decrease in suction, resulting in the increase in the stress ratio (q/p'') as principal stress ratio *R* and mean net stress were kept constant during soaking process. Therefore, the unsaturated samples with higher principal stress ratio *R* experienced higher stress ratio (q/p'') during soaking path, resulted in the larger deviatoric strain as the deviatoric strain is directly proportional to the stress ratio (q/p'').

Another factor affecting the collapse behavior of unsaturated samples is the density. The density does not only influence on the soaking induced collapse behavior of unsaturated soil under isotropic conditions as discussed in the previous section, but also under anisotropic conditions. The induced axial and volumetric strains of the denser samples were less than that of the looser samples due to soaking process under constant principal stress ratio *R* and mean net stress as shown in Figures 3.7 and 3.8. This is because the denser samples had higher initial degree of saturation and mean effective stress (higher strength) than the looser samples under the same suction and mean net stress conditions, which affected to the lower movement of the state boundary surface including the normally consolidated line *NCL* and the critical state line *CSL* from the saturated state in the proposed model. In the beginning of soaking process, the denser unsaturated samples, having higher degree of saturation, had lower positons of the *NCL* and *CSL*. However, after all samples were soaked to the saturated state, the *NCL* and *CSL* of all samples became the same position at this saturated state. This is the reason that the looser samples showed the larger volumetric and axial strains under the same suction reduction conditions compared with the denser samples.

Figure 3.9 shows that the density obviously affected both the volumetric strain and the axial strain, but the principal stress ratio *R* had the significant effect only on the axial strain. The principal stress ratio *R* has much higher impact on the deviatoric strain than the volumetric strain at the low stress ratio, and the axial strain is influenced by the contribution of the volumetric strain and the deviatoric strain. This is the reason that the principal stress ratio *R* influenced significantly only on the axial strain in this simulation. The density has the direct effect on the strength of unsaturated soils, therefore, it had the effects on both of volumetric and axial strains.

3.2 PARAMETRIC STUDY OF THE HYDRAULIC COLLAPSE BEHAVIOR OF UNSATURATED SOILS

A series of simulations of soaking tests under isotropic and anisotropic conditions was performed on Pearl clay, used to validate the proposed model, to provide the typical hydraulic collapse behavior of unsaturated soils under a wide range of densities and stress conditions which it is difficult to conduct the experiment tests. Moreover, the effects of soaking history on the hydraulic collapse behavior and the soaking induced instability of unsaturated soils are explained. The parameters of Pearl clay for stress-strain characteristics and soil-water characteristic curves are shown in Table 3.1 and 3.2, respectively.

3.2.1 A parametric study of the hydraulic collapse behavior of unsaturated soils under isotropic condition

A series of simulations of isotropic consolidation tests under constant suction and subsequent soaking tests was performed on Pearl clay to study the effects of density and mean net stress on the hydraulic collapse behavior of unsaturated soils under isotropic condition. In the simulation, the unsaturated samples had been firstly set to the prescribed void ratio (initial void ratio: 1.10 to 1.50) at the suction of 147 kPa and mean net stress of 20 kPa. Each sample was, then, consolidated to the prescribed mean net stress varying from 20 to 600 kPa under constant suction of 147 kPa, and was finally saturated by decreasing suction to 0 kPa (soaking process) under constant mean net stress varying from 20 to 600 kPa. Stress paths of the simulation are shown in Figure 3.10. The results of a series of simulations are shown in Figures 3.11 (3D space) and Figure 3.12 (2D space) for simple interpretation. In the simulation results, volumetric strain is the change of volumetric strain due to the soaking process; mean net stress is the constant mean net stress during the soaking process; and void ratio is the initial void ratio before conducting the consolidation process.

The simulation results show that density and mean net stress have the effects on the hydraulic collapse behavior under isotropic conditions as reported by Sun et al. (2007). The change of volumetric strain due to soaking depends directly on the void ratio. The denser unsaturated soils have lower hydraulic collapse potential under the same stress conditions, and the highly over consolidated soils are able to expand due to soaking. However, the mean net stress does not show direct variation to the hydraulic collapse potential, i.e., the change of volumetric strain due to soaking increases as the mean net stress increases until reaching to the certain mean net stress level, then, the hydraulic collapse potential decreases as the mean net stress increases.

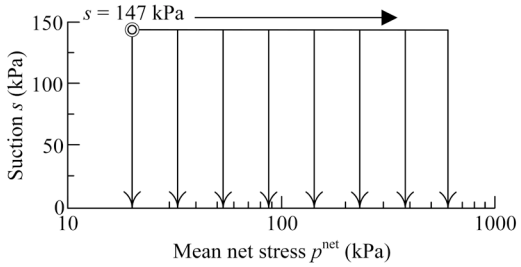

Figure 3.10 Stress paths for a parametric study of the hydraulic collapse behavior of unsaturated soils under isotropic condition

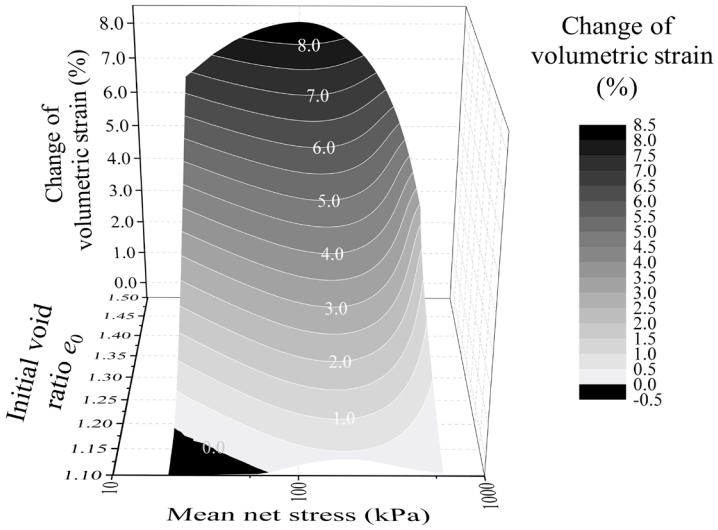

Figure 3.11 Three-dimensional surface of the hydraulic collapse behavior under isotropic condition: effects of density and mean net stress (first soaking paths)

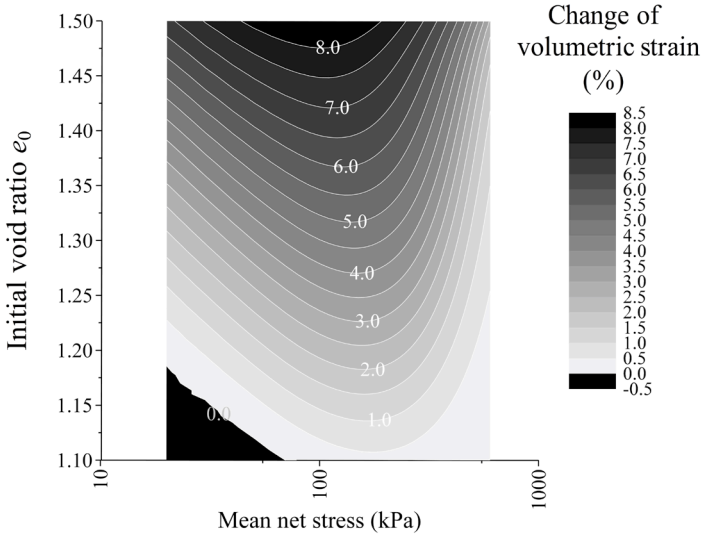

Figure 3.12 Effects of density and mean net stress on the hydraulic collapse behavior under isotropic condition (first soaking paths)

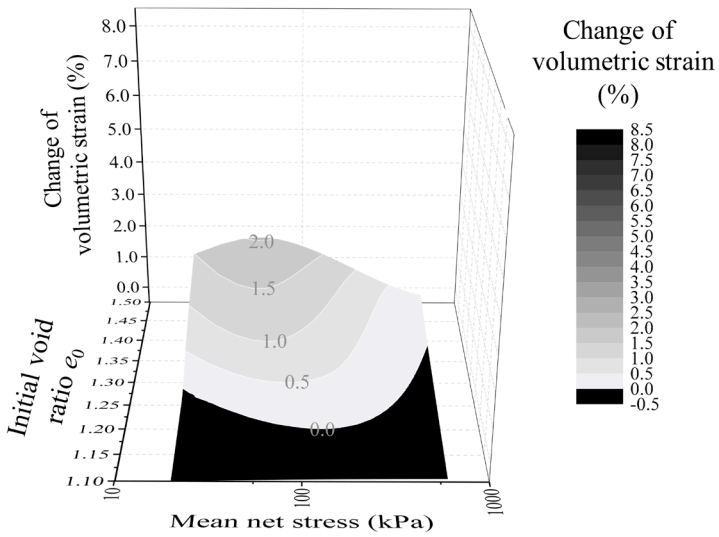

Figure 3.13 Three-dimensional surface of the repeated hydraulic collapse behavior under isotropic condition: effects of density and mean net stress (second soaking paths)

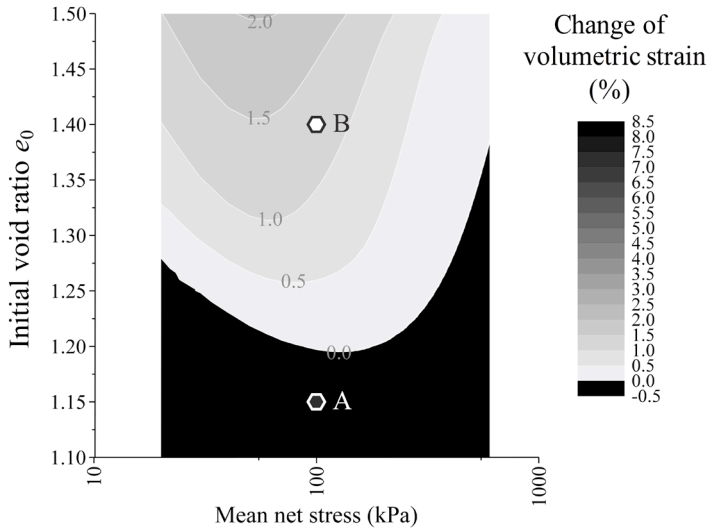

Figure 3.14 Effects of density and mean net stress on the hydraulic collapse behavior under isotropic condition (second soaking paths)

Moreover, the saturated samples at the end of the first soaking process were again increased the suction pressures to 147 kPa (drying process), and then were decreased the suction pressures to 0 kPa (second soaking process) to study the effect of soaking history on the hydraulic collapse behavior of unsaturated soils under isotropic conditions. The simulation results of second soaking test are shown in Figure 3.13 (3D space) and Figure 3.14 (2D space) for simple interpretation. In the simulation results, volumetric strain is the change of volumetric strain due to the second soaking process; mean net stress is the constant mean net stress during the second

soaking process; and void ratio is the initial void ratio before conducting the consolidation process.

The simulation results show that the hydraulic collapse potential of the unsaturated soils due to the second soaking test is much less than that of the first soaking test, and the unsaturated soils also show higher potential of soaking induced expansion due to the second soaking test as the volumetric expansion can be seen at a wider range of void ratio and mean net stress comparing with the first soaking results (see Figures 3.12 and 3.14). The reason for this is that the samples became over consolidated soils after the first hydraulic collapse. Therefore, after samples had been dried by increasing suction with the same initial value of 147 kPa, the degree of saturation of these samples at the beginning of second soaking process were higher than that of the first soaking process. In this case, samples with low initial void ratio still had high degree of saturation at the beginning of second soaking process, thus, they exhibited like saturated soil under unloading condition during the second soaking process. This is the reason that the unsaturated soils show higher potential of soaking induced expansion due to the second soaking in the simulation. Figure 3.15 shows the examples of the simulation results obtained from Figure 3.14 at the initial void ratio of 1.15 (point A) and 1.40 (point B) under mean net stress of 100 kPa. Figure 3.15a shows that the unsaturated sample with initial void ratio of 1.15 had been compressed by the first soaking, however, it showed the expansion behavior due to the second soaking as it became highly over consolidated soil with high degree of saturation of 92.8% at the initial state of the second soaking process. While the sample with initial void ratio of 1.40 had higher void ratio and lower degree of saturation of 83.8% at the initial state of the second soaking process as shown in Figure 3.15b. This effect of soaking history on the hydraulic collapse behavior of unsaturated soils as shown in the simulation results could be observed in the experiment tests as following examples. Rao and Revanasiddappa (2006) indicated that the repeated wetting-drying induced the increase in the degree of expansiveness and the decrease in hydraulic collapse potential of compacted residual soil. Milatz et al. (2016) conducted cyclic drying-wetting tests under oedometric stress conditions on medium coarse sand, which the experiment results showed the significant decrease in the hydraulic collapse potential due to the repeated soaking.

A parametric study of the hydraulic collapse behavior of unsaturated soils under isotropic condition provides the typical hydraulic collapse behavior of unsaturated soils under a wide range of density and mean net stress conditions. The effect of soaking history on the hydraulic collapse behavior under isotropic condition of unsaturated soils is also presented.

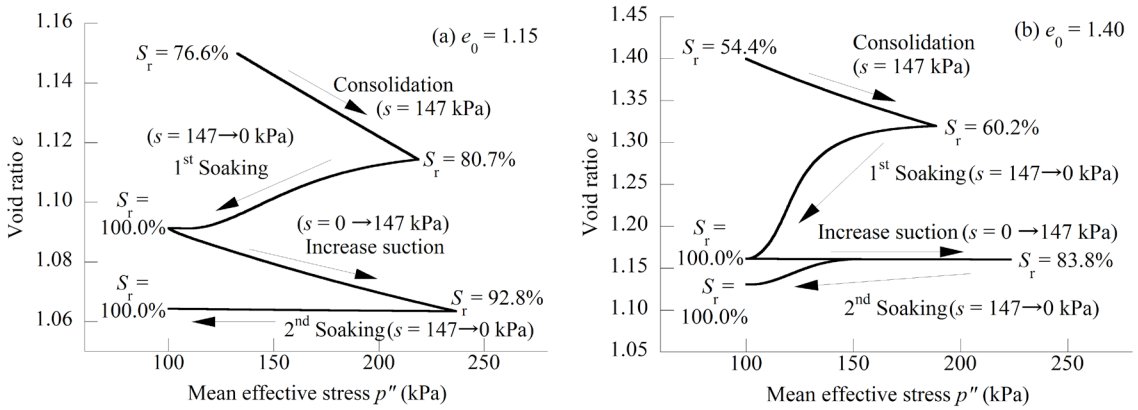

Figure 3.15 Simulation results of repeated soaking tests under mean net stress of 100 kPa on the unsaturated samples: (a) e_0 = 1.15 and (b) e_0 = 1.40

3.2.2 A parametric study of the hydraulic collapse behavior of unsaturated soils under anisotropic condition

A series of simulations of triaxial compression tests under constant suction and mean net stress, and subsequent soaking tests was performed on Pearl clay to study the effects of density and deviatoric stress on the hydraulic collapse behavior of unsaturated soils under anisotropic conditions. In the simulation, the unsaturated samples with the initial void ratio varying from 1.10 to 1.50 had been firstly consolidated from the mean net stress of 20 kPa to 196 kPa under constant suction of 147 kPa. The triaxial compression tests under constant suction and constant mean net stress were, then, carried out to the prescribed deviatoric stress varying from 0 to 250 kPa. After shearing, the samples were finally saturated by decreasing suction to 0 kPa while the deviatoric stress and mean net stress were kept constant. Stress paths of the simulation are shown in Figure 3.16. The results of a series of simulations of triaxial compression tests under constant suction and mean net stress, and subsequent soaking tests are shown in Figures 3.17 to 3.21. In the simulation results, deviatoric stress is the constant deviatoric stress during soaking process; void ratio is the initial void ratio before conducting the consolidation process; degree of saturation and hardening parameter are the final values after soaking process; and deviatoric strain and volumetric strain are the final values obtained from soaking process.

Figure 3.17 shows that deviatoric stress and density had the significant effect on the soaking induced deviatoric strain under anisotropic condition. The soaking induced deviatoric strain increased as deviatoric stress and void ratio increased under the same initial mean net stress and suction conditions. However, density showed higher influence on the soaking induced volumetric strain under anisotropic condition than that of deviatoric stress as shown in Figure 3.18.

The looser samples had a larger induced volumetric strain due to soaking under the same deviatoric stress condition. An increase in deviatoric stress resulted in a decrease in soaking induced volumetric strain under the same initial void ratio, however, this tendency could be more clearly seen at the higher initial void ratio. This decrease in soaking induced volumetric strain under anisotropic condition was caused by the volumetric dilation resulted from an increase in stress ratio due to a decrease in mean effective stress which deviatoric stress was kept constant.

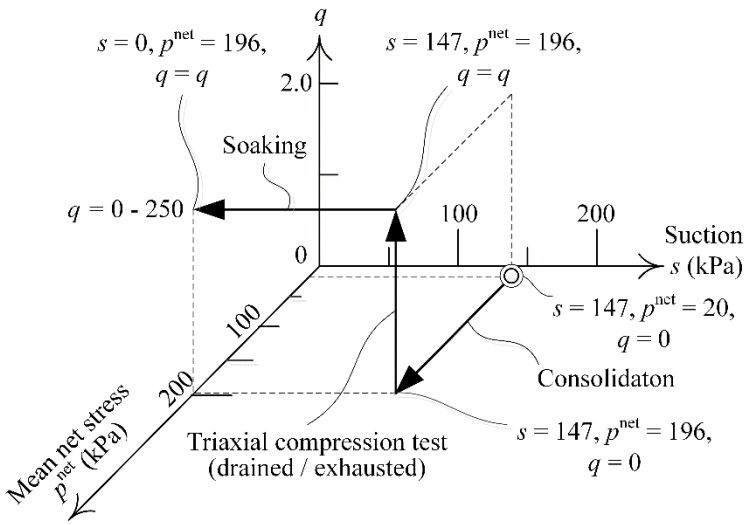

Figure 3.16 Stress paths for a parametric study of the hydraulic collapse behavior of unsaturated soils under anisotropic condition

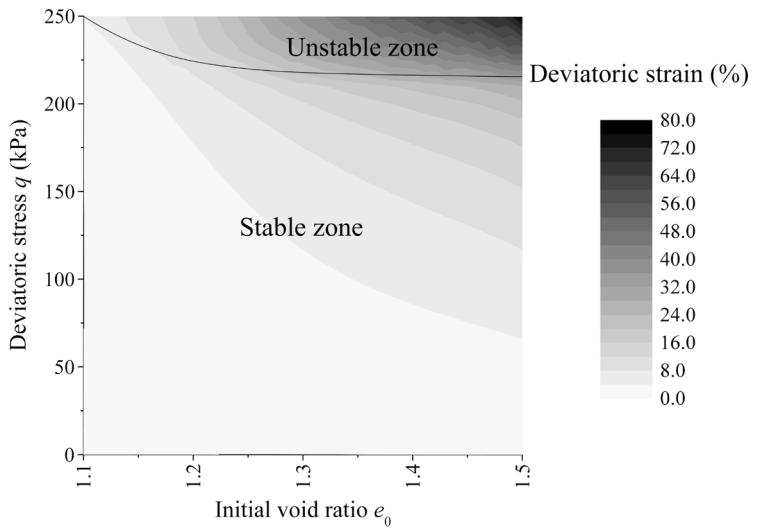

Figure 3.17 The effects of density and deviatoric stress on deviatoric strain obtained during first soaking under anisotropic condition (under constant p^{net} of 196 kPa)

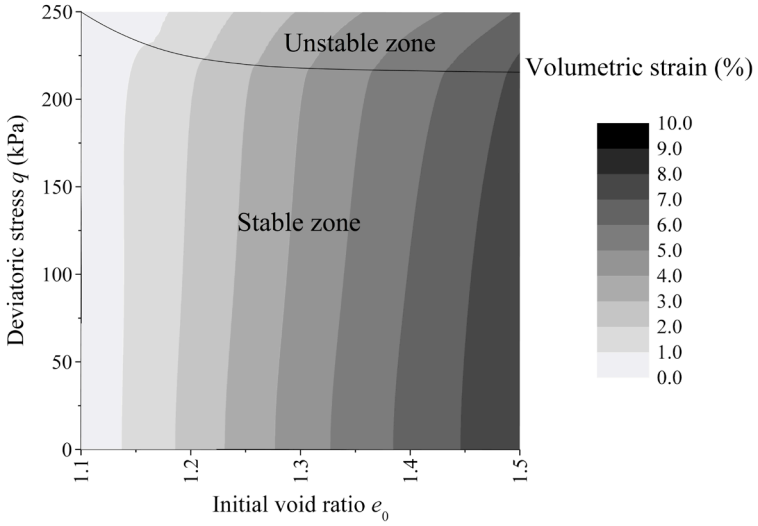

Figure 3.18 The effects of density and deviatoric stress on volumetric strain obtained during first soaking under anisotropic condition (under constant p^{net} of 196 kPa)

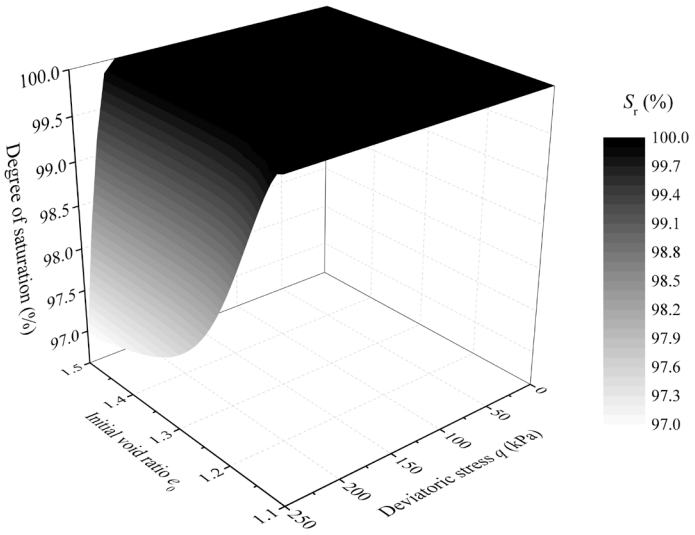

Figure 3.19 Three-dimensional surface of the effects of density and deviatoric stress on degree of saturation obtained after first soaking under anisotropic condition (under constant p^{net} of 196 kPa)

Figure 3.19 shows the final degree of saturation due to soaking test under anisotropic condition. The final degree of saturation of the unsaturated samples subjected to the high value of deviatoric stress could not increase to 100% in the simulation. This is because these unsaturated samples failed during soaking under anisotropic condition in the simulation. This failure can be named as the soaking induced instability of unsaturated soils. In the proposed model, the hardening parameter H ,as shown in Equation (39), can be used as the determination of the instability or the

failure in the simulations. It is usually known that we could not simulate the softening behavior of overconsolidated soil (see dash line in Figure 2.6) after the peak strength under stress controlled loading condition. In the simulation of soaking tests under anisotropic condition, the stress ratio η increased in a similar manner as the simple stress-strain relationship of soil observed from the stress controlled loading tests, i.e., the mean effective stress ($p'' = p_{\text{net}} + sS_{\text{r}}$) of unsaturated samples decreased due to the decrease in suction resulting in the increase in the stress ratio ($\eta = q/p''$) as deviatoric stress q and mean net stress p_{net} were kept constant during soaking process. Therefore, suction could not be further decreased after the stress ratio η reached to the peak strength ($H = 0$) because the simulation started failing at this point. This is the reason that the final degree of saturation of the samples, failed in the simulation, could not increase to 100%. Figure 3.20 shows the zone which the simulation of soaking test under anisotropic condition was successfully simulated (S_{r} = 100%) and the zone which had the instability in the simulation (S_{r} < 100%), called the stable zone and the unstable zone, respectively. Figure 3.21 shows the final values of hardening parameter H obtained after soaking process. The final values of hardening parameter decrease with an increase in deviatoric stress which converged to 0 when arrived the unstable zone at the high deviatoric stress. This almost zero values of hardening parameter mean that the calculations started failing at this state as mentioned above. Figures 3.22 shows the examples of the simulation results of soaking under anisotropic condition at the initial void ratio of 1.30 under constant q of 150 kPa (simulation did not fail, point A) and 240 kPa (simulation failed, point B).

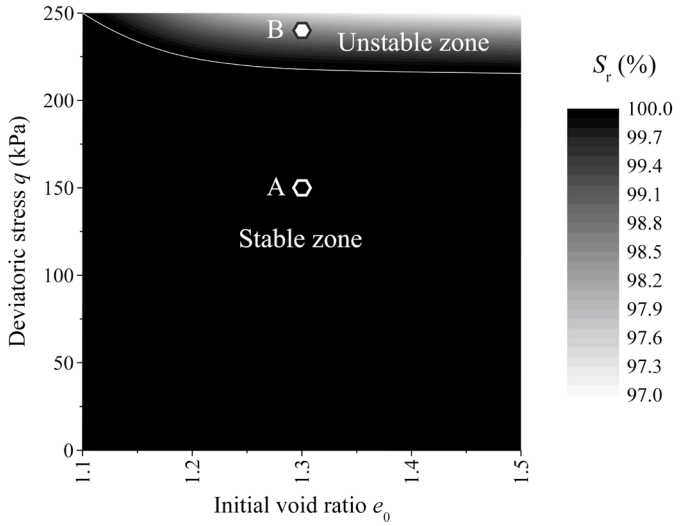

Figure 3.20 The effects of density and deviatoric stress on degree of saturation obtained after first soaking under anisotropic condition (under constant p^{net} of 196 kPa)

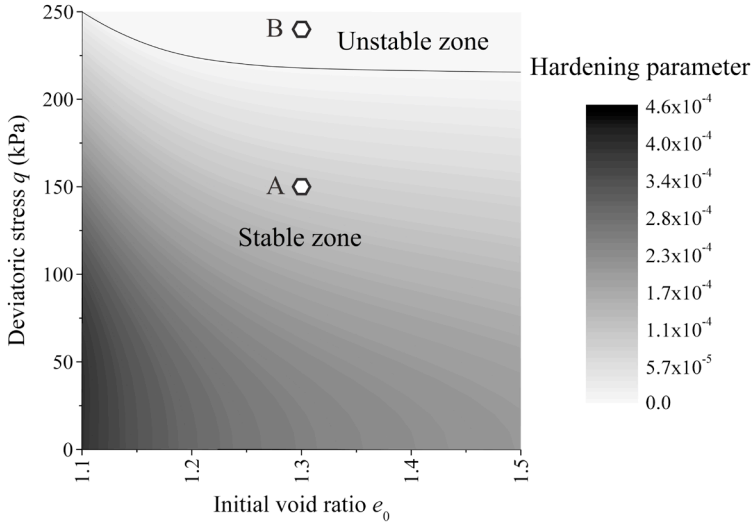

Figure 3.21 The effects of density and deviatoric stress on the hardening parameter obtained after first soaking under anisotropic condition (under constant p^{net} of 196 kPa)

Regarding to the simulation results in the unstable zone, the soaking induced deviatoric strain increased significantly as deviatoric stress increased in the unstable zone as shown in Figure 3.17 and the effect of deviatoric stress on the soaking induced volumetric strain, i.e. the soaking induced volumetric strain decreased as deviatoric stress increased, could be easily recognized as deviatoric stress increased in the unstable zone as shown in Figure 3.18. It can be concluded that the unsaturated samples subjected to the high stress ratio will experience high deviatoric strain, resulted in the failure due to soaking under anisotropic condition. Several examples of the soaking induced instability of unsaturated soils in practice were summarized in the literatures (e.g., Houston et al., 1988; Lawton et al., 1992). Therefore, this parametric study can be used as a reminder in the engineering practice, for example, the embankment or shallow foundation in the area subjected to the high potential of heavy rain or flooding should be more concerned in the engineering design as the embankment or subgrade beneath the shallow foundation may be soaked by the heavy rain or flooding resulting in the failure due to the soaking induced instability under anisotropic condition.

Moreover, the saturated samples at the end of the first soaking process had been dried by increasing suction pressures to 147 kPa (drying process), and were then soaked by decreasing suction pressures to 0 kPa (second soaking process) under constant deviatoric stress and mean net stress to study the effect of soaking history on the hydraulic collapse behavior of unsaturated soils under anisotropic conditions.

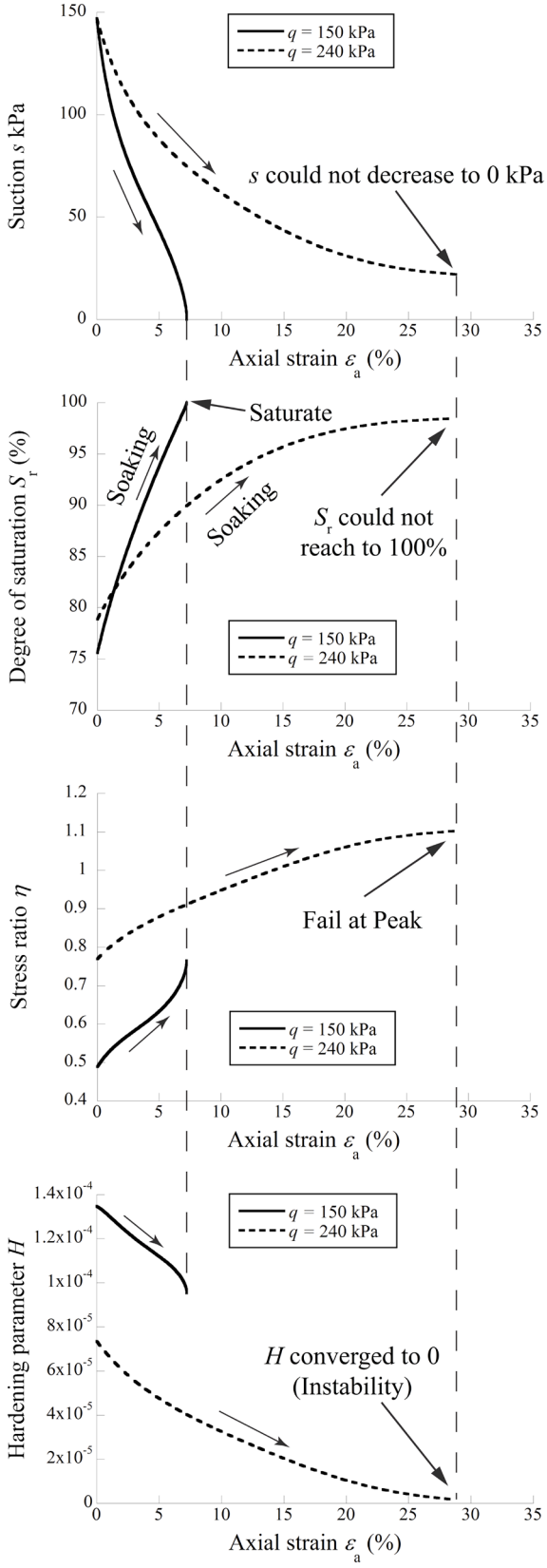

Figure 3.22 Simulation results of soaking under anisotropic condition at the initial void ratio of 1.30 under constant *q*: (a) 150 kPa and (b) 240 kPa

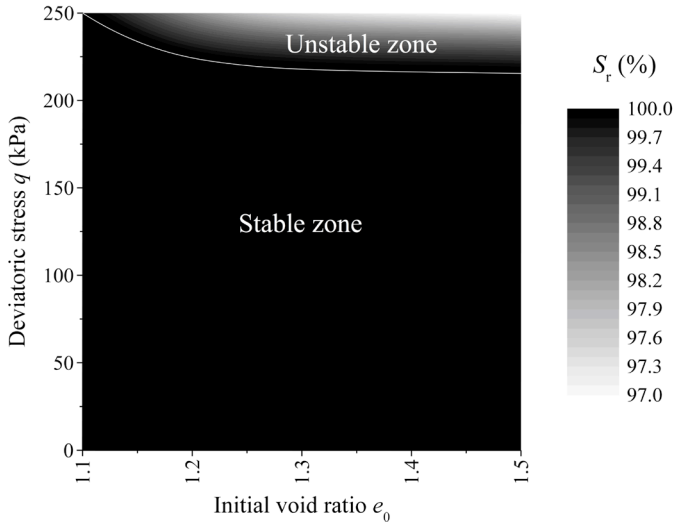

Figure 3.23 The effects of density and deviatoric stress on degree of saturation obtained after second soaking under anisotropic condition (under constant p^{net} of 196 kPa)

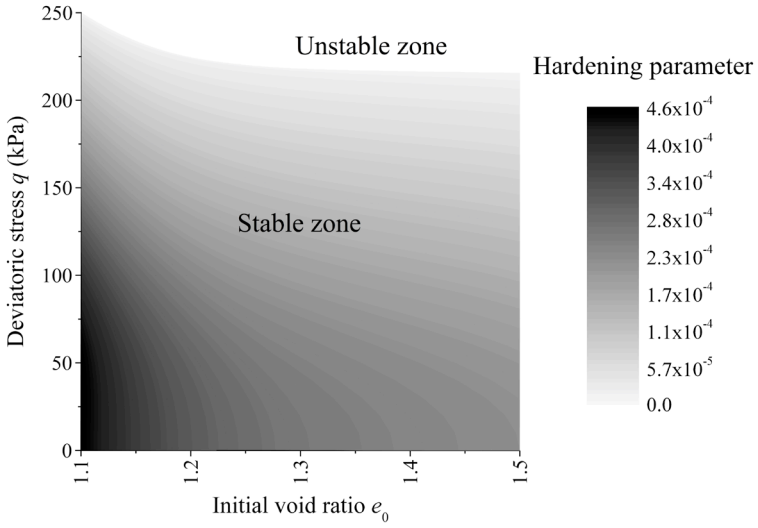

Figure 3.24 The effects of density and deviatoric stress on the hardening parameter obtained after second soaking under anisotropic condition (under constant p^{net} of 196 kPa)

Figure 3.23 shows the final degree of saturation after second soaking process which is exactly same as the results obtained from the first soaking simulation (see Figure 3.20); and the boundary lines between stable zone and unstable zone of both cases also lay exactly in the same position. This is because the simulations in unstable zone had already failed since the first soaking process, and there was no more soaking induced instability after the first soaking process in the stable zone. Therefore, all simulation results after first soaking process in unstable zone are not shown as the simulations had failed since the first soaking process. Figure 3.24 shows the simulation results of hardening parameter after second soaking process. The hardening parameter

after second soaking was higher than that of first soaking, which was an evidence that there was no more soaking induced instability after the first soaking.

Regarding to the effects of soaking history on the deviatoric strain and volumetric strain of unsaturated soils, the soaking induced deviatoric strain obtained from first soaking simulation (see Figure 3.17) was much higher than that of second soaking simulation as shown in Figure 3.25. The soaking induced volumetric strain obtained from first soaking simulation (see Figure 3.18) was also much higher than that of second soaking simulation as shown in Figure 3.26. In addition, the soaking induced expansion behavior could be seen in second soaking simulation at the low initial void ratio as shown in Figure 3.26. This is because the samples became overconsolidated soils after first soaking process as shown in Figure 3.27. Figure 3.27 shows the initial void ratio before conducting first soaking simulation and second soaking simulation. As the samples before conducting first soaking simulation were looser than that of second soaking simulation, therefore, S_{r} of samples before conducting first soaking simulation was lower than that of second soaking simulation because both cases were under same suction of 147 kPa before conducting soaking as shown in Figure 3.28. It can be seen that the dense samples before conducting second soaking tests had high S_{r} which closed to saturated condition, thus, they exhibited like saturated soils under unloading condition during soaking process, which showed expansion behavior.

Figures 3.29 and 3.30 shows the simulation results of deviatoric strain and volumetric strain, respectively, obtained since the beginning of first soaking process until finished second soaking process. Both soaking induced deviatoric strain and volumetric strain were a bit higher than that of first soaking simulation. Therefore, it can be concluded that the significant hydraulic collapse occurred only at the first soaking, and the soaking induced instability occurred only at the first soaking as well. Regarding to the effects of deviatoric stress and initial void ratio on the hydraulic collapse behavior of unsaturated soils under anisotropic condition, the soaking induced deviatoric strain increased as deviatoric stress and initial void ratio increased; and the soaking induced volumetric strain increased as initial void ratio increased and deviatoric stress decreased.

A parametric study of the hydraulic collapse behavior of unsaturated soils under anisotropic condition provides the typical hydraulic collapse behavior of unsaturated soils under a wide range of density and deviatoric stress conditions. The effects of the density and deviatoric stress on the soaking induced deviatoric and volumetric strains under anisotropic condition are presented. Moreover, the soaking induced instability of unsaturated soils which is the failure of the unsaturated soils due to soaking under anisotropic condition and the effects of soaking history on the hydraulic collapse behavior of unsaturated soils under anisotropic condition are proposed.

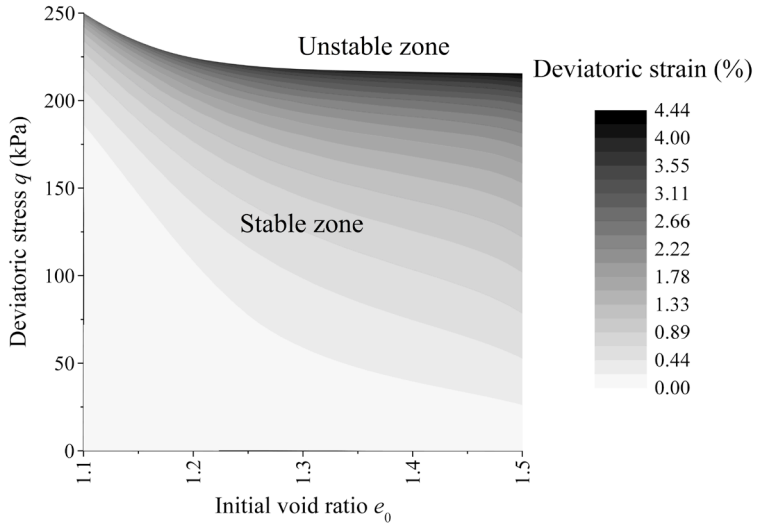

Figure 3.25 The effects of density and deviatoric stress on deviatoric strain obtained during second soaking under anisotropic condition (under constant p^{net} of 196 kPa)

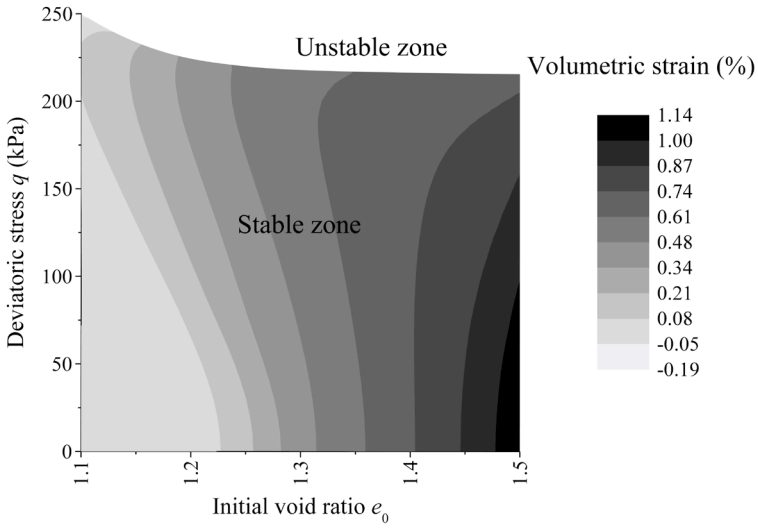

Figure 3.26 The effects of density and deviatoric stress on volumetric strain obtained during second soaking under anisotropic condition (under constant p^{net} of 196 kPa)

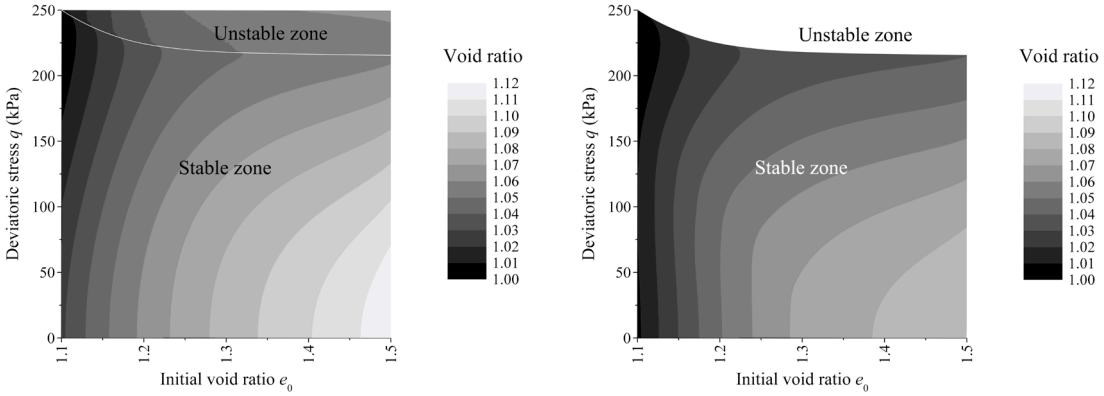

(a) First soaking (b) Second soaking

Figure 3.27 Void ratio before conducting (a) first soaking simulation and (b) second soaking simulation (under constant p^{net} of 196 kPa)

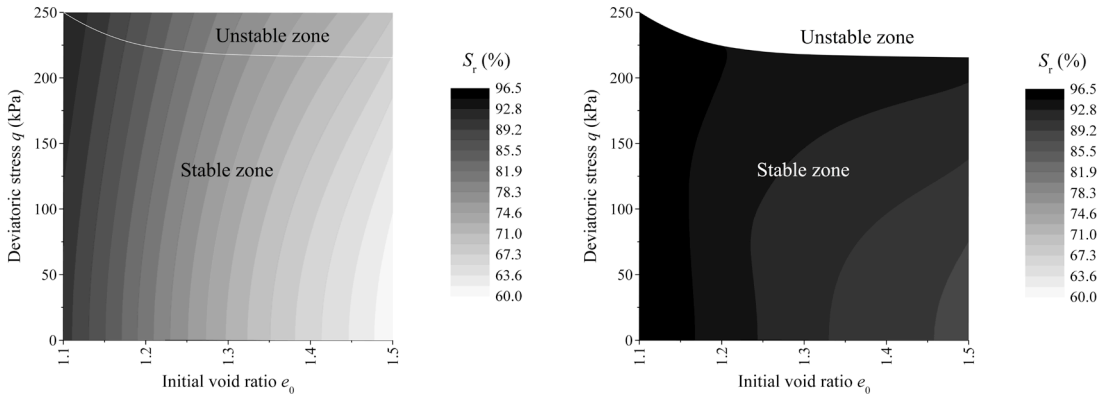

(a) First soaking (b) Second soaking

Figure 3.28 Degree of saturation S_r before conducting (a) first soaking simulation and (b) second soaking simulation (under constant p^{net} of 196 kPa)

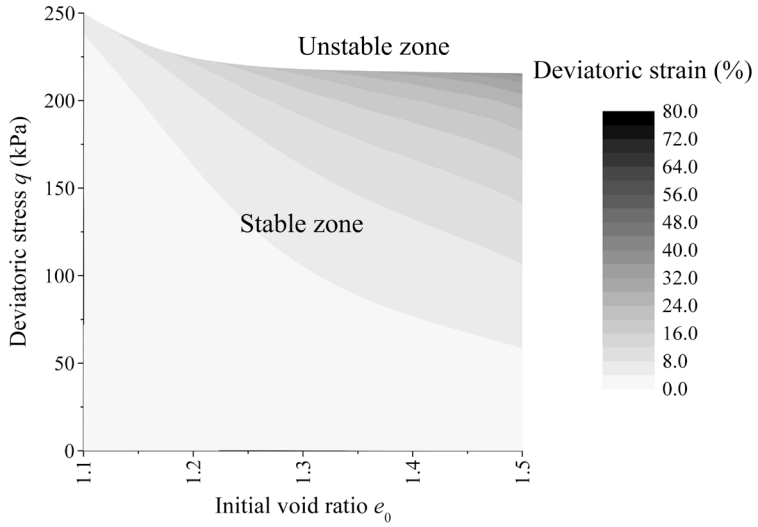

Figure 3.29 The effects of density and deviatoric stress on deviatoric strain obtained since the beginning of first soaking process until finished second soaking process (under constant p^{net} of 196 kPa)

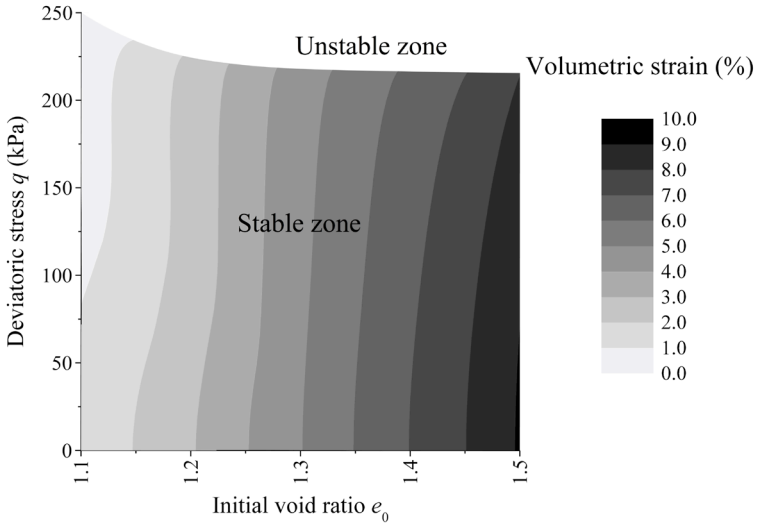

Figure 3.30 The effects of density and deviatoric stress on volumetric strain obtained since the beginning of first soaking process until finished second soaking process (under constant p^{net} of 196 kPa)

3.3 CONCLUSIONS

This chapter presented the validation of the proposed elastoplastic constitutive model for unsaturated soils on the hydraulic collapse behavior of unsaturated soils and a parametric study of the hydraulic collapse behavior of unsaturated soils under isotropic and anisotropic conditions.

The validity of the proposed model was verified through a series of one-dimensional compression test on Catapol clay under constant suction, and a series of soaking tests on Pearl clay under isotropic and anisotropic conditions. The simulation results show that the typical behaviors of unsaturated soils such as the compression behavior, and the soaking induced collapse phenomena under isotropic and anisotropic conditions were suitably described by the proposed model.

A parametric study of the hydraulic collapse behavior induced by soaking under isotropic condition showed that the hydraulic collapse potential decreases with the increase in density which the highly over consolidated soils are able to expand due to soaking. In addition, the hydraulic collapse potential increases as the mean net stress increases until reaching to the certain mean net stress level, then, the hydraulic collapse potential decreases as the mean net stress increases. Moreover, the hydraulic collapse potential decreases significantly due to the repeated drying and wetting, and the repeated drying and wetting also increases the expansion potential of unsaturated soils.

A parametric study of the hydraulic collapse behavior of unsaturated soils under anisotropic condition showed that the soaking induced deviatoric strain and volumetric strain decrease as the density increases, and the soaking induced deviatoric strain increases and the soaking induced volumetric strain decreases as the deviatoric stress increases. Moreover, the effect of soaking under anisotropic condition on deviatoric strain and volumetric strain decreases significantly after unsaturated soils experience first soaking, and the soaking induced volumetric expansion can be found in case of overconsolidated soils with high degree of saturation at the second soaking process. In addition, the soaking induced instability of unsaturated soils which is the failure of the unsaturated soils due to soaking under anisotropic condition is explained.

CHAPTER 4

NUMERICAL STUDY OF THE CYCLIC BEHAVIOR OF UNSATURATED SOILS

Soils are often subjected to cyclic loading under unsaturated conditions in practical situations, such as the deformation of embankments and reclaimed areas during an earthquake. In Japan, the Sanriku-Minami earthquake triggered a landslide in the town of Tsukidate on May 26, 2003. An artificial fill in this disaster area lost its effective confining stress under cyclic loading although the degree of saturation was around 70% (Unno et al., 2006). The landfills along the northeastern shorelines of Tokyo Bay were liquefied because of the Great East Japan Earthquake in 2011, which caused soil subsidence in an area of around 42 km^2 (Konagai et al., 2013). Thus far, several questions have been raised about the liquefaction potential of unsaturated soils.

Recently, many researchers have investigated the cyclic behavior of unsaturated soils by conducting laboratory tests under fully undrained cyclic loading conditions. Ishihara et al. (2004) studied the effects of the relative density and degree of saturation on the undrained behavior of nearly saturated sand through multiple series of monotonic and cyclic triaxial tests. Selim and Burak (2006) conducted a torsional shear test on unsaturated silty clay to explore the small and large strain behavior of unsaturated soils. Okamura and Noguchi (2009) observed the influence of air and suction pressure on the liquefaction resistance of unsaturated soils through a series of cyclic triaxial tests on a fine clean sand and a non-plastic silt under fully undrained conditions. Liu and Xu (2013) studied the effects of the degree of saturation, relative density, and confining pressure on the cyclic behavior of saturated and unsaturated sand by conducting a series of strain-controlled cyclic triaxial tests under fully undrained conditions. Tsukamoto et al. (2014) conducted a series of undrained stress-controlled cyclic triaxial tests on unsaturated sand in order to examine the changes in the cyclic resistance of silty sand with different grain compositions. Further, Unno et al. (2006, 2008, and 2013) conducted a series of strain-controlled cyclic triaxial tests on unsaturated soils under fully undrained conditions in order to study the liquefaction behavior of such soils.

Importantly, the existing experimental studies have revealed that the mean effective stress of an unsaturated soil having a relatively high degree of saturation gradually decreases and such a soil can be finally liquefied in a manner similar to saturated soils. So as to predict the cyclic behavior of unsaturated soils, the coupling effects of mechanical and hydraulic behaviors need to be considered. Over the past decade, many researchers have proposed the coupling of an

elastoplastic constitutive model and a water retention curve model to capture the behavior of unsaturated soils as mentioned in Chapter 2.

The main objectives of this chapter are as follows: (1) to extend the simple elastoplastic model proposed by Kikumoto et al. (2010) to three-dimensional problems in order to predict the liquefaction behavior of unsaturated soils; (2) to present a series of simulations of fully undrained cyclic loading on unsaturated soils using the above-mentioned model; and (3) to propose a standard for the liquefaction resistance of unsaturated soils in relation to the degree of saturation, specific volume, and effective confining pressure.

4.1 MODEL VALIDATION FOR THE CYCLIC BEHAVIOR OF UNSATURATED SOILS

To verify the validity of the constitutive elastoplastic model proposed in Chapter 2, the comparison between simulation and experimental results (Unno et al, 2013) of fully undrained cyclic triaxial tests are presented. All the analyses were performed using the parameters of Tsukidate volcanic sand (non-plastic sand), which has a specific gravity of 2.478 (see Tables 4.1 and 4.2). In the simulation of the cyclic triaxial tests for the calibration of the model parameters and validation of the model, three types of initial shearing states were considered (see Table 4.3). Saturated soil was used in case c-1, while unsaturated soils having different degrees of saturation were considered under varying pore air pressure in cases c-2 and c-3. Then, cyclic shearing, for which the axial strain amplitude was increased every ten cycles as shown in Figure 4.1, was applied to the specimens under the fully undrained conditions at a constant confining pressure.

Table 4.1 Parameters of Tsukidate volcanic sand for stress–strain characteristics

Parameters	Tsukidate volcanic sand	Descriptions
λ	0.123	Compression index
κ	0.022	Swelling index
M	1.5	Stress ratio in critical state
ν_e	0.3	Poisson's ratio
N	1.90	Reference specific volume on the state boundary surface under $p'' = p_a$, $q = 0$, and $S_r = 1$
ω	90.0	Effect of density
ψ	0.90	Effect of S_r on the position of the state boundary surface

Table 4.2 Parameters of Tsukidate volcanic sand for water retention curves

Parameters	Tsukidate volcanic sand	Descriptions
$S_{\max}$	1.0	Parameters for main wetting and drying curves described by van Genuchten's SWCC equation
$S_{\min}$	0.20	
α^{d} (1/kPa)	0.04	
α^{w} (1/kPa)	2.00	
n	1.724	
m	0.42	
ξ_{h}	10.0	Influence of suction histories
ξ_{e}	2.5	Influence of void ratio
e_{ref}	0.90	Reference void ratio

Table 4.3 Initial state of cyclic shearing simulation (Unno et al., 2013)

Case No.	c-1	c-2	c-3
Air pressure u_{a} (kPa)	-	6.0	14.8
Water pressure u_{w} (kPa)	0.0	0.0	0.0
Suction s (kPa)	-	6.0	14.8
Mean net stress p_{net} (kPa)	-	18.6	19.9
Mean effective stress p'' (kPa)	20.8	23.3	30.8

Note: The mean effective stress is calculated on the basis of Bishop's effective stress equation with the effective stress parameter $\chi = S_{\mathrm{r}}$, and the pressure is gauge pressure, which excludes atmospheric pressure (98 kPa).

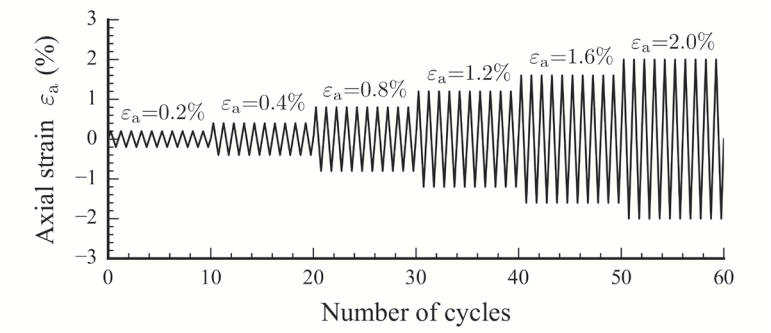

Figure 4.1 Time history of axial strain during cyclic shearing

4.1.1 Definition of fully undrained condition

The fully undrained condition, i.e., unexhausted air and undrained water, is the condition where air and water are unable to drain out of the soil. In other words, the mass of water and air are constant. In order to simulate the unexhausted air condition, we assumed that air is an ideal gas and the temperature is constant. Therefore, Boyle's law, which states that the absolute pressure of a given mass of an ideal gas is inversely proportional to its volume at a constant temperature, can be

used as

$$u_{\mathrm{a}}V_{\mathrm{a}} = \text{constant} \tag{4.1}$$

where u_a is the pore air pressure and V_a is the volume of pore air. As the volume of soil particles, V_s, is constant, we get

$$u_{\mathrm{a}}\frac{V_{\mathrm{a}}}{V_{\mathrm{s}}} = u_{\mathrm{a}}e(1 - S_{\mathrm{r}}) = \text{constant} \tag{4.2}$$

A classical equation for solving problems involving three-phrase relationships (solid, water, and air) can be used to satisfy the undrained water condition as

$$w = \frac{eS_{\mathrm{r}}}{G_{\mathrm{s}}} = \text{constant} \tag{4.3}$$

where w, e, and G_s are the water content, void ratio, and specific gravity of the soil particles, respectively. As G_s is constant, we get

$$eS_{\mathrm{r}} = \text{constant} \tag{4.4}$$

For the detailed procedure of the simulation, please refer to the Appendix A.

4.1.2 The simulations of fully undrained cyclic triaxial tests

The proposed constitutive model and its parameters for stress-strain characteristics (Table 4.1) were first calibrated through undrained cyclic triaxial tests on saturated samples (case c-1), as shown in Figure 4.2. The model captures the gradual increase in the excess pore water pressure and the associated decrease in the mean effective stress, which finally leads to liquefaction after around 30 cycles of shearing. However, the decrease in the mean effective stress observed in the initial shearing cycles is, however, larger in the test. The soil-water characteristic curve and its parameters (Table 4.2) were also calibrated using the water retention test under drying and wetting paths (Unno et al., 2006), as shown in Figure 4.3.

Next, to verify the validity of the proposed model, we conducted a series of simulations of cyclic triaxial tests on unsaturated soils under fully undrained conditions. Unno et al. (2013) had performed cyclic triaxial tests on unsaturated samples with the same initial void ratio of 0.93 under two different initial degrees of saturation. In the simulations, the initial cyclic shearing state was first set as cases c-2 and c-3 for S_{r} of 78.9% and 73.5%, respectively, by applying an increasing pore air pressure to an initially saturated sample under constant pore water pressure. The initial value of I_{h} was set to satisfy the degree of saturation and suction observed in cases c-2 and c-3. Then, cyclic shearing with a step-wise increase in axial strain amplitude, as shown in Figure 4.1, was applied to the specimens under unexhausted air and undrained water conditions at a constant confining pressure. Finally, the experimental results and the corresponding simulation results, i.e.,

the time histories of mean effective stress, void ratio, air pressure, water pressure, and suction, were compared, as shown in Figures 4.4 and 4.5 for cases c-2 and c-3, respectively.

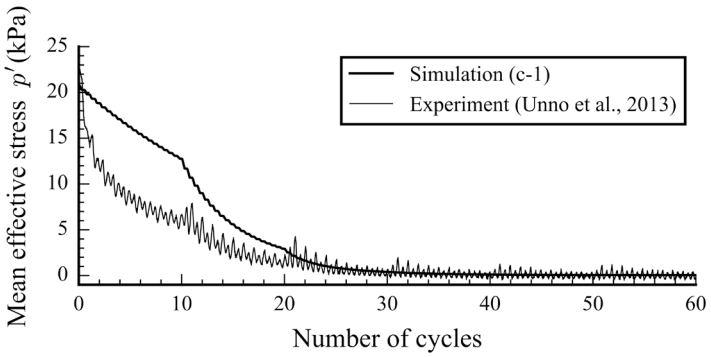

(a) Time histories of mean effective stress

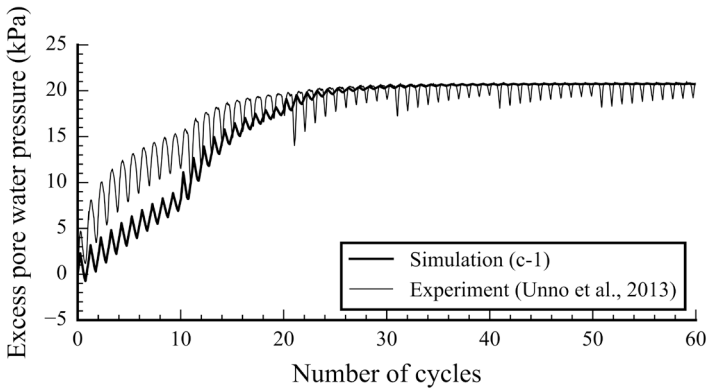

(b) Time histories of water pressure

Figure 4.2 Comparison between the simulation results and the experimental results of case c-1 (S_r = 100%, e_0 = 1.09 kPa)

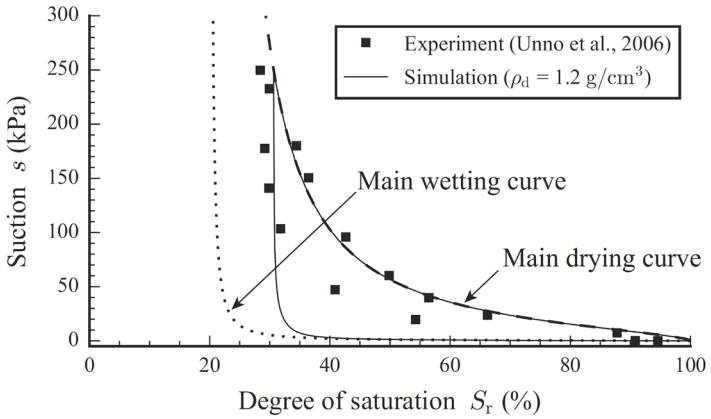

Figure 4.3 Comparison between the simulation results and the experimental results of the water retention test under drying and wetting paths (ρ_d = 1.2 g/cm^3)

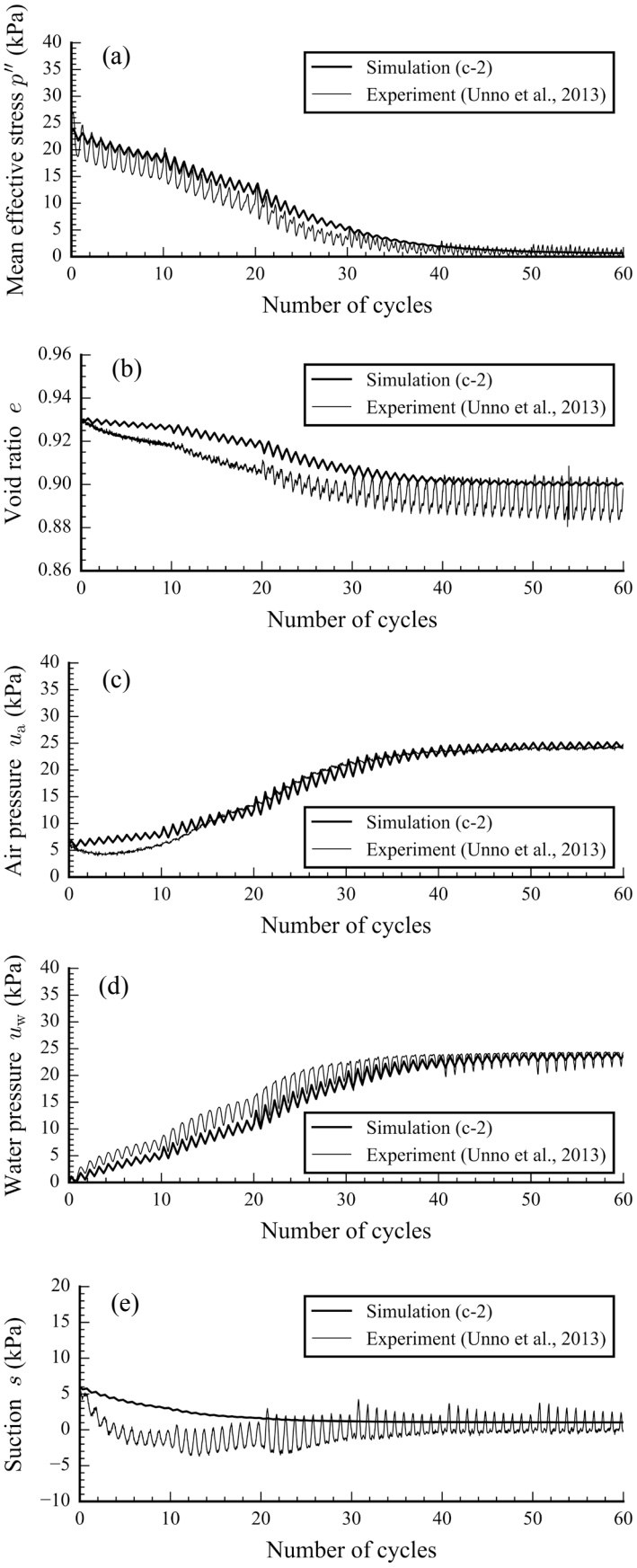

Figure 4.4 Comparison between the simulation results and the experimental results of case c-2 (S_r = 78.9%, s = 6.0 kPa)

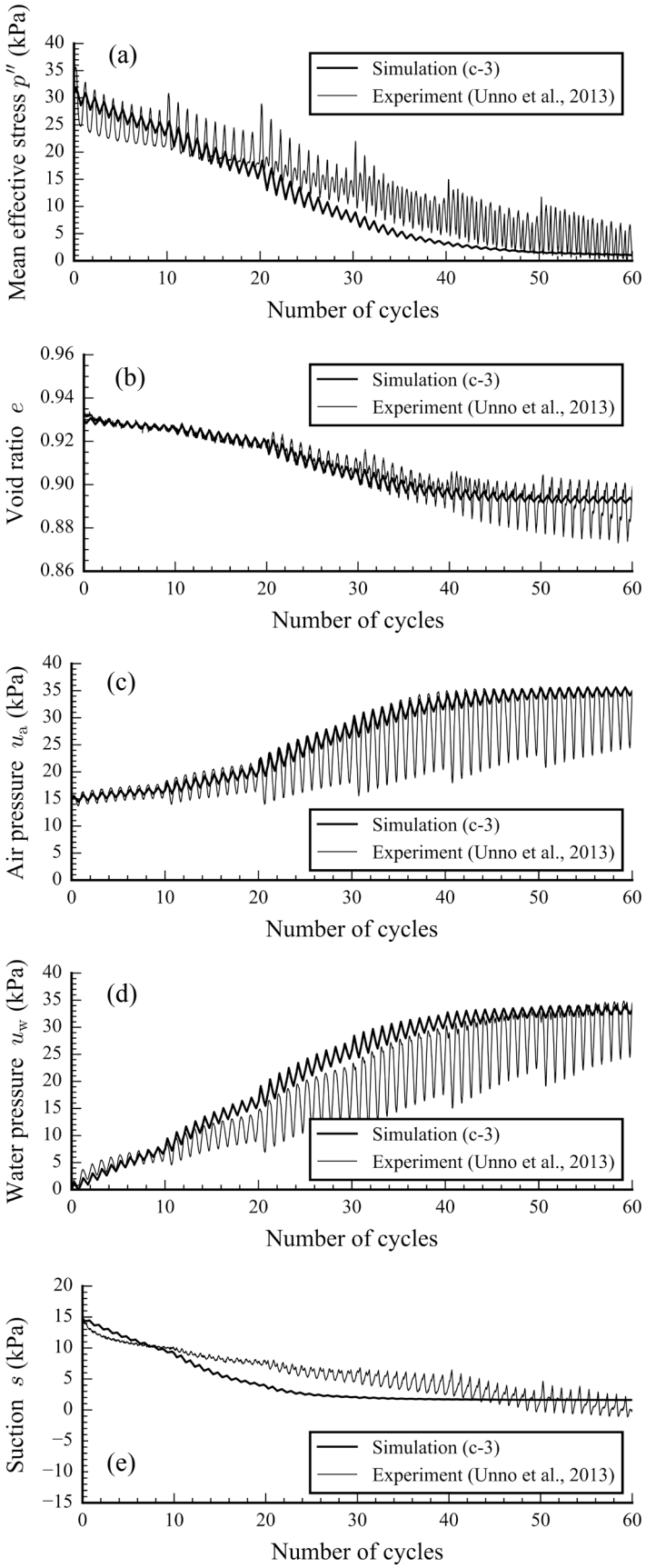

Figure 4.5 Comparison between the simulation results and the experimental results of case c-3 (S_r = 73.5%, s = 14.8 kPa)

Both unsaturated soil samples lost their mean effective stress (as shown in Figures 4.4(a) and 4.5(a)) because of the development of pore air and pore water pressures (Unno et al., 2008). The increase in pore pressure occurs because the generated excess pore pressure within the unsaturated soil cannot be drained out of the soil under fully undrained conditions.

The volumetric behavior, i.e., the magnitude of the decrease in the void ratio, shown in Figures 4.4(b) and 4.5(b), was also predicted accurately. By incorporating Boyle's law, the proposed model can capture the compression behavior of unsaturated soils under fully undrained conditions. As the air pressure increases during cyclic loading, the air volume will automatically decrease following Boyle's law, as shown in Figure 4.6. This decrease in air volume is assumed to be equal to that of the unsaturated soils under the assumption that the soil particles and pore water are incompressible materials. In Figure 4.6, the dashed lines represent the inverse relationship between air void (or air content), e_a, and air pressure according to Boyle's law; in other words, the product of the air void and the absolute air pressure is constant. The simulation results indicate that the variations in air void with air pressure are consistent with Boyle's law. Moreover, the air void in case c-3 is higher than that in case c-2 at arbitrary air pressure. This is because the air void of unsaturated soil depends on the degree of saturation. At the same void ratio, the lower the degree of saturation, the higher is the air void.

In addition, the increase in the pore air pressure (as shown in Figures 4.4(c) and 4.5(c)) is higher than that in the pore water pressure (as shown in Figures 4.4(d) and 4.5(d)). As mentioned above, the pore air can absorb the generated excess pore pressure by compressing its volume (Okamura and Soga, 2006). However, the pore water is an incompressible material; hence, the generated excess pore water pressure cannot be reduced. In other words, the water void (or water content) was kept constant during the test under the undrained water condition. Figure 4.7 shows that the water void remains constant when the water pressure increases in cases c-2 and c-3. As with the air void, the water void of case c-3 is lower than that of case c-2 at arbitrary water pressure. This is because the water void of unsaturated soil depends on the degree of saturation. At the same void ratio, the lower the degree of saturation, the lower is the water void. Finally, this difference between the increase in the pore air pressure and the pore water pressure results in a decrease in the suction pressure under cyclic shear, as shown in Figures 4.4(e) and 4.5(e).

The proposed soil water characteristic curve model considering the effects of density and hydraulic hysteresis can also predict the increase in the degree of saturation owing to volumetric contraction (Unno et al., 2006), as shown in Figure 4.8.

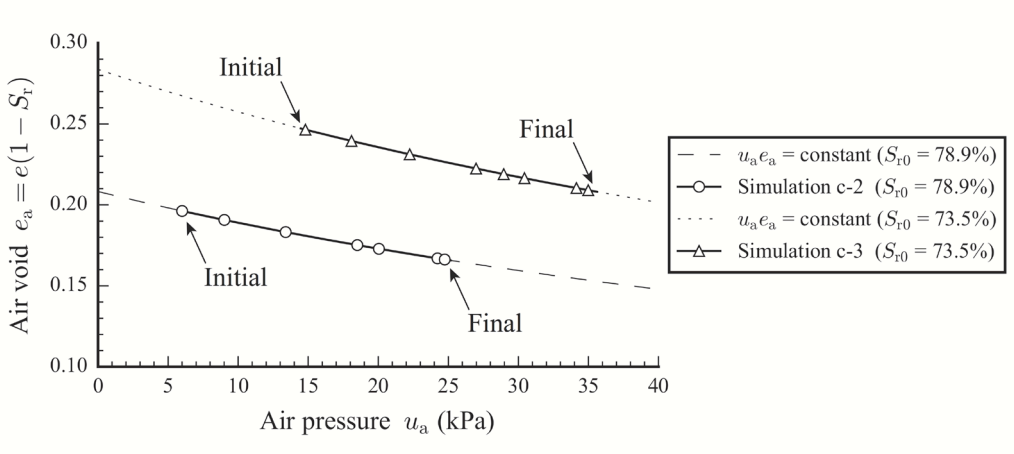

Figure 4.6 Relationship between air void and air pressure of cases c-2 and c-3, following Boyle's law (air pressure is gauge pressure)

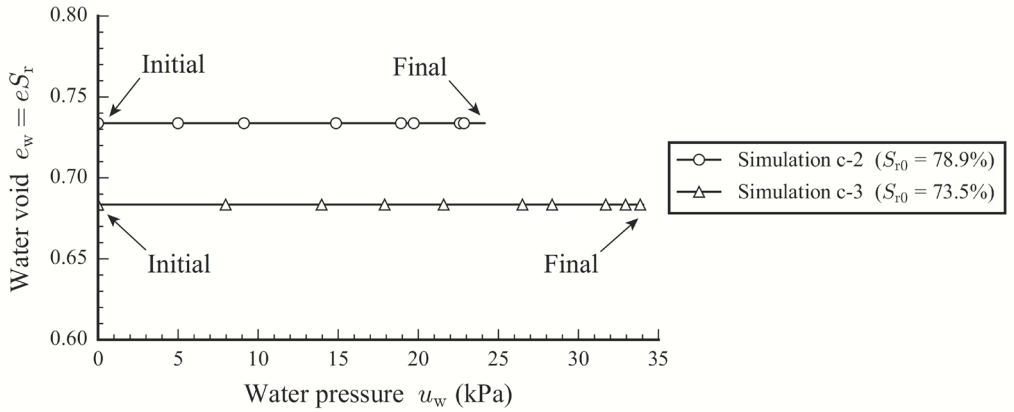

Figure 4.7 Relationship between water void and water pressure of cases c-2 and c-3

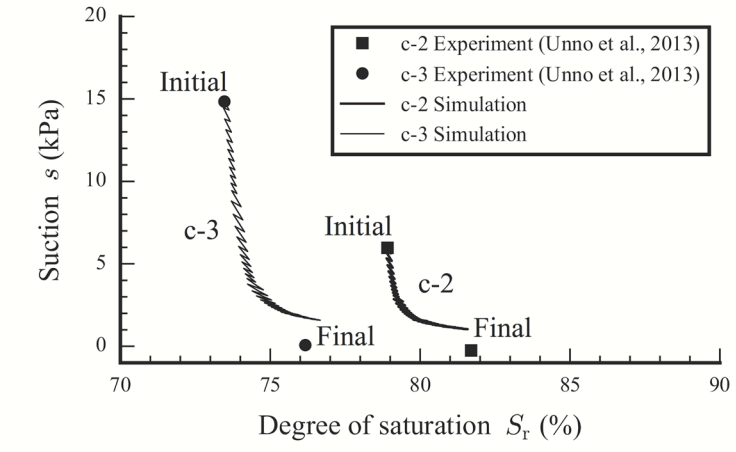

Figure 4.8 Increase in the degree of saturation during fully undrained cyclic triaxial tests of cases c-2 and c-3

Figures 4.9 and 4.10 show the stress-strain curve obtained from the cyclic loading simulation of unsaturated soils under fully undrained conditions for cases c-2 and c-3, respectively. It can be seen that the shear stiffness gradually decreases as the number of cycles increases. The shear strength, i.e., the peak deviatoric stress, slightly increases until the third stage of cyclic shearing (20–30 cycles), but it decreases as the axial strain amplitude is increased further. Finally, the stress–strain curve becomes rather flat, at which point the liquefaction of unsaturated soil is considered to occur (Kazama et al., 2000).

Figures 4.11 and 4.12 show the stress path obtained from the cyclic loading simulation of unsaturated soils under fully undrained conditions for cases c-2 and c-3, respectively. These figures indicate that the unsaturated soil loses its strength under cyclic loading in a manner similar to saturated soils.

A comparison between the simulation results and the experimental results shows that the proposed model precisely describes the cyclic behavior of unsaturated soils under fully undrained cyclic loading conditions.

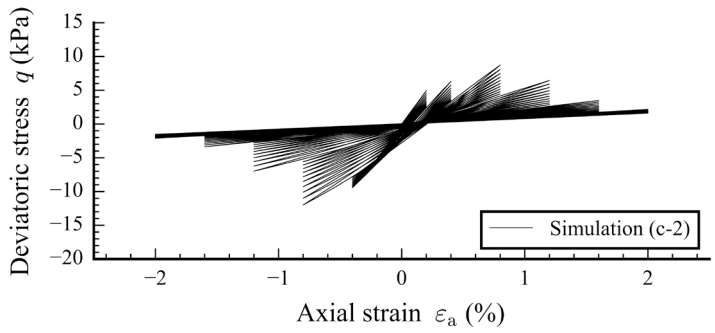

Figure 4.9 Stress-strain curve obtained from the cyclic loading simulation of case c-2 (S_r = 78.9%, s = 6.0 kPa)

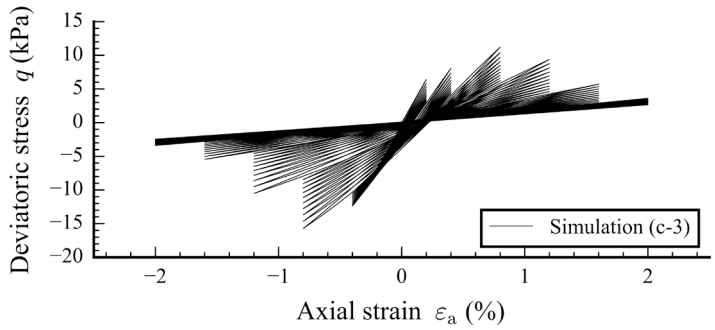

Figure 4.10 Stress-strain curve obtained from the cyclic loading simulation of case c-3 (S_r = 73.5%, s = 14.8 kPa)

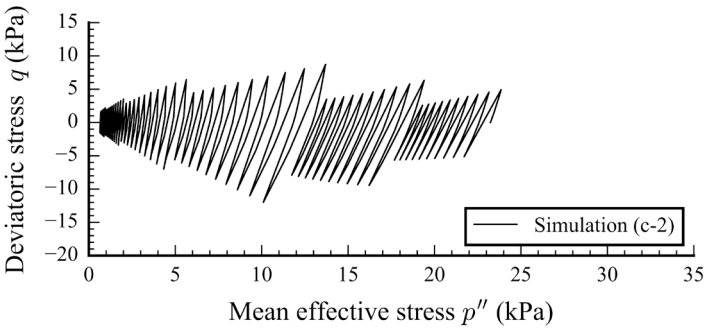

Figure 4.11 Stress path obtained from the cyclic loading simulation of case c-2 (S_r = 78.9%, s = 6.0 kPa)

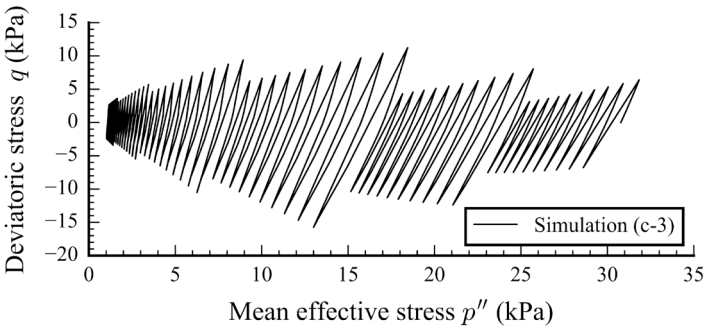

Figure 4.12 Stress path obtained from the cyclic loading simulation of case c-3 (S_r = 73.5%, s = 14.8 kPa)

4.2 PARAMETRIC STUDY OF THE CYCLIC STRENGTH OF UNSATURATED SOILS

A series of simulations of fully undrained cyclic loading on unsaturated soils are presented here to propose a standard for the liquefaction resistance of unsaturated soils in relation to the degree of saturation, specific volume, and effective confining pressure. In this parametric study, the parameters of Tsukidate volcanic sand as shown in Table 4.1 and 4.2, used to validate the proposed model, are used in a series of simulations.

4.2.1 A parametric study of the effects of the degree of saturation and the void ratio on the cyclic strength of unsaturated soils

A series of simulations of cyclic triaxial tests was performed on unsaturated soils using the prescribed void ratio (initial void ratio: 0.60 to 1.09) and degree of saturation (initial degree of saturation: 100% to 40%) under unexhausted air and undrained water conditions at a constant confining pressure of 20 kPa in order to study the effects of the degree of saturation and the void

ratio on the cyclic strength of the unsaturated soils. In order to achieve the desired degree of saturation, suction was increased by decreasing the water pressure. In the simulation, the cyclic axial strain amplitude, as shown in Figure 4.1, was applied again to the specimens. The results of a series of simulations at a constant total confining pressure of 20 kPa are shown in Figures 4.13 (3D space) and 4.14 (2D space) for simple interpretation.

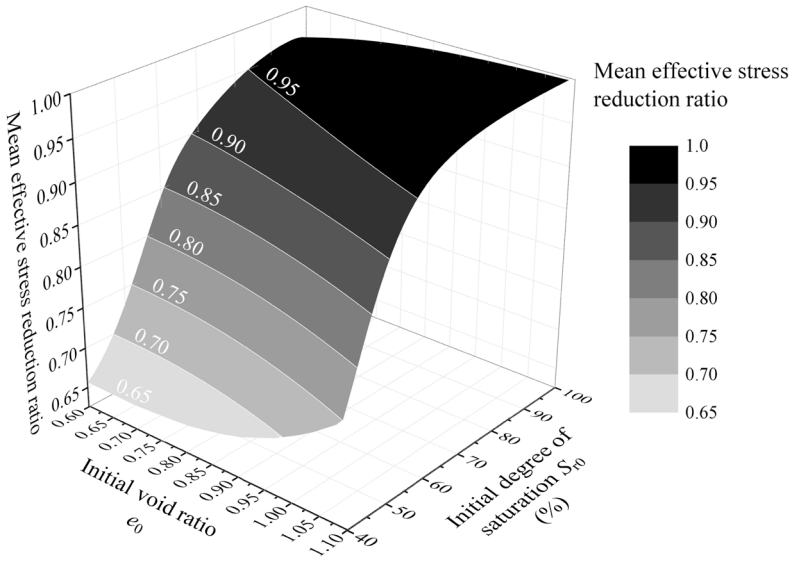

Figure 4.13 Three-dimensional surface of cyclic strength of unsaturated soils: effect of degree of saturation and void ratio (constant total confining pressure of 20 kPa)

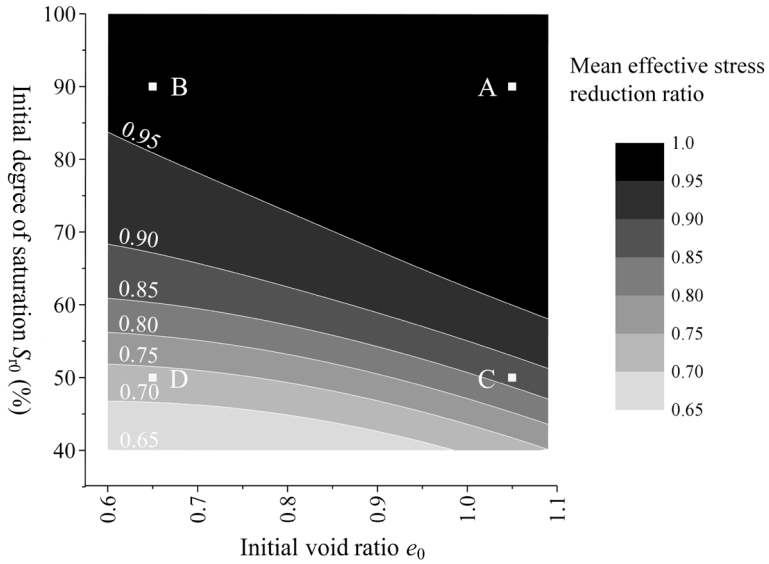

Figure 4.14 Effect of void ratio and degree of saturation on the cyclic strength of unsaturated soils (constant total confining pressure of 20 kPa)

The mean effective stress reduction ratio (Unno et al., 2008) is the rate of decrease in the mean effective stress p'' of unsaturated soils after they are subjected to cyclic shear loading, and it can be used to describe the liquefaction resistance of unsaturated soils. The higher the mean effective stress reduction ratio, the lower is the liquefaction resistance of unsaturated soils.

$$\text{Mean effective stress reduction ratio} = 1 - \frac{p''}{p_0''} \tag{4.5}$$

The mean effective stress reduction ratio is equal to 1 in the complete liquefaction state.

Points A, B, C, and D in Figure 4.14 represent examples of unsaturated soils having different initial degrees of saturation and void ratios: A represents loose unsaturated soil with a high degree of saturation (S_{r0} = 90%, e_0 = 1.05); B represents dense unsaturated soil with a high degree of saturation (S_{r0} = 90%, e_0 = 0.65); C represents loose unsaturated soil with a low degree of saturation (S_{r0} = 50%, e_0 = 1.05); and D represents dense unsaturated soil with a low degree of saturation (S_{r0} = 50%, e_0 = 0.65).

All the specimens experience a reduction in the mean effective stress during cyclic shearing simulation, and specimen A, which is a loose unsaturated soil with a high degree of saturation, is finally liquefied after approximately 38 cycles, as shown in Figure 4.15. The cyclic strength of unsaturated soils can be evaluated by the mean effective stress reduction ratio, as shown in Figure 4.16. Specimen A shows a drastic loss in mean effective stress compared with the other specimens, and its mean effective stress reduction ratio reaches 1.0 after around 38 cycles. For specimen B, which has a high degree of saturation and high density, the mean effective stress reduction ratio nearly reaches 1.0 at the end of the simulation. However, even though specimens C and D, which have low degrees of saturation, show a decrease in shear strength as the mean effective stress decreases, they are not liquefied during the cyclic shearing simulation.

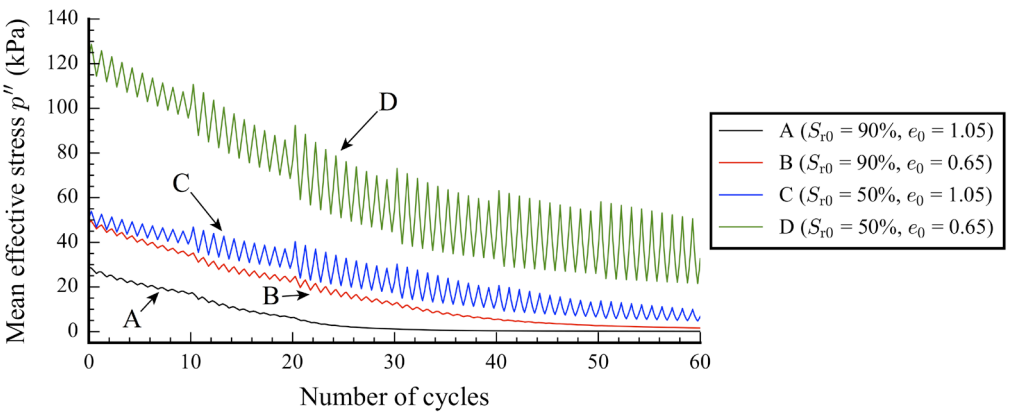

Figure 4.15 Time histories of mean effective stress at points A, B, C, and D (as shown in Figure 4.14)

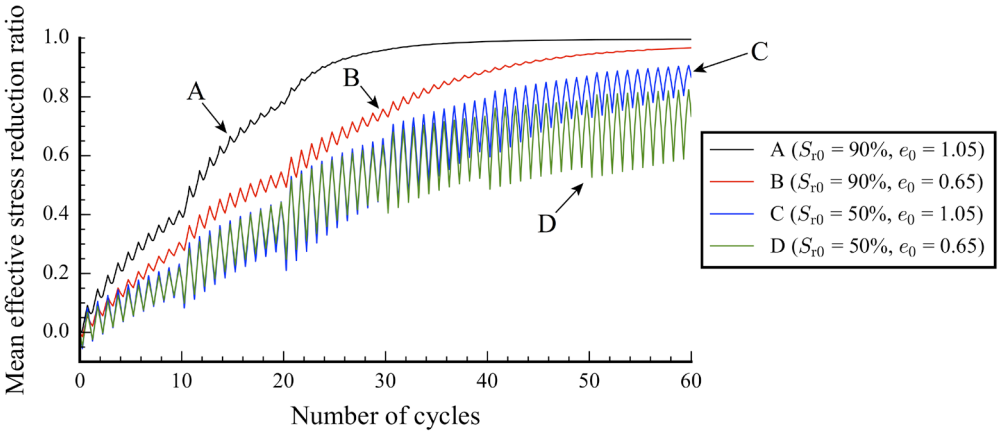

Figure 4.16 Time histories of mean effective stress reduction ratio at points A, B, C, and D (as shown in Figure 4.14)

Figure 4.17 shows the variation in the void ratio during the simulation. The void ratios of specimens A and B remain nearly constant. This is because a change in the volume of the unsaturated soils under fully undrained conditions depends only on the volume of air. Specimens A and B have a high degree of saturation; therefore, the volume of air that affects the variation in the void ratio is limited. On the other hand, the variations in the void ratios of specimens C and D are higher than those of specimen A and B because specimens C and D have a low degree of saturation. As shown in Figure 4.18, Specimens A and C, which are loose unsaturated soils, exhibit compression behavior during the cyclic shearing simulation. However, the normalized void ratio of specimen A becomes constant as it approaches the liquefaction state, while that of specimen C continuously decreases until the end of the simulation. Specimens B and D, which are dense unsaturated soils, exhibit dilatancy at the beginning of the simulation, followed by compression behavior. It is also seen that the normalized void ratio of specimen B becomes nearly constant as it approaches the liquefaction state.

The pore air pressure and pore water pressure of all the specimens increased during the simulation, as shown in Figures 4.19 and 4.20, respectively. However, there was a decrease in the air pressure of specimens B and D in the first 10 cycles, because the variation in the air pressure is inversely proportional to the variation in the void ratio, as per Boyle's law (Equation 4.2). Moreover, the pore air pressure and pore water pressure of specimen A stopped increasing after around 38 cycles, once the liquefaction state was reached, as did those of specimen B at the end of the simulation.

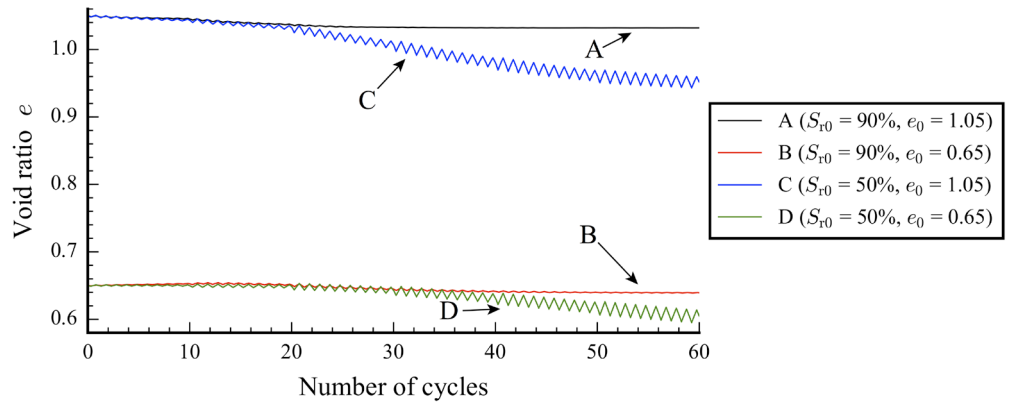

Figure 4.17 Time histories of void ratio at points A, B, C, and D (as shown in Figure 4.14)

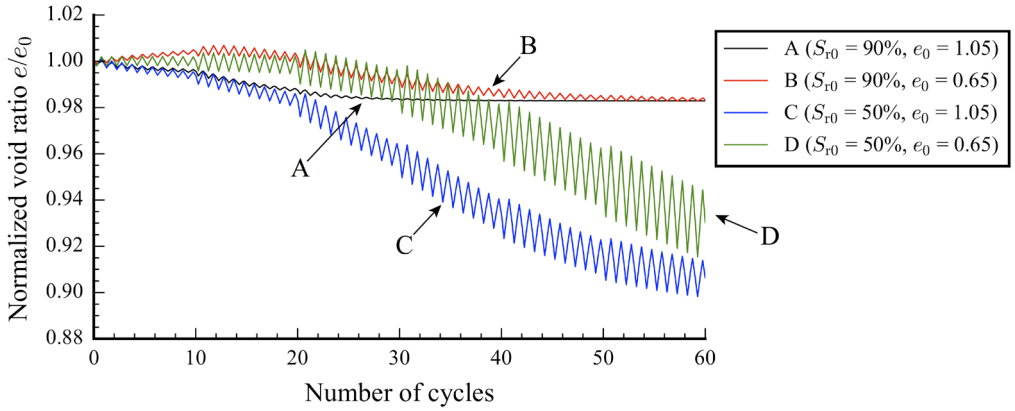

Figure 4.18 Time histories of normalized void ratio at points A, B, C, and D (as shown in Figure 4.14)

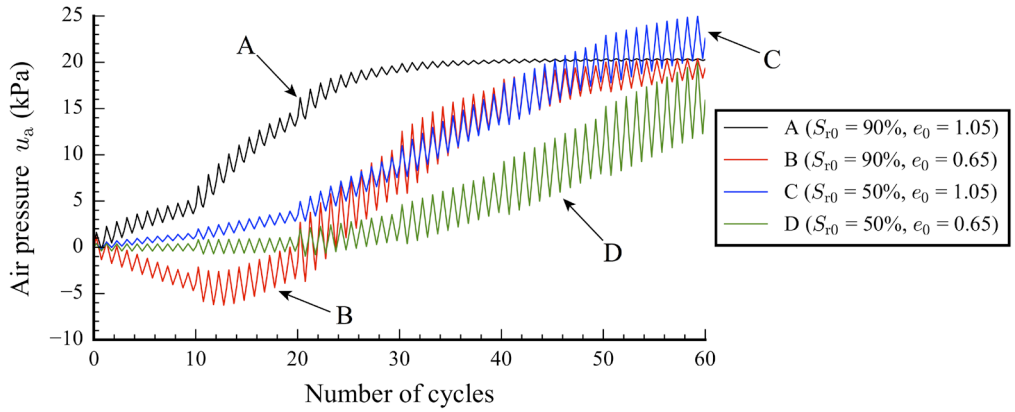

Figure 4.19 Time histories of air pressure at points A, B, C, and D (as shown in Figure 4.14)

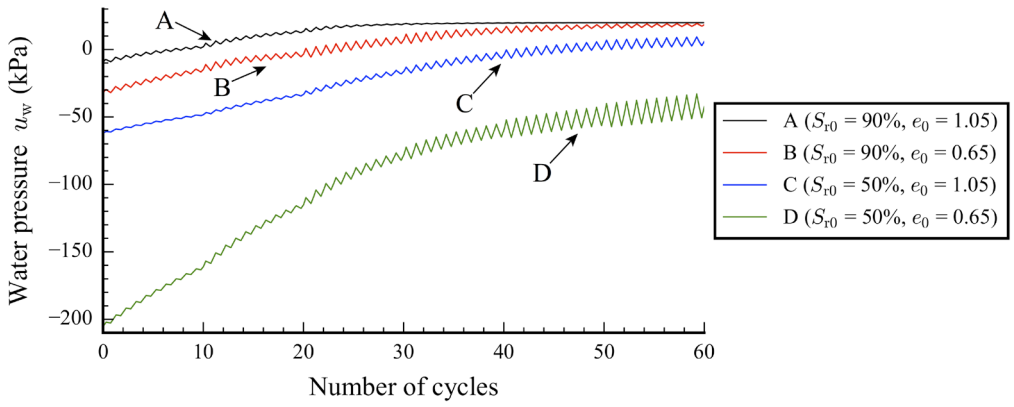

Figure 4.20 Time histories of water pressure at points A, B, C, and D (as shown in Figure 4.14)

Figures 4.21 shows that the suction decreased in all the specimens. However, the reduction rate of the suction in specimens A and B were significantly higher than that in specimens C and D, as shown in Figure 4.22. This is because specimens A and B had a higher degree of saturation than specimens C and D; moreover, the initial pore air pressure and initial pore water pressure were closer to each other in specimens A and B than in specimens C and D. This reduction in suction, which depends on the initial degree of saturation, was also observed in the experimental results obtained by Unno et al. (2006) and Liu and Xu (2013).

Furthermore, this result can be explained by the following factors. Based on the volumetric movement of the state boundary surface owing to the variation in the degree of saturation, unsaturated soils behave more similarly to dense soils, which gain cyclic strength owing to their dilatancy characteristics (Kazama et al., 2000). Figures 4.23 and 4.24 show examples of the stress–strain curve obtained from specimens A and D; under cyclic loading, the cyclic strength decreases as the number of cycles increases in both cases. When the initial degree of saturation is high, the peak deviatoric stress decreases as the axial strain increases owing to the compression behavior, as shown in Figure 4.23. On the other hand, the peak deviatoric stress of unsaturated soils having a low initial degree of saturation increases with the axial strain owing to their dilatancy characteristics, as shown in Figure 4.24.

In conclusion, the liquefaction resistance of unsaturated soils increases as the degree of saturation and void ratio decrease. However, the degree of saturation has a greater effect than the void ratio on the liquefaction resistance of unsaturated soils.

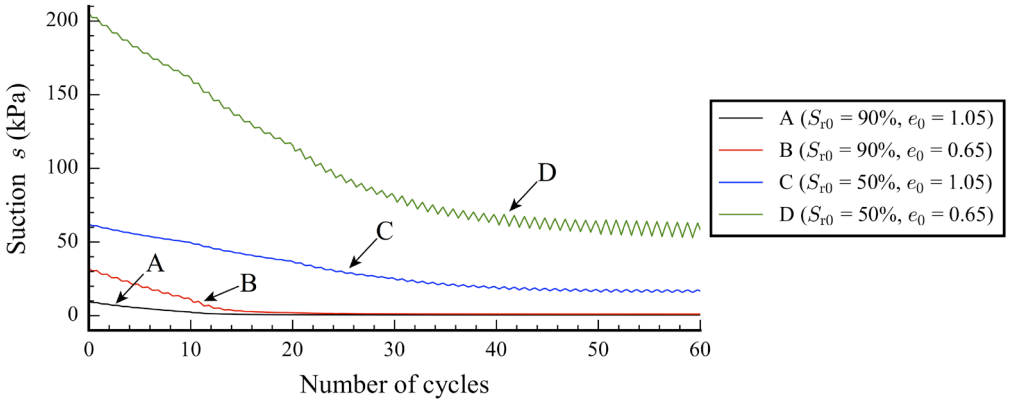

Figure 4.21 Time histories of suction at points A and B (as shown in Figure 4.14)

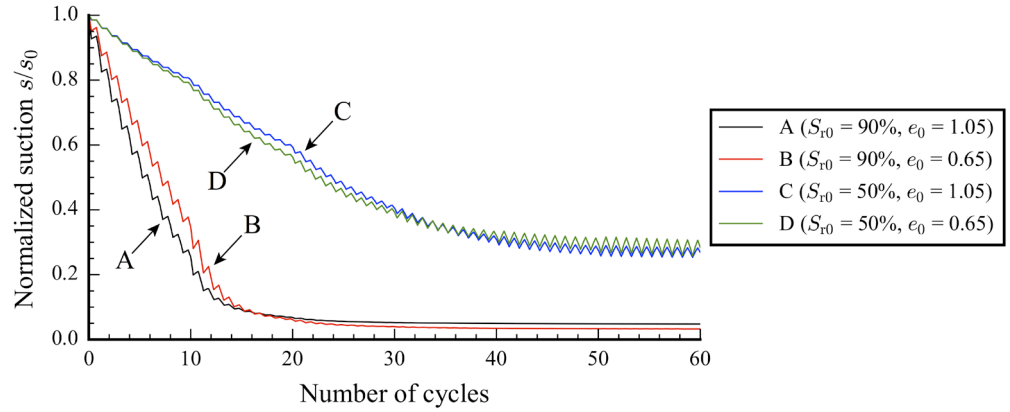

Figure 4.22 Time histories of normalized suction at points A and B (as shown in Figure 4.14)

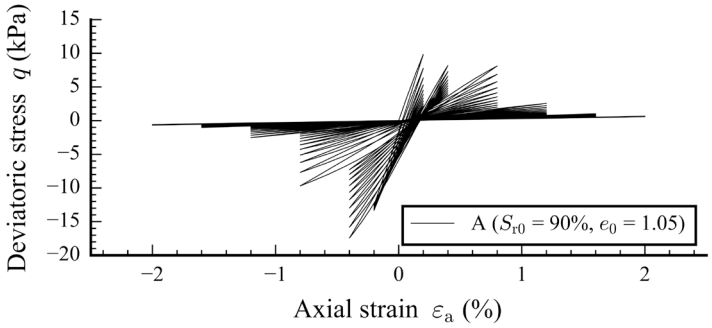

Figure 4.23 Stress-strain curve obtained from specimen A (as shown in Figure 4.14)

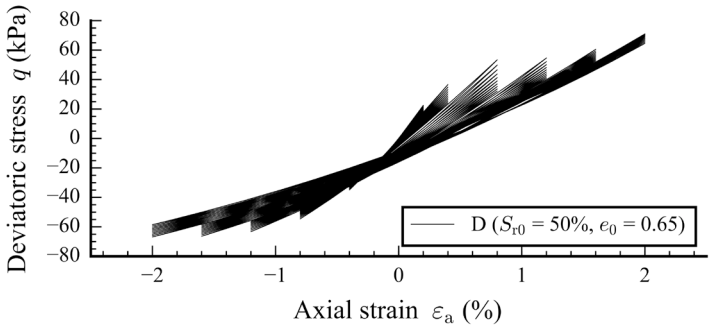

Figure 4.24 Stress-strain curve obtained from specimen D (as shown in Figure 4.14)

4.2.2 A parametric study of the effects of the confining pressure on the cyclic strength of unsaturated soils

To consider the effect of the confining pressure on the cyclic strength of unsaturated soils, a series of simulations of cyclic triaxial tests were performed on the specimens of unsaturated soils under unexhausted air and undrained water conditions at a constant total confining pressure varying from 20 to 300 kPa. In the simulations, each saturated specimen with an initial void ratio of 1.09 was first consolidated from 20 kPa to the desired confining pressure up to 300 kPa. Suction was then applied to each specimen by decreasing the water pressure until the desired initial degree of saturation, varying from 40% to 100%, was reached. Subsequently, cyclic axial strain was applied to all the specimens under fully undrained conditions at a constant total confining pressure, as shown in Figure 4.1. The results of the simulations are shown in Figures 4.25 (3D space) and 4.26 (2D space) for simple interpretation.

Points A, B, C, and D in Figure 4.26 represent examples of unsaturated soils having different initial degrees of saturation and total confining pressures: A represents unsaturated soil with a high degree of saturation and low total confining pressure (S_{r0} = 90%, σ_{c0} = 40 kPa); B represents unsaturated soil with a high degree of saturation and high total confining pressure (S_{r0} = 90%, σ_{c0} = 280 kPa); C represents unsaturated soil with a low degree of saturation and low total confining pressure (S_{r0} = 50%, σ_{c0} = 40 kPa); and D represents unsaturated soil with a low degree of saturation and high total confining pressure (S_{r0} = 50%, σ_{c0} = 280 kPa).

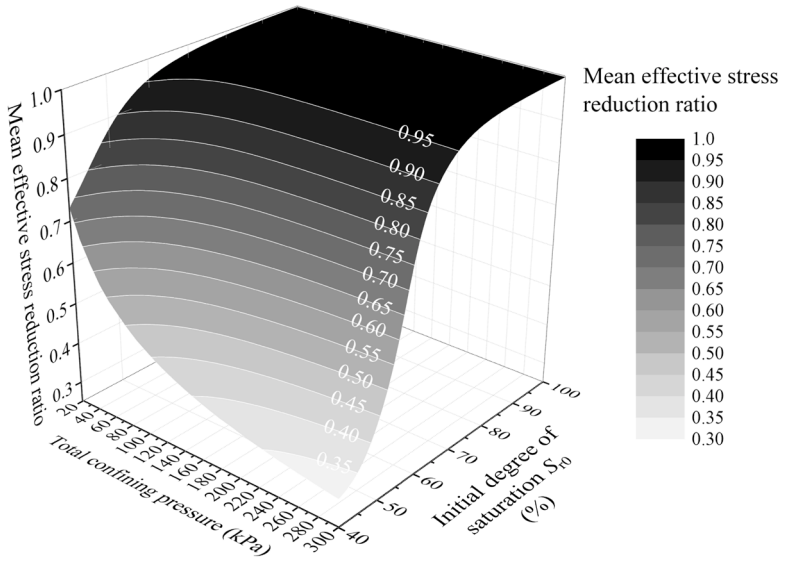

Figure 4.25 Three-dimensional surface of cyclic strength of unsaturated soils: effect of confining pressure and degree of saturation

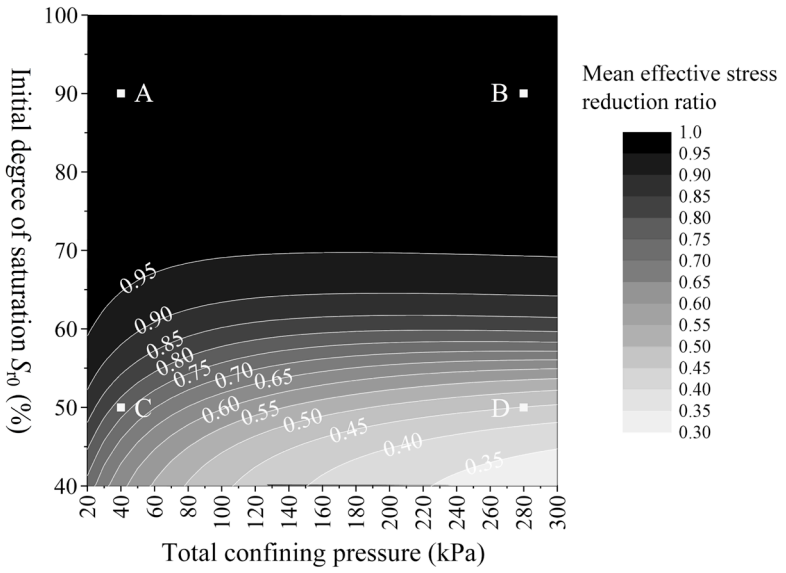

Figure 4.26 Effect of confining pressure and degree of saturation on the cyclic strength of unsaturated soils

All the specimens lost their mean effective stress during the cyclic shearing simulation, in which specimens A and B liquefied after around 28 and 40 cycles, respectively, as shown in Figure 4.27. However, as shown in Figure 4.28, the mean effective stress reduction ratio of specimen A was nearly the same as that of specimen B, which is higher than that of specimens C and D. This indicates that the cyclic strength of unsaturated soils is highly dependent on the degree of saturation, while the effect of the total confining pressure on the cyclic strength of unsaturated soils is more evident at lower degrees of saturation. These simulation results are in good agreement with the experimental results obtained by Liu and Xu (2013).

Figure 4.29 shows the variation in the void ratio during the simulation. The initial void ratio of specimens A and C are higher than those of specimens B and D because of the total confining pressure. As discussed in Section 4.2.1, the void ratio of specimens A and B remain nearly constant, while specimens C and D show a greater reduction in the void ratio during the simulation owing to the difference in the initial degrees of saturation. However, if we consider only the effect of the total confining pressure on the variation in the void ratio by using the normalized void ratio at different degrees of saturation, as shown in Figure 4.30, it can be seen that the higher the confining pressure, the higher is the compression rate of the void ratio. Specimens A, B, C, and D are found to exhibit compression behavior during the fully undrained cyclic loading simulation even though specimens B and D are dense soils, because dense soils usually show compression behavior under low strain, followed by dilation behavior at higher strain. Therefore, it is possible that dense soils will show only compression behavior if they are subjected to low strain (Liu and Xu, 2013).

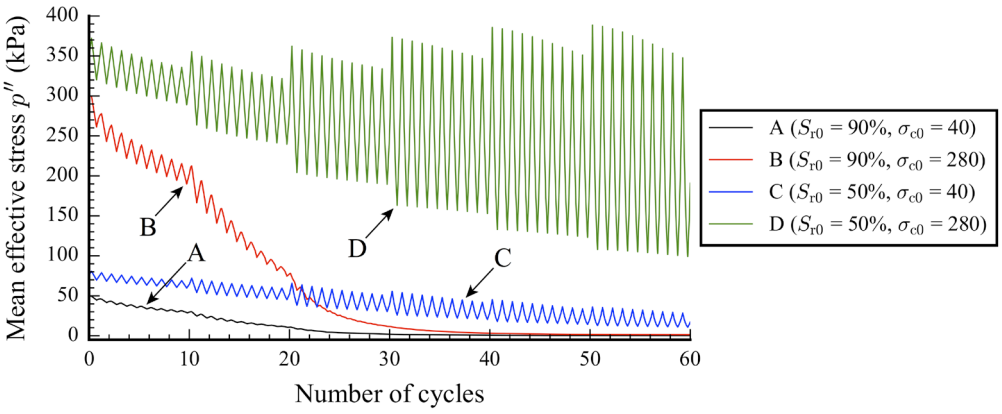

Figure 4.27 Time histories of mean effective stress at points A, B, C, and D (as shown in Figure 4.26)

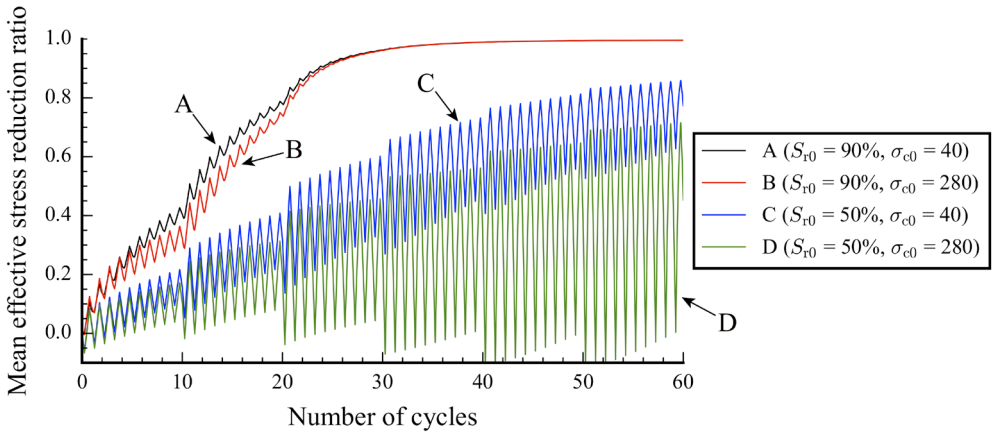

Figure 4.28 Time histories of mean effective stress reduction ratio at points A, B, C, and D (as shown in Figure 4.26)

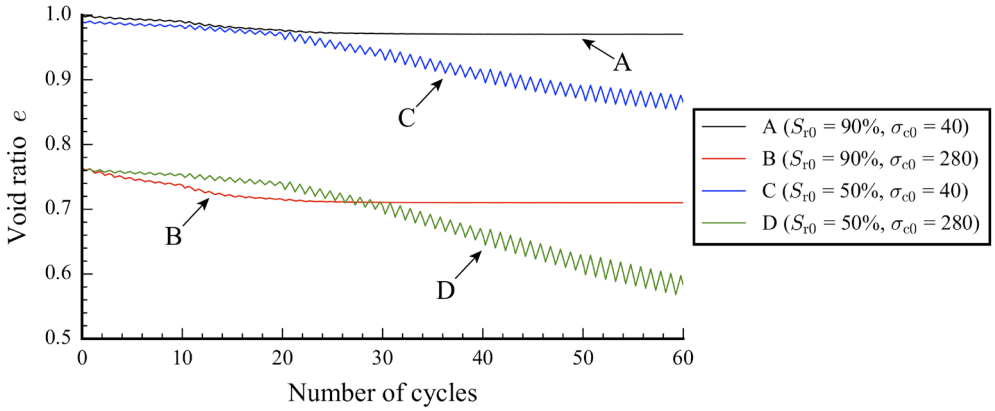

Figure 4.29 Time histories of void ratio at points A, B, C, and D (as shown in Figure 4.26)

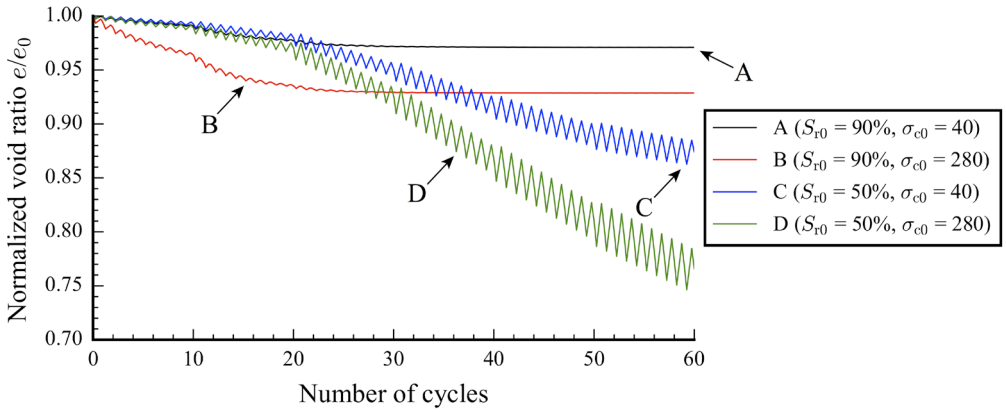

Figure 4.30 Time histories of normalized void ratio at points A, B, C, and D (as shown in Figure 4.26)

The pore air pressure and pore water pressure of all the specimens increased during the simulation owing to the decrease in the void ratio (as shown in Figures 4.31 and 4.32, respectively). At each degree of saturation, it is seen that an increase in the pore air pressure and pore water pressure depends on the total confining pressure. The higher the total confining pressure, the higher is the increase in the pore air and pore water pressure. Moreover, the pore air pressure and pore water pressure of specimens A and B stopped increasing after reaching the total confining pressure. In this state, specimens A and B were completely liquefied. This development in the pore air and pore water pressure leads to a decrease in the mean effective stress of unsaturated soils, as mentioned above.

The initial suction of each specimen was different depending on the desired degree of saturation, as shown in Figure 4.33. It is seen that the suction in all the specimens decreased during the simulation. Moreover, the reduction rate of suction of specimens with higher total confining pressure is higher than that of specimens with lower total confining pressure, as shown in Figure 4.34.

Figure 4.35 shows the stress–strain curves obtained from specimens C and D. At the same initial degree of saturation, the deviatoric stress of specimen C was less than that of specimen D under the same axial strain level. It can be concluded that the deviatoric stress of unsaturated soils increases with the total confining pressure under the same initial degree of saturation. A stronger soil naturally experiences a higher deviatoric stress than a weaker soil under the same axial strain level. Thus, the higher the confining pressure, the higher is the cyclic strength of the soil.

In conclusion, the liquefaction resistance of unsaturated soils increases with the total

confining pressure. However, as indicated by the simulation using the parameters of Tsukidate volcanic sand with cyclic loading history shown in Figure 4.1 that the effect of the total confining pressure on the cyclic strength of unsaturated soils is insignificant when the degree of saturation is higher than 70%, whereas it is more evident at lower degrees of saturation. Furthermore, the unsaturated soils are observed to easily liquefy when the degree of saturation is higher than 70% (i.e., when the mean effective stress reduction ratio is higher than 0.9), regardless of the initial confining pressure.

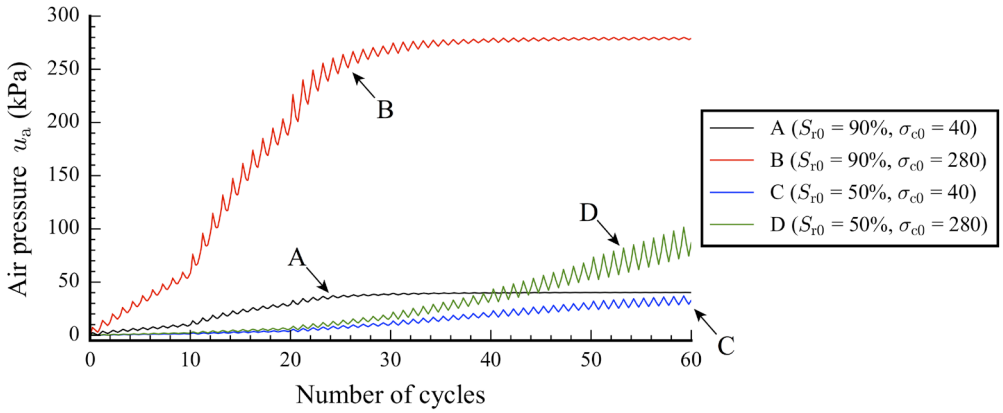

Figure 4.31 Time histories of air pressure at points A, B, C, and D (as shown in Figure 4.26)

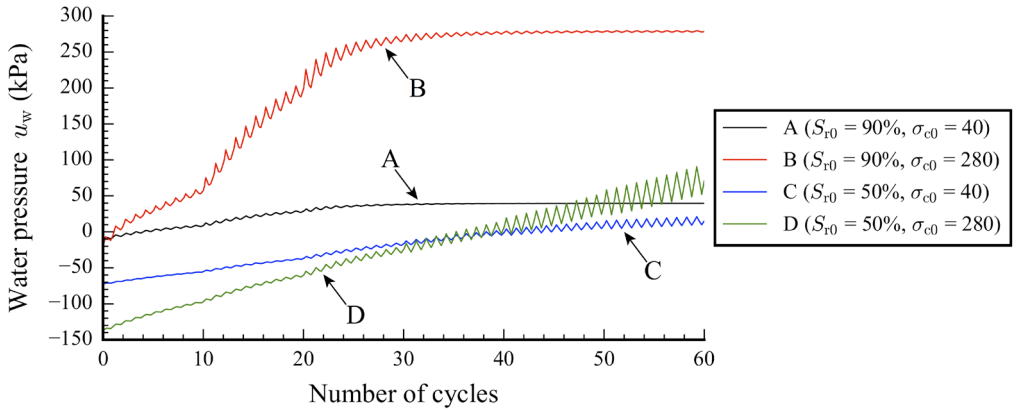

Figure 4.32 Time histories of water pressure at points A, B, C, and D (as shown in Figure 4.26)

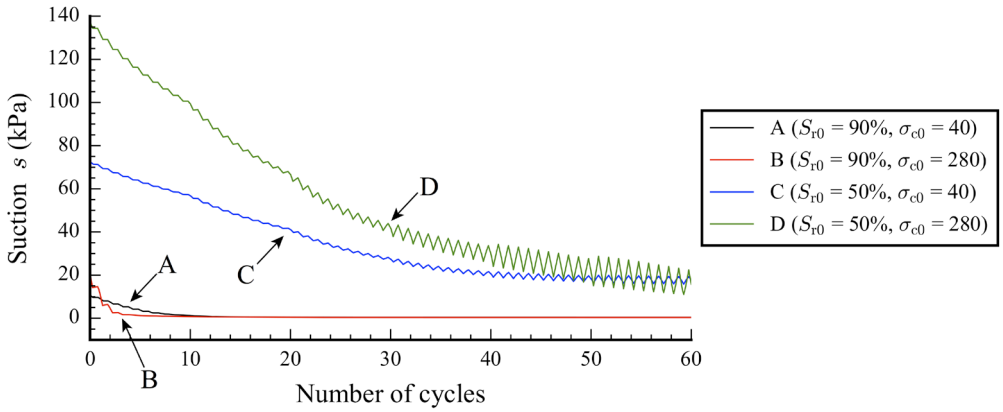

Figure 4.33 Time histories of suction at points A and B (as shown in Figure 4.26)

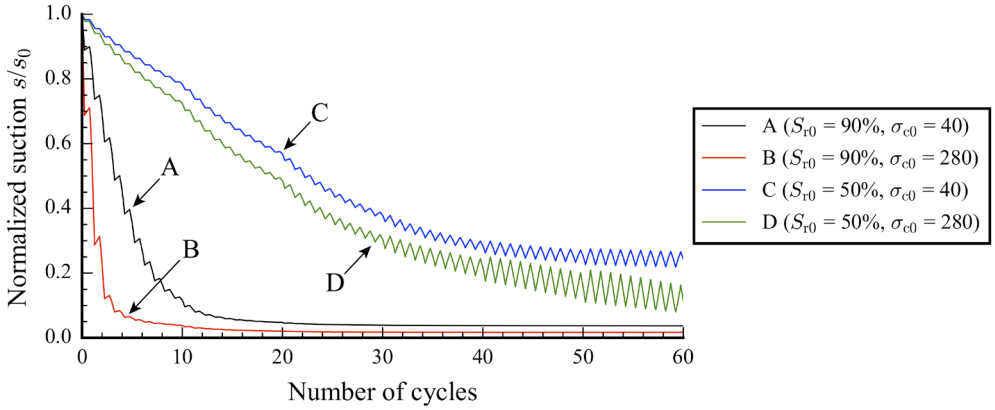

Figure 4.34 Time histories of normalized suction at points A and B (as shown in Figure 4.26)

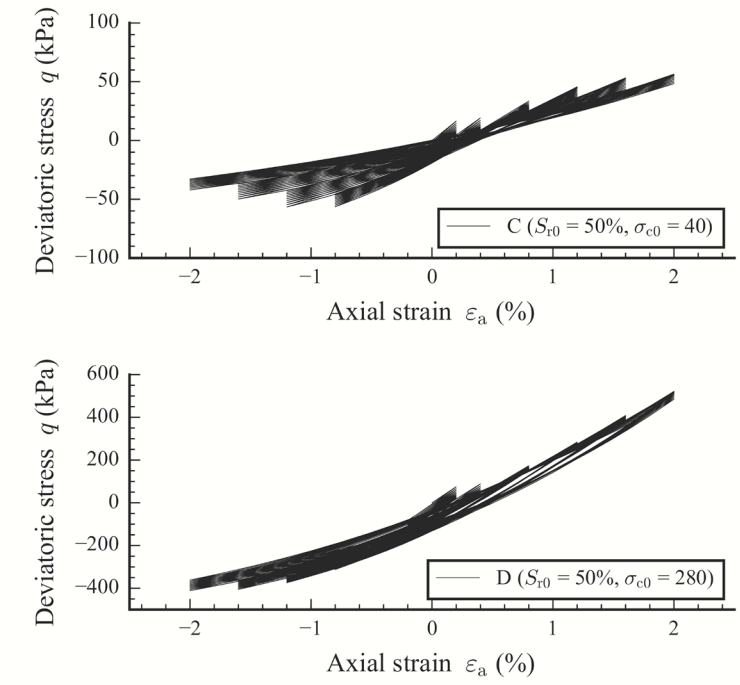

Figure 4.35 Stress-strain curves obtained from specimens C and D (as shown in Figure 4.26)

4.3 CONCLUSIONS

This chapter presented the validation of a three-dimensional extension of the simple elastoplastic constitutive model proposed by Kikumoto et al. (2010) on the cyclic behavior of unsaturated soils and a parametric study of the cyclic behavior of unsaturated soils under fully undrained condition.

The validity of the proposed model was verified through a series of cyclic triaxial tests on saturated and unsaturated soils under fully undrained conditions. The results showed that the proposed model properly describes the fully undrained cyclic behavior of unsaturated soils, such as liquefaction, compression associated with Boyle's law, and an increase in the degree of saturation owing to a decrease in suction and volumetric compression.

The results also showed that unsaturated soils with a low degree of saturation and low void ratio have high cyclic strength. Moreover, the cyclic strength increases with the total confining pressure. Among various factors, the degree of saturation has a significant effect on the liquefaction resistance of unsaturated soils.

CHAPTER 5

EXTENSION OF THE CONSTITUTIVE MODEL FOR UNSATURATED SOILS TO ANISOTROPY

In general, soils subjected to load which is not under isotropic condition show anisotropic behaviors (e.g., the cyclic behavior of soils due to cyclic loading). Regarding the assumption of isotropic hardening, soils exhibit purely elastic behavior if stress condition is inside yield surface. Therefore, isotropic hardening cannot predict the cyclic behavior of soils as soils show purely elastic under unloading paths in isotropic hardening. Although the cyclic behavior of soils is well reproduced as mentioned in Chapter 4 by using the model proposed in Chapter 2 which includes subloading concept, there is an issue about the stress path obtained from cyclic loading which should be improved as the cyclic mobility could not be well predicted by only subloading concept. Thus, the elastoplastic model needs to be improved for simulating anisotropic behaviors.

Kinematic hardening (i.e. the translation of yield surface) is one of the concepts which succeed in describing the anisotropic or cyclic behaviors. However, there is a limitation that kinematic hardening cannot be used to simulate the behavior of soils as the yield surface of kinematic hardening cannot keep the stress space of soil at the origin. Sekiguchi and Ohta (1977) firstly proposed the method to simulate the anisotropic behavior of soils by assuming the yield surface rotates around the origin of stress space if soils have the inherent anisotropy, however, yield function proposed by Sekiguchi and Ohta (1977) did not obey the critical state concept. Dafalias (1986) proposed the yield surface including rotational hardening concept which is able to follow the critical state concept and derived from the plastic work dissipation equation. Hashiguchi and Chen (1998) proposed the method to control the rotation of yield surface around the origin of stress space by introducing the rotational hardening variable.

In this chapter, the formulation of extension of the constitutive model for unsaturated soils to anisotropy is presented. This model is modified from the model described in Chapter 2 by incorporating the rotational hardening concept (Hashiguchi and Chen, 1998) as well as the critical state soil model for rotational hardening (Dafalias, 1986). The effective stress, soil water characteristic curves and elastic stress-strain relationship, which have been described in Chapter 2, will not be shown here. The regulations of notations and symbols are given at the end of Chapter 1. Finally, the simulation results calculated by using the proposed model are shown to reveal the performance of the proposed model.

5.1 MODEL FORMULATION OF A ROTATIONAL HARDENING ELASTOPLASTIC CONSTITUTIVE MODEL FOR UNSATURATED SOILS

The formulation of a rotational hardening elastoplastic constitutive model for unsaturated soils, which is modified from the model proposed in Chapter 2 by incorporating the rotational hardening concept for predicting anisotropic behaviors, is presented here. An associated flow rule is assumed in the new model, i.e. yield function is used as plastic potential function. The evolution law of rotational hardening variable $\boldsymbol{\beta}$ and its assumptions are firstly described. Then, yield function including rotational hardening and subloading concepts is presented. Finally, the elastoplastic stress–strain relationship based on rotational hardening and subloading surface concepts is proposed.

5.1.1 The evolution law of the rotational hardening variable $\boldsymbol{\beta}$

Hashiguchi and Chen (1998) proposed the rotational hardening variable $\boldsymbol{\beta}$ and the assumptions to formulate the evolution law of the rotational hardening variable $\boldsymbol{\beta}$ which can be described as follows:

- Yield surface rotates around the origin of stress space.
- As the rotational hardening is the concept to deal with the anisotropic behavior of soils, the rotation of yield surface should depend only on the plastic deviatoric strain. In other words, yield surface should not be rotated when the plastic volumetric strain occurs. Therefore, the rotational rate of yield surface is proportional to the magnitude of plastic deviatoric strain rate tensor $\|\dot{\boldsymbol{e}}^{\mathrm{p}}\|$.
- In case that the loading path traces the central axis of yield surface in the principal stress space ($\|\boldsymbol{\eta}-\boldsymbol{\beta}\|=0$), i.e. anisotropic consolidation, yield surface is not be rotated as shown in Figure 5.1.
- There is a restriction of the rotation of yield surface, i.e. yield surface cannot be rotated over the limit surface which is defined as $m_{\mathrm{r}}\frac{\boldsymbol{\eta}-\boldsymbol{\beta}}{\|\boldsymbol{\eta}-\boldsymbol{\beta}\|}-\boldsymbol{\beta}$. In this study, the limit of rotation of yield surface cannot be set over than the critical state line (*M-line*) in p-q space as shown in Figure 5.1 (i.e., $m_{\mathrm{r}}<\sqrt{\frac{2}{3}}M$).

Finally, the evolution law of the rotational hardening variable $\boldsymbol{\beta}$ can be expressed as

$$\dot{\boldsymbol{\beta}}=b_{\mathrm{r}}\|\dot{\boldsymbol{e}}^{\mathrm{p}}\|\|\boldsymbol{\eta}-\boldsymbol{\beta}\|\left[m_{\mathrm{r}}\frac{\boldsymbol{\eta}-\boldsymbol{\beta}}{\|\boldsymbol{\eta}-\boldsymbol{\beta}\|}-\boldsymbol{\beta}\right] \tag{5.1}$$

where b_{r} is the material constant parameter and m_{r} is the limit of rotation.

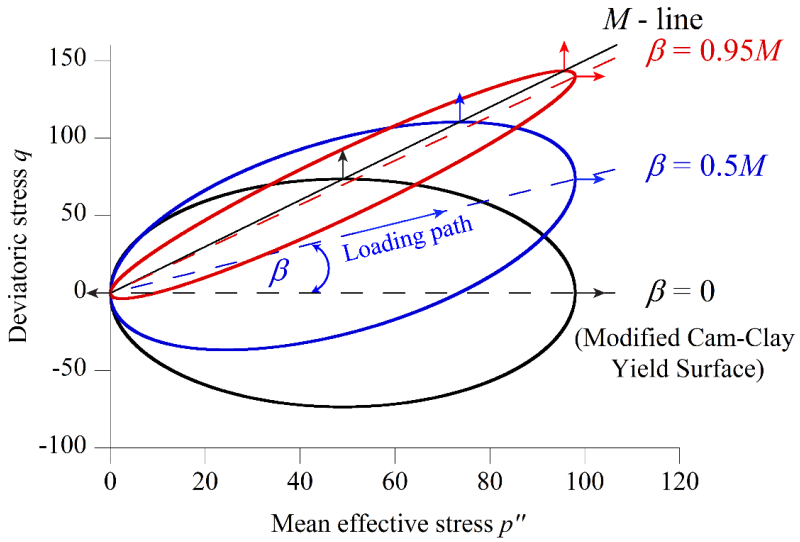

Figure 5.1 The rotation of yield surface due to an increase in the rotational hardening variable $\boldsymbol{\beta}$ in p-q space

As $\dot{\boldsymbol{e}}^{\mathrm{p}}$ is the deviatoric part of plastic strain rate tensor (i.e., $\dot{\boldsymbol{\varepsilon}}^{\mathrm{p}} - \frac{1}{3}\mathrm{tr}(\dot{\boldsymbol{\varepsilon}}^{\mathrm{p}})\mathbf{1}$), Equation (5.1) can be rearranged in the function of $\langle\dot{\Lambda}\rangle$ as

$$\dot{\boldsymbol{\beta}} = \langle\dot{\Lambda}\rangle \boldsymbol{A} \tag{5.2}$$

where $\boldsymbol{A} = b_{\mathrm{r}} \left\| \frac{\partial f}{\partial \boldsymbol{\sigma}''} - \frac{1}{3}\mathrm{tr}\left(\frac{\partial f}{\partial \boldsymbol{\sigma}''}\right)\mathbf{1} \right\| \|\boldsymbol{\eta} - \boldsymbol{\beta}\| \left[m_{\mathrm{r}} \frac{\boldsymbol{\eta} - \boldsymbol{\beta}}{\|\boldsymbol{\eta} - \boldsymbol{\beta}\|} - \boldsymbol{\beta} \right]$.

5.1.2 Yield function for unsaturated soil based on rotational hardening and subloading surface concepts

Dafalias (1986) proposed yield function base on the rotational hardening concept which can be written in $p - q$ space as

$$f = \frac{(q - p'\beta)^2}{M^2 - \beta^2} + p''(p'' - p_{\mathrm{c}}) = 0 \tag{5.3}$$

where β is a rotational hardening variable ($\beta = \sqrt{\frac{3}{2}}\|\boldsymbol{\beta}\|$) and p_{c} is the preconsolidation pressure including the isotropic hardening law. In case of $\beta = 0$, which means that there is no rotation of yield surface, Equation (5.3) becomes

$$f = \frac{q^2}{M^2} + p'(p' - p_{\mathrm{c}}) = 0 \tag{5.4}$$

which is the modified Cam clay yield function (Roscoe and Burland, 1968) used to formulate the isotropic hardening model proposed in Chapter 2. The advantage of yield function proposed by Dafalias (1986) is that yield surface follows the critical state concept even though the shape of

yield surface is distorted and yield surface rotates around the origin of stress space, i.e., yield surface is distorted and rotated by an increase in the rotational hardening variable β but it cannot be rotated over the critical state line (*M*-line), and yield surface always intersect with the critical state line (*M*-line) at the maximum value of q on yield surface ($\frac{\partial f}{\partial \boldsymbol{p'}} = 0$) as shown in Figure 5.1. Figure 5.1 shows the distorted yield surface and the rotation of yield surface as an increase in the rotational hardening variable β. The arrows in Figure 5.1 are perpendicular to the yield surface ($f = 0$), which $\frac{\partial f}{\partial \boldsymbol{p''}} = 0$ at the vertical arrows and $\frac{\partial f}{\partial q} = 0$ at the horizontal arrows.

As $q = \sqrt{\frac{3}{2}}\|\boldsymbol{s}\|$ and $\beta = \sqrt{\frac{3}{2}}\|\boldsymbol{\beta}\|$, Equation (5.3) can be rewritten in three-dimensional stress space as

$$f = \frac{3}{2}\frac{\|\boldsymbol{s} - p'\boldsymbol{\beta}\|^2}{M^2 - \frac{3}{2}\|\boldsymbol{\beta}\|^2} + p'(p' - p_c) = 0. \tag{5.5}$$

Substituting $\boldsymbol{\eta} = \frac{\boldsymbol{s}}{p''}$ and $m_d = \sqrt{\frac{2}{3}}M$, which m_d is the function of stress ratio in critical state *M*, into Equation (5.5), we get

$$f = \frac{\|\boldsymbol{\eta} - \boldsymbol{\beta}\|^2}{m_d^2 - \|\boldsymbol{\beta}\|^2} + 1 - \frac{p_c}{p'} = 0. \tag{5.6}$$

Taking the natural logarithms of Equation (5.6), we get

$$f = \ln\frac{p'}{p_c} + \ln\left\{1 + \frac{\|\boldsymbol{\eta} - \boldsymbol{\beta}\|^2}{m_d^2 - \|\boldsymbol{\beta}\|^2}\right\} = 0. \tag{5.7}$$

The hardening law as described in preconsolidation pressure p_c can be expressed as

$$p_c = p_0' \exp\left(\frac{v_0}{\lambda - \kappa}\varepsilon_v^p\right). \tag{5.8}$$

By substituting Equation (5.8) into Equation (5.7), we get

$$f = \frac{\lambda - \kappa}{v_0}\left[\ln\frac{p'}{p_0'} + \ln\left\{1 + \frac{\|\boldsymbol{\eta} - \boldsymbol{\beta}\|^2}{m_d^2 - \|\boldsymbol{\beta}\|^2}\right\}\right] - \varepsilon_v^p. \tag{5.9}$$

To consider the effect of degree of saturation and the effect of specific volume on the unsaturated soil behaviors, the movement of state boundary surface variable Ψ and the subloading surface variable Ω as proposed in Chapter 2 are applied to yield function in Equation (5.9), we finally get the yield function for unsaturated soil based on rotational hardening and subloading surface concepts as

$$f = \frac{\lambda - \kappa}{v_0}\left[\ln\frac{p''}{p_0''} + \ln\left\{1 + \frac{\|\boldsymbol{\eta} - \boldsymbol{\beta}\|^2}{m_d^2 - \|\boldsymbol{\beta}\|^2}\right\}\right] - \frac{\Psi - \Psi_0}{v_0} + \frac{\Omega - \Omega_0}{v_0} - \varepsilon_v^p. \tag{5.10}$$

5.1.3 Elastoplastic stress–strain relationship based on rotational hardening and subloading surface concepts

Regarding the consistency conditions, taking the time derivative of the yield function $f\left(\boldsymbol{\sigma}'', \boldsymbol{\beta}, \Psi, \Omega, \varepsilon_{\mathrm{v}}^{\mathrm{p}}\right)$ given by Equation (5.10), we get the consistency condition as

$$\dot{f} = \frac{\partial f}{\partial \boldsymbol{\sigma}''} : \dot{\boldsymbol{\sigma}''} + \frac{\partial f}{\partial \boldsymbol{\beta}} : \dot{\boldsymbol{\beta}} + \frac{\partial f}{\partial \Psi}\dot{\Psi} + \frac{\partial f}{\partial \Omega}\dot{\Omega} + \frac{\partial f}{\partial \varepsilon_{\mathrm{v}}^{\mathrm{p}}}\dot{\varepsilon}_{\mathrm{v}}^{\mathrm{p}} = 0. \tag{5.11}$$

Substituting an associated flow as shown in Equation (2.31) and the evolution laws of $\boldsymbol{\beta}$, Ψ and Ω, given by Equations (5.2), (2.22) and (2.24), respectively, into Equation (5.11), we get

$$\frac{\partial f}{\partial \boldsymbol{\sigma}''} : \dot{\boldsymbol{\sigma}''} + \frac{\partial f}{\partial \boldsymbol{\beta}} : \langle \dot{\Lambda} \rangle \boldsymbol{A} + \frac{\psi}{v_0}\dot{S}_{\mathrm{r}} - \omega\Omega|\Omega|\langle \dot{\Lambda} \rangle \left\| \frac{\partial f}{\partial \boldsymbol{\sigma}''} \right\| - \langle \dot{\Lambda} \rangle \frac{\partial f}{\partial \boldsymbol{\sigma}''} : \mathbf{1} = 0. \tag{5.12}$$

Thus, we get the rate of the plastic multiplier from Equations (5.12) and (2.37) as follows.

$$\langle \dot{\Lambda} \rangle = \left\langle \frac{\frac{\partial f}{\partial \boldsymbol{\sigma}''} : \boldsymbol{D}^{\mathrm{e}} : \dot{\boldsymbol{\varepsilon}} + \frac{\psi}{v_0}\dot{S}_{\mathrm{r}}}{\frac{\partial f}{\partial \boldsymbol{\sigma}''} : \mathbf{1} - \frac{\partial f}{\partial \boldsymbol{\beta}} : \boldsymbol{A} + \omega\Omega|\Omega| \left\| \frac{\partial f}{\partial \boldsymbol{\sigma}''} \right\| + \frac{\partial f}{\partial \boldsymbol{\sigma}''} : \boldsymbol{D}^{\mathrm{e}} : \frac{\partial f}{\partial \boldsymbol{\sigma}''}} \right\rangle \tag{5.13}$$

where $\frac{\partial f}{\partial \boldsymbol{\sigma}''} : \mathbf{1} - \frac{\partial f}{\partial \boldsymbol{\beta}} : \boldsymbol{A} + \omega\Omega|\Omega| \left\| \frac{\partial f}{\partial \boldsymbol{\sigma}''} \right\|$ is the hardening parameter H of the proposed model.

Finally, we get the rate form of the elastoplastic stress–strain relationship from Equations (2.13), (2.18), (2.31), and (5.13).

$$\dot{\boldsymbol{\sigma}''} = \boldsymbol{D}^{\mathrm{e}} : \dot{\boldsymbol{\varepsilon}} - \left\langle \frac{\frac{\partial f}{\partial \boldsymbol{\sigma}''} : \boldsymbol{D}^{\mathrm{e}} : \dot{\boldsymbol{\varepsilon}} + \frac{\psi}{v_0}\dot{S}_{\mathrm{r}}}{\frac{\partial f}{\partial \boldsymbol{\sigma}''} : \mathbf{1} - \frac{\partial f}{\partial \boldsymbol{\beta}} : \boldsymbol{A} + \omega\Omega|\Omega| \left\| \frac{\partial f}{\partial \boldsymbol{\sigma}''} \right\| + \frac{\partial f}{\partial \boldsymbol{\sigma}''} : \boldsymbol{D}^{\mathrm{e}} : \frac{\partial f}{\partial \boldsymbol{\sigma}''}} \right\rangle \boldsymbol{D}^{\mathrm{e}} : \frac{\partial f}{\partial \boldsymbol{\sigma}''} \tag{5.14}$$

When the rate of the plastic multiplier $\dot{\Lambda}$ is positive, the rate form of the elastoplastic stress–strain relationship can be expressed in the similar manner as shown in Equation (2.40) as

$$\dot{\boldsymbol{\sigma}''} = \boldsymbol{D}^{\mathrm{ep}} : \dot{\boldsymbol{\varepsilon}} - \boldsymbol{D}^{\mathrm{Sr}}\dot{S}_{\mathrm{r}} \tag{5.15}$$

where $\boldsymbol{D}^{\mathrm{ep}}$ and $\boldsymbol{D}^{\mathrm{Sr}}$ are defined as follows.

$$\boldsymbol{D}^{\mathrm{ep}} = \boldsymbol{D}^{\mathrm{e}} - \frac{\boldsymbol{D}^{\mathrm{e}} : \frac{\partial f}{\partial \boldsymbol{\sigma}''} \otimes \frac{\partial f}{\partial \boldsymbol{\sigma}''} : \boldsymbol{D}^{\mathrm{e}}}{\frac{\partial f}{\partial \boldsymbol{\sigma}''} : \mathbf{1} - \frac{\partial f}{\partial \boldsymbol{\beta}} : \boldsymbol{A} + \omega\Omega|\Omega| \left\| \frac{\partial f}{\partial \boldsymbol{\sigma}''} \right\| + \frac{\partial f}{\partial \boldsymbol{\sigma}''} : \boldsymbol{D}^{\mathrm{e}} : \frac{\partial f}{\partial \boldsymbol{\sigma}''}} \tag{5.16}$$

$$\boldsymbol{D}^{\mathrm{Sr}} = \frac{\boldsymbol{D}^{\mathrm{e}} : \frac{\partial f}{\partial \boldsymbol{\sigma}''}\frac{\psi}{v_0}}{\frac{\partial f}{\partial \boldsymbol{\sigma}''} : \mathbf{1} - \frac{\partial f}{\partial \boldsymbol{\beta}} : \boldsymbol{A} + \omega\Omega|\Omega| \left\| \frac{\partial f}{\partial \boldsymbol{\sigma}''} \right\| + \frac{\partial f}{\partial \boldsymbol{\sigma}''} : \boldsymbol{D}^{\mathrm{e}} : \frac{\partial f}{\partial \boldsymbol{\sigma}''}} \tag{5.17}$$

Rate forms of the stress-strain relationship under various testing conditions (e.g., fully drained condition, constant water content condition, and fully undrained condition) are proposed in the Appendix.

Table 5.1 Parameters of unsaturated sample for stress–strain characteristics

Parameters	sample	Descriptions
λ	0.123	Compression index
κ	0.022	Swelling index
M	1.5	Stress ratio in critical state
ν_{e}	0.3	Poisson's ratio
N	1.90	Reference specific volume on the state boundary surface under $p'' = p_{\mathrm{a}}$, $q = 0$, and $S_{\mathrm{r}} = 1$
ω	90.0	Effect of density
ψ	0.90	Effect of S_{r} on the position of the state boundary surface
b_{r}	200.0	Rotational rate of yield surface
m_{r}	0.82	Limit of rotation

Table 5.2 Parameters of unsaturated sample for water retention curves

Parameters	sample	Descriptions
$S_{\max}$	1.0	Parameters for main wetting and drying curves described by van Genuchten's SWCC equation
$S_{\min}$	0.20	
α^{d} (1/kPa)	0.04	
α^{w} (1/kPa)	2.00	
n	1.724	
m	0.42	
ξ_{h}	10.0	Influence of suction histories
ξ_{e}	2.5	Influence of void ratio
e_{ref}	0.90	Reference void ratio

5.2 SIMULATION RESULTS OBTAINED FROM NEW ELASTOPLASTIC CONSTITUTIVE MODEL FOR UNSATURATED SOILS

To reveal the performance of extension of the constitutive model for unsaturated soils to anisotropy, the simulation results calculated by using the proposed model are discussed here.

In this chapter, all the analyses were calculated by using the parameters for stress-strain characteristics and water retention curves as shown in Tables 5.1 and 5.2, respectively. All simulations were also performed on unsaturated samples with the initial void ratio of 1.05 and the initial degree of saturation of 90% at a net confining pressure of 20 kPa ($e_0 = 1.05$, $S_{\mathrm{r0}} = 90\%$, and $\sigma_{\mathrm{c}}^{\mathrm{net}} = 20$ kPa).

5.2.1 The simulations of triaxial tests on unsaturated soils

A series of simulations of triaxial tests on unsaturated soils under various testing conditions (i.e., drained water & exhausted air conditions, undrained water & exhausted air conditions, and undrained water & unexhausted air conditions) was performed to assure that the

proposed model with rotational hardening follows the critical state theory.

Firstly, the simulations of triaxial monotonic loading tests under various testing conditions (i.e., drained water & exhausted air conditions, undrained water & exhausted air conditions, and undrained water & unexhausted air conditions) were performed on the unsaturated samples. Figure 5.2 shows the stress paths of triaxial monotonic loading tests under various testing conditions. The simulation results show that all unsaturated samples were successfully reached to the unique critical state stress ratio line.

Secondly, the simulations of stress-controlled triaxial cyclic loading tests under fully undrained condition and subsequent strain-controlled triaxial monotonic loading tests under various testing conditions (i.e., drained water & exhausted air conditions, undrained water & exhausted air conditions, and undrained water & unexhausted air conditions) were performed on the unsaturated samples. Figure 5.3 shows the stress paths of triaxial cyclic loading under fully undrained condition and subsequent triaxial monotonic loading tests under various testing conditions. The simulation results show that all unsaturated samples were successfully reached to the unique critical state stress ratio line.

Regarding all simulation results, the extension of the constitutive model for unsaturated soils to anisotropy is able to satisfy the critical state concept as all unsaturated samples with the same initial condition, which were subjected to complex loading conditions under various testing conditions, was finally approached to the unique critical state stress ratio line.

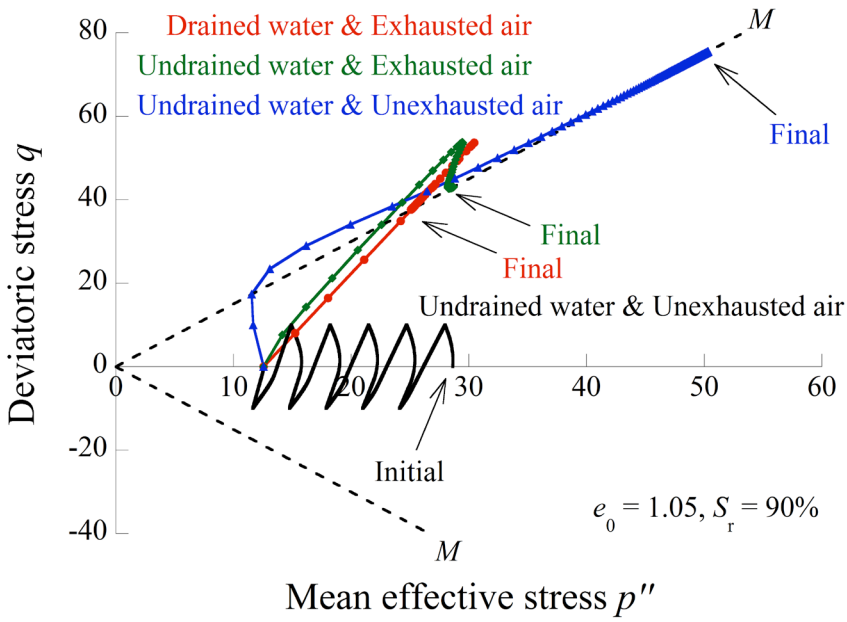

Figure 5.2 The simulation results of triaxial monotonic loading tests under various testing conditions

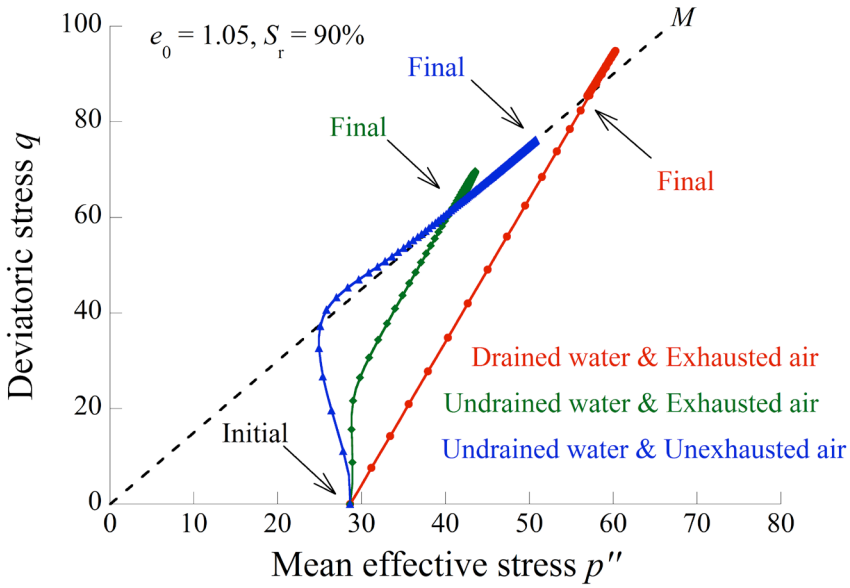

Figure 5.3 The simulation results of triaxial cyclic loading under fully undrained condition and subsequent triaxial monotonic loading tests under various testing conditions

5.2.2 The simulations of stress-controlled cyclic triaxial tests on unsaturated soils under fully undrained condition

To verify the performance of the extension of the constitutive model for unsaturated soils to anisotropy on the cyclic behavior of unsaturated soils, the simulations of stress-controlled cyclic triaxial tests on unsaturated soils under fully undrained conditions were performed by using the proposed model including rotational hardening and then comparing with the simulation results obtained from the model without rotational hardening proposed in Chapter 2. In the simulations, the same initial condition of unsaturated samples (e_0 = 1.05, S_{r0} = 90%, and σ_c^{net} = 20 kPa) was set for both model with rotational hardening and model without rotational hardening. Then, the deviatoric stress controlled cyclic shearing, as shown in Figure 5.4, was applied to the unsaturated samples under fully undrained conditions at a constant net confining pressure.

Figures 5.5 and 5.6 show the simulation results of stress-controlled triaxial cyclic loading tests under fully undrained conditions obtained from the model without rotational hardening and the proposed model with rotational hardening, respectively. Both simulation results show that unsaturated soil samples lost their mean effective stresses during cyclic loading at the beginning of the simulations and finally exhibited the cyclic mobility. However, the stress paths showing the cyclic mobility of unsaturated soils obtained from both models were rather different as shown in Figures 5.7 and 5.8 for the model without rotational hardening and the proposed model with rotational hardening, respectively.

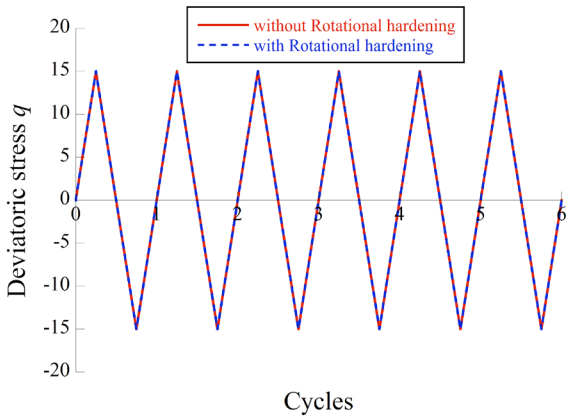

Figure 5.4 Time history of deviatoric stress during cyclic loading

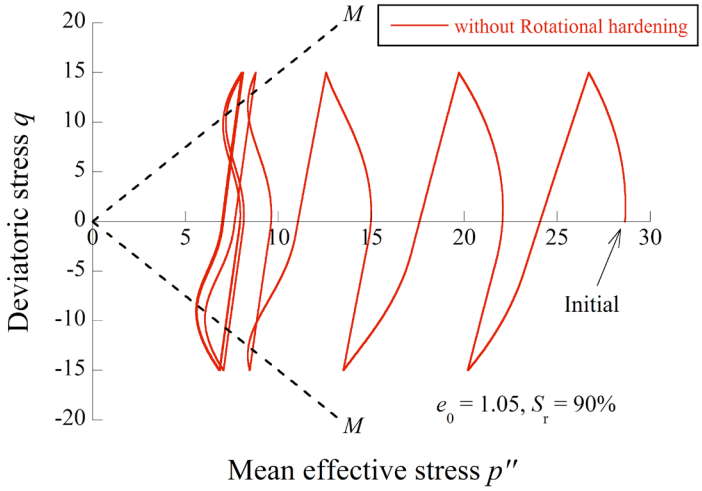

Figure 5.5 The simulation results of triaxial cyclic loading tests under fully undrained conditions (without Rotational Hardening)

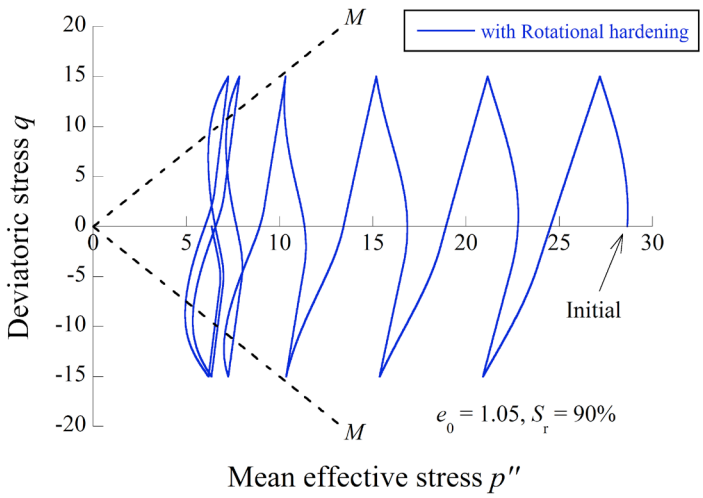

Figure 5.6 The simulation results of triaxial cyclic loading tests under fully undrained conditions (with Rotational Hardening)

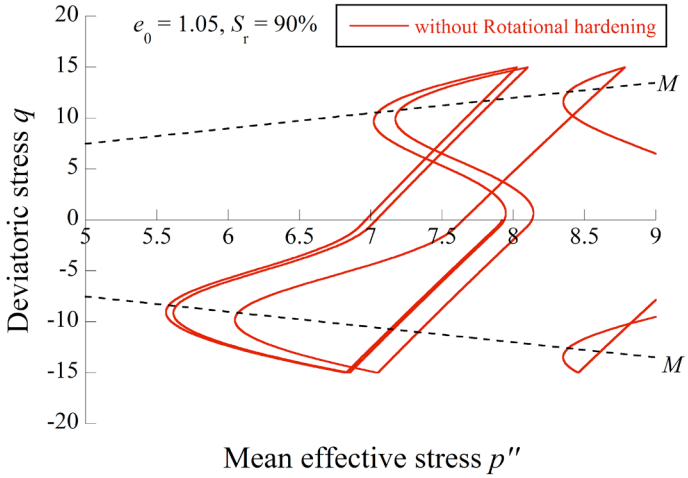

Figure 5.7 The simulation results at the final loading cycle of triaxial cyclic loading tests under fully undrained conditions (without Rotational Hardening)

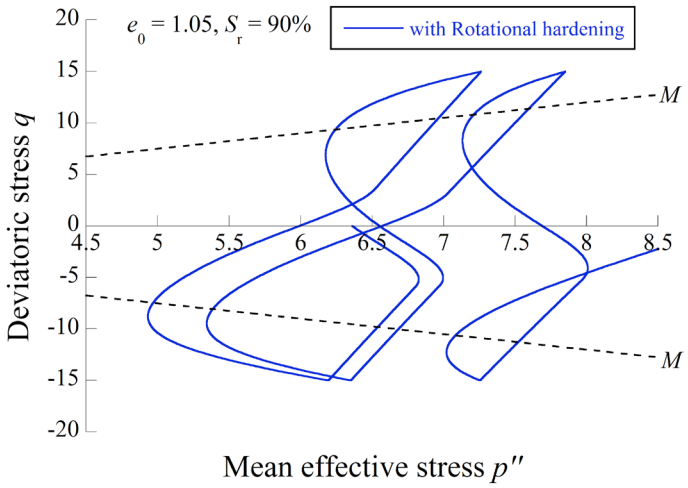

Figure 5.8 The simulation results at the final cycles of triaxial cyclic loading tests under fully undrained conditions (with Rotational Hardening)

The stress paths of unsaturated samples obtained from the model without rotational hardening (see Figure 5.7) exhibited the unrealistic behavior as unsaturated samples showed only elastic behaviors during unloading paths, while the stress paths of unsaturated samples obtained from the proposed model with rotational hardening (see Figure 5.8) showed more natural cyclic behavior as the cyclic mobility was clearly seen and unsaturated samples exhibited elastoplastic behaviors during unloading paths. This is because the stress paths were only inside the yield surface during unloading paths in the model without rotational hardening. Therefore, the results were only based on elastic behaviors following the assumption of the elastoplastic theory. While the results of the proposed model were able to show elastoplastic behavior during unloading paths

because the unloading paths from one side of the yield surface were only inside the yield surface at the beginning, then, reached to another side of yield surface within the unloading process as the yield surface rotated due to an increased in plastic deviatoric strain (see Figure 5.1 for the rotation of yield surface). Figure 5.9 shows the stress paths with their corresponding norm of plastic strain obtained from the models with and without rotational hardening.

To conclude, an extension of the constitutive model for unsaturated soils to anisotropy is able to predict the realistic cyclic behavior of unsaturated soils as the stress paths due to cyclic loading (or cyclic mobility) were well predicted and the elastoplastic behavior could be simulated in the unloading processes.

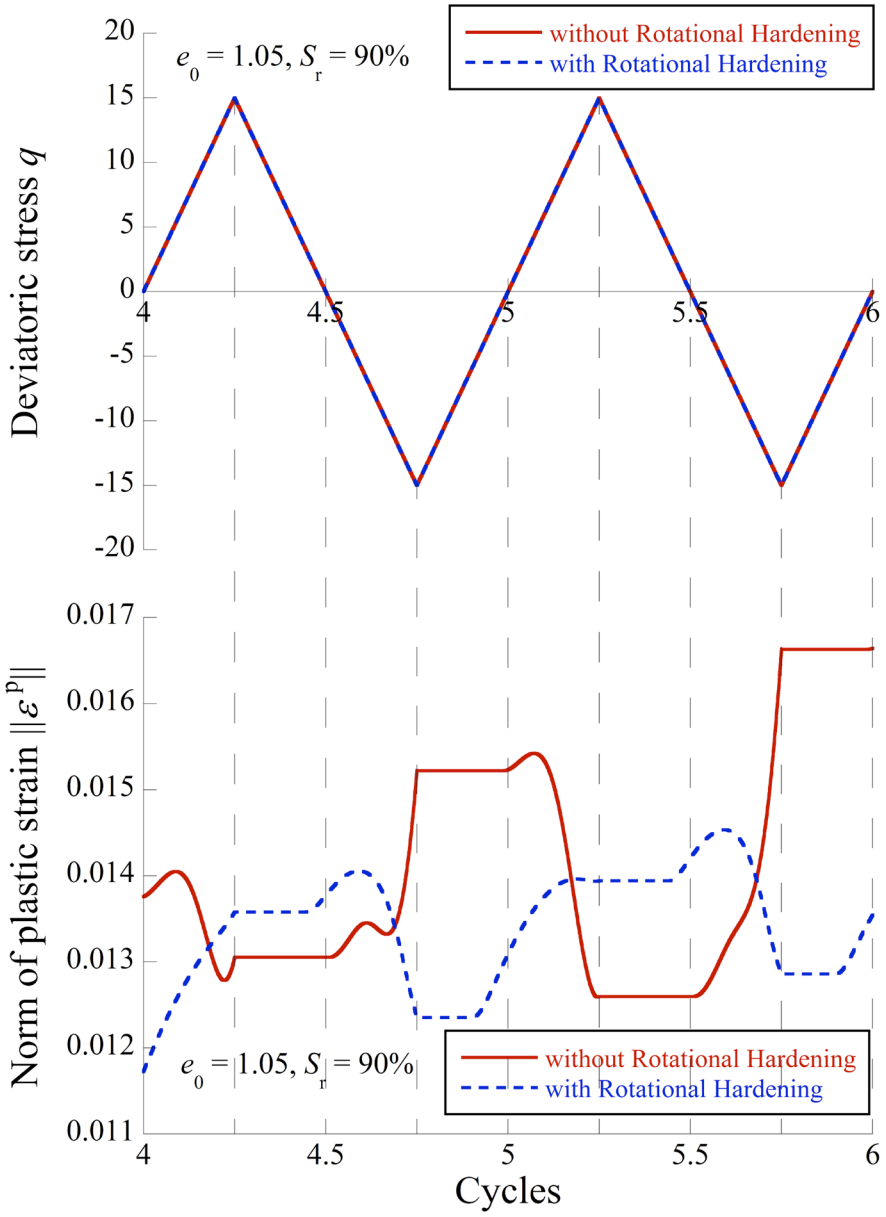

Figure 5.9 Time histories of deviatoric stress and norm of plastic strain obtained from the simulation results of triaxial cyclic loading tests under fully undrained conditions

5.3 CONCLUSIONS

This chapter presented an extension of the constitutive model for unsaturated soils to anisotropy. This proposed model is modified from the model described in Chapter 2 by incorporating the rotational hardening concept (Hashiguchi and Chen, 1998) as well as the critical state soil model for rotational hardening (Dafalias, 1986).

Regarding the simulation results, an extension of the constitutive model for unsaturated soils to anisotropy is able to satisfy the critical state concept as the unique critical state stress ratio is proved through the simulations of triaxial tests on unsaturated soils under complex loading and testing conditions. Moreover, the stress paths due to cyclic loading (cyclic mobility) were well predicted, and the elastoplastic behavior could be simulated in the unloading processes.

CHAPTER 6

CONCLUDING REMARKS AND FUTURE RESEARCH

This dissertation investigated the factors that play an important role on the hydraulic collapse behavior and the cyclic behavior of unsaturated soils, as well as proposed the elastoplastic constitutive model for predicting the anisotropy of unsaturated soils. In this final chapter, the substantive findings and the novelty of this research are summarized, and the prospects for the future research are discussed.

6.1 CONTRIBUTIONS

The key findings and the novelty of this dissertation are summarized as follows.

To begin with the hydraulic collapse behavior of unsaturated soils, the hydraulic collapse behavior of unsaturated soils was studied through the simulations. The simulation results showed that the density, mean net stress and deviatoric stress affected the hydraulic collapse behavior of unsaturated soils. Regarding to isotropic condition, the hydraulic collapse potential decreased with an increase in density; and the hydraulic collapse potential increased as the mean net stress increased until reaching to the certain mean net stress level, then, the hydraulic collapse potential decreased as the mean net stress increased. Regarding to anisotropic condition, the soaking induced deviatoric strain and the soaking induced volumetric strain decreased as the density increased; and the soaking induced deviatoric strain increased and the soaking induced volumetric strain decreased as the deviatoric stress increased. The soaking history also had a significant influence on the hydraulic collapse behavior of unsaturated soils. The hydraulic collapse potential, the soaking induced deviatoric strain, and the soaking induced volumetric strain decreased significantly if unsaturated soils had experienced first soaking. Moreover, the soaking induced instability of unsaturated soils was explained through the simulations by using the hardening parameter.

Secondly, the cyclic behavior of unsaturated soils was studied and discussed through the simulations of fully undrained cyclic triaxial tests. The liquefaction phenomenon of unsaturated soils was well reproduced the proposed elastoplastic constitutive model for unsaturated soils. The simulation results showed that the density, effective confining pressure and degree of saturation affected the cyclic strength of unsaturated soils. Among various factors, the degree of saturation had a significant effect on the liquefaction resistance of unsaturated soils. Unsaturated soils with a low degree of saturation and low void ratio had high cyclic strength. Moreover, the cyclic strength

of unsaturated soils increased with the total confining pressure.

Finally, an extension of the elastoplastic constitutive model for unsaturated soils to anisotropy by incorporating rotational hardening was proposed. The cyclic mobility of unsaturated soils, which is the effect of anisotropy on unsaturated soil behaviors, was well predicted.

6.2 FUTURE RESEARCH

In this dissertation, the unsaturated soil behaviors were discussed through the simulation results by using the proposed elastoplastic constitutive model for unsaturated soils. In the future, the initial / boundary value problems of unsaturated reclaimed ground under earthquake-induced cyclic loading will be solved by using a finite element method based on the critical state model for unsaturated soils proposed in this study. Thus, I expect to obtain information about the effect of cyclic loading on unsaturated soil layers in practical situations.

REFERENCES

Alonso, E. E., Gens, A. & Josa, A. (1990). A constitutive model for partially saturated soils. *Geotechnique* **40**, No. 3, 405–430.

Been, K. & Jefferies, M. (1985). A state parameter for sands. *Geotechnique* **35**, No.2, 99–112.

Bishop, A. W. (1959). The principal of effective stress. *Teknisk Ukeblad* **106**, No.39, 859–863.

Borja, R. I. (2006). On the mechanical energy and effective stress in saturated and unsaturated continua. *International Journal of Solids and Structures* **43**, 1764-1786.

Brooks, R. H. & Corey, A. T. (1964). Hydraulic properties of porous media. *Hydrology Paper*, No. 3, Colorado State University, Fort Collins, Colorado.

Dafalias, Y. F. (1986). An anisotropic critical state soil plasticity model. *Mechanics Research Communications* **13**, No. 6, 341–347.

Dafalias, Y. F. & Taiebat, M. (2013). Anatomy of rotational hardening in clay plasticity. *Geotechnique* **63**, No. 16, 1406–1418.

Fredlund, D. G. & Xing, A. (1994). Equation for the soil–water characteristic curve. *Canadian Geotechnical Journal* **31**, No.3, 521–532.

Gallipoli, D., Gens, A., Sharma, R. & Vaunat, J. (2003). An elasto-plastic model for unsaturated soil incorporating the effects of suction and degree of saturation on mechanical behaviour. *Geotechnique* **53**, No. 1, 123–135.

Gallipoli, D., Wheeler, S. J. & Karstunen M. (2003a). Modelling the variation of degree of saturation in a deformable unsaturated soil. *Geotechnique* **53**, No. 1, 105–112.

Gardner, W. R. (1958). Some steady state solutions of the unsaturated moisture flow equation with application to evaporation from a water table. *Soil Science Journal* **85**, No.4, 228–232.

Gens, A. (1996). Constitutive modelling: application to compacted soils. *Proceedings of the first international conference on unsaturated soils*, Paris, 1179-1200.

Haines, W. B. (1930). Studies in the physical properties of soil. V. The hysteresis effect in capillary properties, and the modes of moisture distribution associated therewith. *The Journal of Agricultural Science* **20**, No.1, 97–116.

Hashiguchi, K. & Chen, Z. -P. (1998). Elastoplastic constitutive equation of soils with the subloading surface and the rotational hardening. *International Journal for Numerical and Analytical Methods in Geomechanics* **22**, 197–227.

Hashiguchi, K. & Ueno, M. (1977). Elastoplastic constitutive laws of granular material. *Proceedings of the 9th International Conference on Soil Mechanics and Foundation*

Engineering, Tokyo, 73–82.

Honda, M. (2000). *PhD Thesis*, Kobe university, Japan. (in Japanese).

Houston, S. L., Houston, W. N. & Spadola, D. J. (1988). Prediction of field collapse of soils due to wetting. *Journal of Geotechnical Engineering* **114**, No.1, 40–58.

Huang, H. C., Tan, Y. C., Liu, C. W. & Chen, C. H. (2005). A novel hysteresis model in unsaturated soils. *Hydrological Process* **19**, No.8, 1653–1665.

Ishihara, K., Tsukamoto, Y. & Kamada, K. (2004). Undrained behaviour of near-saturated sand in cyclic and monotonic loading. *Proceedings of the International Conference on Cyclic Behavior of Soils and Liquefaction Phenomena*, Bochum, 27–39.

Jennings, J. E. B. & Burland, J. B. (1962). Limitations to the use of effective stresses in partly saturated soils. *Geotechnique* **12**, No.2, 125-144.

Kato, S. & Kawai, K. (2000). Deformation characteristics of a compacted clay in collapse under isotropic and triaxial stress state. *Soils and foundations* **40**, No.5, 75-90.

Kazama, M., Yamaguchi, A. & Yanagisawa, E. (2000). Liquefaction resistance from a ductility viewpoint. *Soils and Foundations* **40**, No.6, 47–60.

Khalili, N., Habte, M. A. & Zargarbashi, S. (2008). A fully coupled flow deformation model for cyclic analysis of unsaturated soils including hydraulic and mechanical hystereses. *Computers and Geotechnics* **35**, No.6, 872–889.

Kikumoto, M., Kyokawa, H., Nakai, T. & Shahin, H. M. (2010). A simple elasto–plastic model for unsaturated soils and interpretations of collapse and compaction behaviours. *Proceedings of the 5th International Conference on Unsaturated Soils*, Barcelona, 849–855.

Konagai, K., Kiyota, T., Suyama, S., Asakura, T., Shibuya, K. & Eto, C. (2013). Maps of soil subsidence for Tokyo bay shore areas liquefied in the March 11th, 2011 off the Pacific Coast of Tohoku Earthquake. *Soil Dynamics and Earthquake Engineering* **53,** 240–253.

Komolvilas, V. & Kikumoto, M. (2017). Simulation of liquefaction of unsaturated soil using critical state soil model. *International Journal for Numerical and Analytical Methods in Geomechanics*, DOI: 10.1002/nag.2669.

Kuhn, H. W. & Tucker, A. W. (1951). Nonlinear programming. *Proceedings of 2nd Berkeley Symposium*, University of California Press, Berkeley, 481-492.

Lawton, E. C., Fragaszy, R. J. & Hetherington, M. D. (1992). Review of wetting- induced collapse in compacted soil. *Journal of Geotechnical Engineering* **118**, No.9, 1376–1394.

Liu, C. & Muraleetharan, K. K. (2012a). Coupled Hydro–Mechanical Elastoplastic Constitutive Model for Unsaturated Sands and Silts. I: Formulation. *International Journal of*

Geomechanics **12**, No.3, 239–247.

Liu, C., & Muraleetharan, K. K. (2012b). Coupled Hydro–Mechanical Elastoplastic Constitutive Model for Unsaturated Sands and Silts. II: Integration, Calibration, and Validation. *International Journal of Geomechanics* **12**, No.3, 248–259.

Liu, C. & Xu, J. (2013). Experimental Study on Effects of Initial Conditions on Liquefaction of Saturated and Unsaturated Sand. *International Journal of Geomechanics* **15**, No.6.

Milatz, M., Törzs, T. & Grabe, J. (2016). Settlements in unsaturated granular soils induced by changes in saturation and suction. *Proceedings of the 3rd European Conference on Unsaturated Soils*, E3S Web of Conferences **9**, No.14009, Paris, 1–7.

Okamura, M. & Noguchi, K. (2009). Liquefaction resistances of unsaturated non-plastic silt. *Soils and Foundations* **49**, No.2, 221–229.

Okamura, M. & Soga, Y. (2006). Effects of Pore Fluid Compressibility on Liquefaction Resistance of Partially Saturated Sand. *Soils and Foundations* **46**, No.5, 695–700.

Rao, S. M. & Revanasiddappa, K. (2006). Influence of cyclic wetting drying on collapse behaviour of compacted residual soil. *Geotechnical and Geological Engineering* **24**, No.3, 725–734.

Roscoe, K. H. & Burland, J. B. (1968). On the generalised stress–strain behaviour of "wet" clay. *Engineering plasticity*, Cambridge University Press, 535–609.

Schrefler, B. A. (1984). The finite element method in soil consolidation (with applications to surface subsidence). *PhD Thesis*, University College of Swansea, Wales.

Sekiguchi, H. & Ohta, K. (1977). Induced anisotropy and time dependence in clays. *Proceedings of the 9th International Conference on Soil Mechanics and Foundation Engineering*, Tokyo, 229–238.

Selim, A. A. & Burak, G. (2006). Cyclic Stress–Strain Behavior of Partially Saturated Soils. *Proceedings of the 4th International Conference on Unsaturated Soils*, Arizona, 497–507.

Sivakumar, V. (1993). A critical state framework for unsaturated soil. *PhD Thesis*, University of Sheffield, England.

Sun, D. A., Sheng, D. & Xu, Y. (2007). Collapse behaviour of unsaturated compacted soil with different initial densities. *Canadian Geotechnical Journal* **44**, No.6, 673-686.

Tadepalli, R. & Fredlund, D. G. (1991). The collapse behavior of a compacted soil during inundation. *Canadian Geotechnical Journal* **28**, No.4, 477-488.

Tarantino, A. & Tombolato, S. (2005). Coupling of hydraulic and mechanical behaviour in unsaturated compacted clay. *Geotechnique* **55**, No.4, 307–317.

Topp, G. C & Miller, E. E. (1966). Hysteretic moisture characteristics and hydraulic conductivities

for glass–bead media. *Soil Science Society of America Journal* **30**, No.2, 156–162.

Tsukamoto, Y., Kawabe, S., Matsumoto, J. & Hagiwara, S. (2014). Cyclic resistance of two unsaturated silty sands against soil liquefaction. *Soils and Foundations* **54**, No.6, 1094–1103.

Unno, T., Kazama, M., Uzuoka, R. & Sento, N. (2008). Liquefaction of unsaturated sand considering the pore air pressure and volume compressibility of the soil particle skeleton. *Soils and Foundations* **48**, No.1, 87–99.

Unno, T., Kazama, M., Sento, N. & Uzuoka, R. (2006). Cyclic shear behavior of unsaturated volcanic sandy soil under various suction conditions. *Proceedings of the 4th International Conference on Unsaturated Soils*, Arizona, 1133–1144.

Unno, T., Uzuoka, R., Sento, N. & Kazama, M. (2013). Pore air pressure effect on cyclic shear behavior of undrained sandy soil. *Journal of Japan Society of Civil Engineers* **69**, No.3, 386–403.

van Genuchten, M. T. (1980). A closed form equation for predicting the hydraulic conductivity of unsaturated soil. *Soil Science Society of America Journal* **44**, No.5, 892–898.

Wheeler, S. J. & Sivakumar, V. (1995). An elasto-plastic critical state framework for unsaturated soil. *Geotechnique* **45**, No.1, 35–53.

Wheeler, S. J., Sharma, R. J. & Buisson, M. S. R. (2003). Coupling of hydraulic hysteresis and stress–strain behaviour in unsaturated soils. *Geotechnique* **53**, No. 1, 41–54.

Yang, C., Cui, Y. J., Pereira, J. M. & Huang, M. S. (2008). A constitutive model for unsaturated cemented soils under cyclic loading. *Computers and Geotechnics* **35**, No.6, 853–859.

RESEARCH PUBLICATIONS

1) Komolvilas, V. & Kikumoto, M. (2016). Fully undrained cyclic loading simulation on unsaturated soils using an elastoplastic model for unsaturated soils. *Proceedings of the 3rd European Conf. on unsaturated soils (E-UNSAT 2016)*, E3S Web of Conferences Volume 9, Article number 17008, Paris, France. DOI: 10.1051/e3sconf/20160917008.
2) Komolvilas, V. & Kikumoto, M. (2017). Simulation of liquefaction of unsaturated soil using critical state soil model. *International Journal for Numerical and Analytical Methods in Geomechanics*, Volume 41, Issue 10, 1217-1246. DOI: 10.1002/nag.2669.
3) Komolvilas, V. & Kikumoto, M. (2017). A series of fully undrained cyclic loading simulation on unsaturated soils using an elastoplastic model for unsaturated soils. *Proceedings of 19th International Conference on Soil Mechanics and Geotechnical Engineering*, Seoul, Korea.

APPENDIX

A.1 RATE FORM OF THE STRESS–STRAIN RELATIONSHIP

The elastoplastic constitutive model proposed in Chapter 2 and Chapter 5 are capable of describing the behavior of unsaturated soils under various testing conditions, for example, fully drained condition, constant water content condition, and fully undrained condition. The constitutive equations of the proposed model are presented herein.

First, substituting the time derivative of effective stress tensor for unsaturated soils, as shown in Equation (2.2), into Equation (2.40) or Equation (5.15) gives

$$\dot{\boldsymbol{\sigma}}^{\mathrm{net}} + S_{\mathrm{r}}\mathbf{1}\dot{s} + s\mathbf{1}\dot{S}_{\mathrm{r}} = \boldsymbol{D}^{\mathrm{ep}}{:}\dot{\boldsymbol{\varepsilon}} - \boldsymbol{D}^{\mathrm{Sr}}\dot{S}_{\mathrm{r}} \qquad (\mathrm{A}-1)$$

where $\dot{\boldsymbol{\sigma}}^{\mathrm{net}}$ and $\dot{s}$ are the rate of Cauchy's net stress tensor and suction, respectively. Assuming incompressibility of soil particles, we obtain $\dot{e} = -v_0\mathbf{1}{:}\,\dot{\boldsymbol{\varepsilon}}$. Substituting this into Equation (2.12), we obtain

$$\dot{S}_{\mathrm{r}} = \frac{\frac{\partial S_{\mathrm{r}}}{\partial s}\dot{s} - \frac{\partial S_{\mathrm{r}}}{\partial e}v_0\mathbf{1}{:}\,\dot{\boldsymbol{\varepsilon}}}{1 - \frac{\partial S_{\mathrm{r}}}{\partial I_{\mathrm{h}}}\frac{\mathrm{d}I_{\mathrm{h}}}{\mathrm{d}S_{\mathrm{r}}}} \qquad (\mathrm{A}-2)$$

Substituting the rate of the degree of saturation $\dot{S}_{\mathrm{r}}$ into Equation (A-1) gives

$$\dot{\boldsymbol{\sigma}}^{\mathrm{net}} = \boldsymbol{D}^{\mathrm{ep}}{:}\dot{\boldsymbol{\varepsilon}} - S_{\mathrm{r}}\mathbf{1}\dot{s} - (\boldsymbol{D}^{\mathrm{Sr}} + s\mathbf{1})\frac{\frac{\partial S_{\mathrm{r}}}{\partial s}\dot{s} - \frac{\partial S_{\mathrm{r}}}{\partial e}v_0\mathbf{1}{:}\,\dot{\boldsymbol{\varepsilon}}}{1 - \frac{\partial S_{\mathrm{r}}}{\partial I_{\mathrm{h}}}\frac{\mathrm{d}I_{\mathrm{h}}}{\mathrm{d}S_{\mathrm{r}}}} \qquad (\mathrm{A}-3)$$

Equation (A-3) can be rearranged as

$$\dot{\boldsymbol{\sigma}}^{\mathrm{net}} = \boldsymbol{D}^{\mathrm{net}}{:}\dot{\boldsymbol{\varepsilon}} - \boldsymbol{D}^{\mathrm{s}}\dot{s} \qquad (\mathrm{A}-4)$$

where $\boldsymbol{D}^{\mathrm{net}}$ and $\boldsymbol{D}^{\mathrm{s}}$ are defined by

$$\boldsymbol{D}^{\mathrm{net}} = \boldsymbol{D}^{\mathrm{ep}} + \left(\boldsymbol{D}^{\mathrm{Sr}} + s\mathbf{1}\right) \otimes \frac{\frac{\partial S_{\mathrm{r}}}{\partial e}v_0\mathbf{1}}{1 - \frac{\partial S_{\mathrm{r}}}{\partial I_{\mathrm{h}}}\frac{\mathrm{d}I_{\mathrm{h}}}{\mathrm{d}S_{\mathrm{r}}}} \qquad (\mathrm{A}-5)$$

$$\boldsymbol{D}^{\mathrm{s}} = S_{\mathrm{r}}\mathbf{1} + \left(\boldsymbol{D}^{\mathrm{Sr}} + s\mathbf{1}\right)\frac{\frac{\partial S_{\mathrm{r}}}{\partial s}}{1 - \frac{\partial S_{\mathrm{r}}}{\partial I_{\mathrm{h}}}\frac{\mathrm{d}I_{\mathrm{h}}}{\mathrm{d}S_{\mathrm{r}}}} \qquad (\mathrm{A}-6)$$

Substituting $\dot{\boldsymbol{\sigma}}^{\mathrm{net}} = \dot{\boldsymbol{\sigma}} - \dot{u}_{\mathrm{a}}\mathbf{1}$ and $\dot{s} = \dot{u}_{\mathrm{a}} - \dot{u}_{\mathrm{w}}$ into Equation (A-4), we obtain

$$\dot{\boldsymbol{\sigma}} = \boldsymbol{D}^{\mathrm{net}}{:}\dot{\boldsymbol{\varepsilon}} + (\mathbf{1} - \boldsymbol{D}^{\mathrm{s}})\dot{u}_{\mathrm{a}} + \boldsymbol{D}^{\mathrm{s}}\dot{u_{\mathrm{w}}} \qquad (\mathrm{A}-7)$$

where $\dot{u}_{\mathrm{a}}$ and $\dot{u_{\mathrm{w}}}$ are the rates of air pressure and water pressure, respectively.

A.2 TESTING CONDITIONS FOR ELEMENTARY TESTS

The testing conditions for predicting unsaturated soil behavior are varied according to the drainage conditions of pore air and pore water, namely exhausted air condition, unexhausted air condition, drained water condition, or undrained water condition. Moreover, the stress condition of soils is also included in the testing conditions (e.g. the constant total stress condition).

The exhausted air condition is the condition that air is able to drain out of the soil. Therefore, we usually assume that there is no change in air pressure. In other words, the increment in air pressure is constant, which can be written as

$$\dot{u}_{\mathrm{a}} = 0 \text{ (Exhausted air condition)} \qquad (\mathrm{A}-8)$$

The drained water condition is the condition that pore water is able to drain out of the soil. Therefore, we usually assume that there is no change in water pressure. In other words, the increment in water pressure is constant, which can be written as

$$\dot{u_{\mathrm{w}}} = 0 \text{ (Drained water condition)} \qquad (\mathrm{A}-9)$$

The unexhausted air condition is the condition that air is unable to drain out of the soil. In other words, the mass of air is constant. We assume that air is an ideal gas and the temperature is constant. Thus, Boyle's law can be applied here as

$$(\dot{V_{\mathrm{a}}u}_{\mathrm{a}}) = 0 \text{ (Unexhausted air condition)} \qquad (\mathrm{A}-10)$$

where V_{a} is the volume of void air. As the volume of soil particles, V_{s}, is assumed to be constant and as $\frac{V_{\mathrm{a}}}{V_{\mathrm{s}}} = e(1 - S_{\mathrm{r}})$, we obtain

$$\{e(1 - \dot{S}_{\mathrm{r}})u_{\mathrm{a}}\} = 0. \qquad (\mathrm{A}-11)$$

Solving Equation (A-11), we obtain the constraint for the unexhausted air condition as

$$\dot{S}_{\mathrm{r}} = (1 - S_{\mathrm{r}})\frac{\dot{u}_{\mathrm{a}}}{u_{\mathrm{a}}} + (1 - S_{\mathrm{r}})\frac{\dot{e}}{e} \qquad (\mathrm{A}-12)$$

where $\dot{e} = -v_0\mathbf{1}{:}\dot{\boldsymbol{\varepsilon}}$. Substituting Equation (A-12) into Equation (A-2), we obtain

$$(1 - S_{\mathrm{r}})\frac{\dot{u}_{\mathrm{a}}}{u_{\mathrm{a}}} - (1 - S_{\mathrm{r}})\frac{v_0\mathbf{1}{:}\dot{\boldsymbol{\varepsilon}}}{e} = \frac{\frac{\partial S_{\mathrm{r}}}{\partial s}\dot{s} - \frac{\partial S_{\mathrm{r}}}{\partial e}v_0\mathbf{1}{:}\dot{\boldsymbol{\varepsilon}}}{1 - \frac{\partial S_{\mathrm{r}}}{\partial I_{\mathrm{h}}}\frac{\mathrm{d}I_{\mathrm{h}}}{\mathrm{d}S_{\mathrm{r}}}} \qquad (\mathrm{A}-13)$$

where $\dot{s} = \dot{u}_{\mathrm{a}} - \dot{u_{\mathrm{w}}}$. Equation (A-13) can be rearranged as

$$\left[\frac{\partial S_{\mathrm{r}}}{\partial e}+\left(1-\frac{\partial S_{\mathrm{r}}}{\partial I_{\mathrm{h}}}\frac{\mathrm{d}I_{\mathrm{h}}}{\mathrm{d}S_{\mathrm{r}}}\right)\frac{(S_{\mathrm{r}}-1)}{e}\right]v_0\mathbf{1}{:}\mathrm{d}\boldsymbol{\varepsilon}=\left[\left(1-\frac{\partial S_{\mathrm{r}}}{\partial I_{\mathrm{h}}}\frac{\mathrm{d}I_{\mathrm{h}}}{\mathrm{d}S_{\mathrm{r}}}\right)\frac{(S_{\mathrm{r}}-1)}{u_{\mathrm{a}}}+\frac{\partial S_{\mathrm{r}}}{\partial s}\right]\dot{u_{\mathrm{a}}}-\frac{\partial S_{\mathrm{r}}}{\partial s}\dot{u_{\mathrm{w}}}\quad(\mathrm{A}-14)$$

The undrained water condition is the condition that water is unable to drain out of the soil. In other words, the mass of water is constant. Therefore, taking the time derivative of water content *w* gives

$$\dot{w}=(e\dot{S_r})=0\text{ (Undrained water condition).}\qquad(\mathrm{A}-15)$$

Thus, we get the constraint for the undrained water condition as

$$\dot{S}_{\mathrm{r}}=-\frac{S_{\mathrm{r}}\dot{e}}{e}\qquad(\mathrm{A}-16)$$

where $\dot{e}=-v_0\mathbf{1}{:}\dot{\boldsymbol{\varepsilon}}$. Substituting Equation (A-16) into Equation (A-2), we obtain

$$\frac{S_{\mathrm{r}}v_0\mathbf{1}{:}\dot{\boldsymbol{\varepsilon}}}{e}=\frac{\frac{\partial S_{\mathrm{r}}}{\partial s}\dot{s}-\frac{\partial S_{\mathrm{r}}}{\partial e}v_0\mathbf{1}{:}\dot{\boldsymbol{\varepsilon}}}{1-\frac{\partial S_{\mathrm{r}}}{\partial I_{\mathrm{h}}}\frac{\mathrm{d}I_{\mathrm{h}}}{\mathrm{d}S_{\mathrm{r}}}}\qquad(\mathrm{A}-17)$$

where $\mathrm{d}s=\mathrm{d}u_{\mathrm{a}}-\mathrm{d}u_{\mathrm{w}}$. Equation (A-17) can be rearranged as

$$\left[\left(1-\frac{\partial S_{\mathrm{r}}}{\partial I_{\mathrm{h}}}\frac{\mathrm{d}I_{\mathrm{h}}}{\mathrm{d}S_{\mathrm{r}}}\right)\left(\frac{S_{\mathrm{r}}}{e}\right)+\frac{\partial S_{\mathrm{r}}}{\partial e}\right]v_0\mathbf{1}{:}\dot{\boldsymbol{\varepsilon}}=\frac{\partial S_{\mathrm{r}}}{\partial s}\dot{u_{\mathrm{a}}}-\frac{\partial S_{\mathrm{r}}}{\partial s}\dot{u_{\mathrm{w}}}.\qquad(\mathrm{A}-18)$$

The constant total stress condition is the condition that the total stress of soil does not change during the test. In other words, the increment in total stress is constant, which can be written as

$$\dot{\boldsymbol{\sigma}}=0\text{ (Constant total stress condition)}\qquad(\mathrm{A}-19)$$

A.3 CONSTITUTIVE RELATIONSHIP

A.3.1 Constitutive relationship for exhausted air and drained water condition (fully drained condition or constant suction condition)

The fully drained condition, that is, exhausted air and drained water, is the condition that air and water are able to drain out of the soil. So as to simulate the fully drained condition, the constitutive equation can be obtained by combining Equations (A-7), (A-8), and (A-9) as

$$\dot{\boldsymbol{\sigma}}=\boldsymbol{D}^{\mathrm{net}}{:}\dot{\boldsymbol{\varepsilon}}\qquad(\mathrm{A}-20)$$

where $\boldsymbol{D}^{\mathrm{net}}$ is given by Equation (A-5).

A.3.2 Constitutive relationship for exhausted air and undrained water condition (constant

water content condition)

The constant water content condition, that is, exhausted air and undrained water, is the condition that air is able to drain out of the soil but water is unable to do so. So as to simulate the constant water content condition, the constitutive equations can be obtained by combining Equations (A-7), (A-8), and (A-18) as

$$\begin{cases} \dot{\boldsymbol{\sigma}} = \boldsymbol{D}^{\mathrm{net}}{:}\dot{\boldsymbol{\varepsilon}} + \boldsymbol{D}^{\mathrm{s}}\dot{u_{\mathrm{w}}} \\ 0 = \left[\left(1 - \dfrac{\partial S_{\mathrm{r}}}{\partial I_{\mathrm{h}}}\dfrac{\mathrm{d}I_{\mathrm{h}}}{\mathrm{d}S_{\mathrm{r}}}\right)\left(\dfrac{S_{\mathrm{r}}}{e}\right) + \dfrac{\partial S_{\mathrm{r}}}{\partial e}\right] v_0 \mathbf{1}{:}\dot{\boldsymbol{\varepsilon}} + \dfrac{\partial S_{\mathrm{r}}}{\partial s}\dot{u_{\mathrm{w}}} \end{cases} \quad (\mathrm{A}-21)$$

where $\boldsymbol{D}^{\mathrm{s}}$ is given by Equation (A-6).

A.3.3 Constitutive equations for unexhausted air and undrained water condition (fully undrained condition)

The fully undrained condition, that is, unexhausted air and undrained water, is the condition that air and water are unable to drain out of the soil. In other words, the masses of water and air are constant. So as to simulate the fully undrained condition, we first subtract Equation (A-14) from Equation (A-18):

$$0 = \left[\left(1 - \frac{\partial S_{\mathrm{r}}}{\partial I_{\mathrm{h}}}\frac{\mathrm{d}I_{\mathrm{h}}}{\mathrm{d}S_{\mathrm{r}}}\right)\frac{1}{e}\right] v_0 \mathbf{1}{:}\dot{\boldsymbol{\varepsilon}} - \left[\left(1 - \frac{\partial S_{\mathrm{r}}}{\partial I_{\mathrm{h}}}\frac{\mathrm{d}I_{\mathrm{h}}}{\mathrm{d}S_{\mathrm{r}}}\right)\frac{(1 - S_{\mathrm{r}})}{u_{\mathrm{a}}}\right]\dot{u_{\mathrm{a}}} \quad (\mathrm{A}-22)$$

Combining Equations (A-4), (A-18), and (A-22), the constitutive equations for the fully undrained condition can be obtained as

$$\begin{cases} \dot{\boldsymbol{\sigma}} = \boldsymbol{D}^{\mathrm{net}}{:}\dot{\boldsymbol{\varepsilon}} + (\mathbf{1} - \boldsymbol{D}^{\mathrm{s}})\dot{u_{\mathrm{a}}} + \boldsymbol{D}^{\mathrm{s}}\dot{u_{\mathrm{w}}} \\ 0 = \left[\left(1 - \dfrac{\partial S_{\mathrm{r}}}{\partial I_{\mathrm{h}}}\dfrac{\mathrm{d}I_{\mathrm{h}}}{\mathrm{d}S_{\mathrm{r}}}\right)\dfrac{1}{e}\right] v_0 \mathbf{1}{:}\dot{\boldsymbol{\varepsilon}} - \left[\left(1 - \dfrac{\partial S_{\mathrm{r}}}{\partial I_{\mathrm{h}}}\dfrac{\mathrm{d}I_{\mathrm{h}}}{\mathrm{d}S_{\mathrm{r}}}\right)\dfrac{(1 - S_{\mathrm{r}})}{u_{\mathrm{a}}}\right]\dot{u_{\mathrm{a}}} \\ 0 = \left[\left(1 - \dfrac{\partial S_{\mathrm{r}}}{\partial I_{\mathrm{w}}}\dfrac{\mathrm{d}I_{\mathrm{w}}}{\mathrm{d}S_{\mathrm{r}}}\right)\left(\dfrac{S_{\mathrm{r}}}{e}\right) + \dfrac{\partial S_{\mathrm{r}}}{\partial e}\right] v_0 \mathbf{1}{:}\dot{\boldsymbol{\varepsilon}} - \dfrac{\partial S_{\mathrm{r}}}{\partial s}\dot{u_{\mathrm{a}}} + \dfrac{\partial S_{\mathrm{r}}}{\partial s}\dot{u_{\mathrm{w}}} \end{cases} \quad (\mathrm{A}-23)$$

A.3.4 Constitutive relationship for constant net stress condition (suction tests)

The constant net stress condition is the condition that air is able to drain out of the soil and the total stress does not change but water is able to increase or decrease during the test (e.g. suction test). In order to simulate the constant net stress condition, the constitutive equations can be obtained by combining Equations (A-7), (A-8), and (A-19) as

$$\boldsymbol{D}^{\mathrm{net}}{:}\dot{\boldsymbol{\varepsilon}} = -\boldsymbol{D}^{\mathrm{s}}\dot{u_{\mathrm{w}}} \quad (\mathrm{A}-24)$$